The role of intracellular and extracellular AGEs on *in vitro* osteoclastogenic model of RAW 264.7 cells

A Dissertation Submitted in Partial Fulfillment of the Requirements for the Degree of
Doctor of Philosophy

Graduate School of Life and Medical Sciences
Department of Medical Life Systems
Doshisha University

Author: TANZIMA TARANNUM LUCY
Student ID: 1414 20 2501
Supervisor: Prof. Dr. Yoshikazu Yonei

Kyoto, Japan
May 2023

Table of Contents

Acknowledgment

I would like to express my gratefulness to the almighty Allah (SWT) for all his blessings and mercy to live my dream and be able to make it come true, for the strength and patience to endure all the stress and hurdles on the way to complete this journey.

It is my pleasure to take this opportunity to convey my gratitude to Prof. Dr. Yoshikazu Yonei, Faculty of Life and Medical Sciences, Department of Medical Life Systems, Doshisha University, Japan; for allowing me to be a part of his laboratory as a post-graduate student. His expertise in the field of anti-aging medicine, knowledgeable comments, and pedagogic advice were very helpful and motivating. Without his kind guidance and immense support, it would have been way more difficult to complete everything on time.

I would like to thank Dr. Masayuki Yagi for his advice and support whenever I needed them. My thankfulness to Dr. Wakako Takabe for her precious time and tireless support in making me able to learn the research techniques and everything related. It was her supervision that made the base of me being a researcher. I would like to express my gratitude to Dr. Akira Kobayashi, Dr. Satoru Funamoto, and Dr. Hiroshi Ichikawa for allowing me to use their laboratory facilities whenever I needed them.

I would like to thank Dr. Chieko Sakiyama, the faculty staff, and every former and present member of Yonei Lab for always being there for me and supporting me in every aspect.

This list will not be completed without acknowledging the most precious person in my life, my beloved husband Dr. A. N. M. Mamun-Or-Rashid whose contribution in completing this journey cannot be documented in sentences. Yet again, it is a token of appreciation to thank him.

Last but not least, I would like to thank my mother, father, brother, in-laws, and all friends and relatives for their support and encouragement.

Tanzima Tarannum Lucy
Kyoto, Japan
May 17, 2023

List of abbreviations

Advanced glycation end products (AGEs)

ATPase H+ Transporting V (Atp6v)

Cathepsin K (CtsK)

Cell counting kit-8 (CCK-8)

Collagen-I (col-I)

Collagen peptide (col-pep)

Dendritic cell-specific transmembrane protein (DC-stamp)

3-Deoxyglucosone (3-DG)

Dulbecco's modified Eagle's medium (DMEM)

Extracellular signal-regulated kinases (ERK)

Fetal bovine serum (FBS)

Fructose (fru)

Glucose (glu)

Glycating agent (GA)

Glycated collagen protein (col-AGE)

Glycated collagen peptide (col-pep-AGE)

Glyceraldehyde 3-phosphate dehydrogenase (GAPDH)

Glyoxal (GO)

High mobility group box 1 (HMGB1)

High-performance liquid chromatography (HPLC)

Integrin alpha-V (Itgav)

Integrin Beta 3 (ItgB3)

Matrix metallopeptidase 9 (MMP-9)

Minutes (mins)

Messenger RNA (mRNA)

Methylglyoxal (MGO)

Microphthalmia-associated transcription factor (MITF)

Nanometer (nm)

Nuclear factor kappa-B ligand (RANKL)

Nuclear factor-κB (NF-κB)

Nuclear factor of activated T-cells cytoplasmic 1 (NFATc1)

N^{ε}-(carboxymethyl)-lysine (CML)

Osteoclast (OC)

Osteoclast differentiation/ osteoclastogenesis (OS)

Osteoclast stimulatory transmembrane protein (OC-stamp)

Pentosidine (pent)

Potential of hydrogen (pH)

P38 mitogen-activated protein kinases (p38 MAPK)

Radioimmunoprecipitation assay buffer (RIPA buffer)

Real-time polymerase chain reaction (RT-PCR)

Receptor activator of nuclear factor kappa-B ligand (RANKL)

Receptor for AGEs (RAGE)

Relative fluorescence units (RFU)

Ribose (rib)

Room temperature (RT)

Sodium borohydride ($NaBH_4$)

Sodium dodecyl sulfate-polyacrylamide gel electrophoresis (SDS-PAGE)

Standard deviation (SD)

Standard error of the mean (SEM)

Tartrate-resistant acid phosphatase (TRAP)

TNF receptor-associated factor (TRAF)

Table of Figures

The role of intracellular and extracellular AGEs on *in vitro* osteoclastogenic model of RAW 264.7 cells

Abstract

Aging is an unavoidable physiological process resulting from the impact of cellular and molecular damage over time having effects all over the body. Glycative stress results from persistently raised blood sugar levels, high sugar and high fat-containing diet, and excessive alcohol consumption which leads to the production of excessive aldehydes that reacts non-enzymatically with protein, producing advanced glycation end products (AGEs). AGEs bind to specific receptors for AGEs (RAGE), which subsequently induce the production of inflammatory cytokines and other substances. The formation and accumulation of AGEs increase with age and have been linked with a wide range of metabolic and inflammatory diseases due to the alteration of the structural and functional integrity of a protein. Collagen-I (col-I) is the main structural protein of bone and is important for maintaining bone strength and quality. Pentosidine (pent), a well-known cross-link, fluorescent AGE that has been found to be elevated in bone collagen, serum, and urine of patients with osteoporosis. Increased osteoclast activity is postulated to induce a state in which bone resorption by osteoclasts exceeds bone formation by osteoblasts, resulting in porous and fragile bone*, i.e.,* a high turnover metabolic disorder.

Aim of this study was to check the effect of col-I glycation using different glycating agents (GAs) as well as the effect of free pent on osteoclast differentiation/osteoclastogenesis (OS) using *in vitro* cell culture model of mouse macrophage RAW 264.7 cells. Moreover, the effect of repetitive cell sub-culturing mimicking the aging of cells on OS was also checked.

Fluorescent AGE-derived fluorescence intensity was measured using a fluorometric plate reader and High-performance liquid chromatography (HPLC) analysis was done to measure AGE and their intermediates formation. Tartrate-resistant acid phosphatase (TRAP) activity and TRAP staining were done to check OS. To check mRNA and protein expression, Real time polymerase chain reaction (RT-PCR) and western blotting were done respectively. An immunofluorescent assay was used to check the morphology of the cells and signaling pathway activation.

Intracellular AGE formation was observed to be increased, and the receptor for AGEs (RAGE) was found to be decreased along with the reduced formation of multinucleated osteoclasts formation with passaging. Maturation and early osteoclastogenic marker gene expression were reduced in cells of higher passages. Larger F-actin rings in lower passage cells than higher passage cells indicate reduced cell-cell fusion which is essential for giant osteoclast formation indicating glycative stress to cells by forming intracellular AGEs due to repeated sub-culturing leading to loss of differentiation potential.

Afterward, early passage cells were treated with glycated col-I (col-AGE) which stimulated receptor activator of nuclear factor kappa-B ligand (RANKL)-induced OS. The amount of pent formation was found to differ in col-AGE based on GA without any significant effect on their stimulatory role for OS suggesting col bound pent might be an epiphenomenon rather than a cause. mRNA expression and pathway activation depended largely on the GA used to prepare col-AGE. Glycated col-I peptide (col-pep-AGE) was used to measure the formation of reactive AGE precursors revealing differences in the amount depending on GA. Free pent was found to inhibit RANKL-induced OS significantly.

From this study, we observed that the formation of intracellular and extracellular AGEs could alter RANKL-induced OS in RAW 264.7 cells. Intracellular AGE formation reduced OS by reducing cell-cell fusion and inhibiting osteoclastogenic gene expression. In contrast, extracellular col-AGEs modulate OS based on the GA. Col-derived AGEs and col-pep-derived AGEs showed a stimulatory effect on OS; whereas free pentosidine significantly reduced OS. This phenomenon seems to be feedback inhibition by the AGE (pent) as protein-bound pent stimulates OS to enhance its removal from the bone part and when it is removed and released into the extracellular space as free pent, it shows feedback inhibition.

These findings suggest that to maintain bone homeostasis, it is important to avoid factors that induce glycative stress and to aim for a healthy lifestyle.

Introduction

The non-enzymatic reaction between the reactive carbonyl group of reducing sugars and the free amino group of protein or nucleic acid produces a harmful heterogeneous molecule called advanced glycation end products (AGEs). This reaction is known as the glycation reaction. It is a continuous life-long process and the accumulation of AGEs increases with normal aging; impaired glucose tolerance, reduced removal of AGEs, and increased oxidative and carbonyl stress are considered as possible reasons for this phenomenon (1). AGEs can also be formed by polyol pathway or lipid peroxidation in the presence or absence of a hyperglycemic state which suggests that they can be formed both endogenously and exogenously under normal or pathological conditions (2). AGEs can produce reactive oxygen species and reactive nitrogen species causing oxidative stress and inflammation. This causes alteration of protein structure and function, cellular dysfunction, and apoptosis resulting in multi-tissue injury which in a term is called glycative stress (3).

Glycative stress has drawn attention in recent years as a factor that significantly affects tissues and organs of the human body and is directly related to health maintenance and aging-related diseases (4). Glycative stress refers to the excessive formation of carbohydrate-derived aldehydes or fatty-acid-derived aldehydes in the body. Unfavorable lifestyle habits involving high-sugar and high-fat diets; excessive alcohol consumption; and conditions like hyperglycemia can cause excessive aldehyde production (5, 6). These aldehydes impact diverse substances such as proteins, lipids, bases in DNA of cells, and subcellular organelles. Proteins in the body are modified by non-enzymatic procedure and abnormal proteins, *i.e.*, carbonylated proteins, advanced glycation end-products (AGEs), are formed and stored intra- and extra-cellularly. AGEs induce endoplasmic reticulum stress, causing the deterioration of cellular functions (5–7).

AGEs play a vital role in altering the functionality and phenotypic characteristics of cells with the passaging number (8, 9) such as inducing the proliferation and migration of cells (10, 11), cell cycle arrest (10), and apoptosis (12). The passaging of cells is a process including culture and subculture to maintain cell viability and cell population required for *in vitro* cell culture studies. It starts from the

seeding of cells followed by incubation for optimal growth and transferring them into a new cell culture flask to regrow. The passage number is the number that expresses how many times the cell line has undergone sub-culturing. Several studies have been conducted to find out the effect of passage number on cell phenotype. Primary cells isolated from living tissues undergo morphological changes and progressive damage with passaging (13, 14). Surprisingly, for some cell lines, these changes occur at relatively low passage numbers, whereas, at high passage numbers for other cell lines (15). Increased generation time, gradual cessation of mitotic activities, and accumulation of cellular debris were observed in different cell lines at high passage numbers (14, 16–18). Opposite to these findings, the LNCaP cell population was found to be over two times higher after five days at passage number 70 than that at passage number 38 (8). Bonab and colleagues found several physiological, functional, and molecular parameter changes occurring in long-term cultures including a gradual decrease in proliferation potential, impairment of functions, typical Hayflick phenomenon of cellular aging, and shortening of the telomeres using the MSC cell line (19). Taken together, passage numbers could be a source of variation in data hence affecting data reproducibility. Our laboratory has been using RAW 264.7 cells for different studies. RAW 264.7 is a monocyte/macrophage cell lineage originating from the Abelson leukemia virus-transformed cell line from BALB/c mice. It has been implicated as an *in vitro* osteoclastogenesis model for many years and is an appropriate model of macrophage. The manufacturer company The American Type Culture Collection (ATCC) recommends the use of the cells until passage 18 for osteoclast (OC) differentiation study (20). We have also noticed a decrease in differentiation potential with increased passage numbers and have always used early passages (21–24) but for other inflammatory cytokine production studies, no variation in reproducibility until passage 20 was observed (25).

We hypothesized that the changes in osteoclastogenic differentiation/osteoclastogenesis (OS) could be due to glycative stress because passaging of cells is actually cellular aging and AGE accumulation increases with age. Henceforth, in the first chapter, we tried to find out the effect of passaging on intracellular AGE formation and accumulation, and on osteoclastogenic differentiation capacity using the RAW 264.7 cell line.

AGEs have also been linked with several age-related diseases like diabetes, Alzheimer's, renal failure, osteoporosis, cancers, and hepatic disease by altering intracellular signaling after binding with its receptor (RAGE). RAGE is a cell surface receptor of the immunoglobulin superfamily having affinity to bind with multiple ligands like HMGB1, amyloid-β peptides, and members of the S100 protein family contributing to different pathophysiology (26). Osteoporosis is a metabolic disease of bone with low bone density and microarchitectural deterioration leaving the bone weak and fragile. Bone remodeling is composed of a coupled process of bone formation and bone resorption to maintain structural integrity and mineralization (27). Osteoblasts are mesenchymal-origin mononuclear cells responsible for bone formation and osteoclasts are hematopoietic-origin multinucleated cells responsible for bone resorption. A healthy balance is always required between these two opposite processes to maintain healthy bone structure and strength. When bone resorption exceeds bone formation bone microstructure alters, and bone mass decreases. Bone mass is a crucial factor as it together with bone quality determines bone strength. Increased bone resorption and decreased calcium absorption cause a reduction in bone mass in advanced age (7). Genetic background, lifestyle, chronic diseases like diabetes, renal impairment, and certain drugs possess a crucial role in bone mass reduction by altering both bone formation and resorption and ultimately reducing bone strength (1). Collagen (col) is secreted by osteoblast cells (28) and is the main structural protein of bone as 90% of bone matrix protein is composed of collagen-I (col-I) which is a big molecule with a molecular weight of 300 kDa, determining the strength of bone (29). It is a triple helix structure in which three polypeptide chains (α chains) are enzymatically crosslinked by a hydrogen bond making a scaffold for the mineralization (30) suggesting any disruption of the structure will hamper the mineralization process and the bone will become weaker. Collagen-peptides (col-pep) are the hydrolyzed form of col protein with a molecular weight ranging from 3-6 kDa. Glycation of col protein causes a non-enzymatic or AGE-induced cross-linking that is disordered bonding between col molecules. This type of cross-linking reduces the elasticity of col, bone becomes rigid and brittle (31). This is how glycation of col plays a key role in determining bone quality.

Pentosidine (pent), is a well-known crosslinking AGE and a surrogate marker of total AGE formation (32). Pent level in serum and urine increases with age (32, 33) as well as the urinary pent level

associates with the prevalence of fractures in women (33, 34), men (34), and diabetic patients (34, 35). In dialysis patients, increased pent in bone has been reported to be correlated with reduced bone formation, bone volume ratio, and mineralization (36). Additionally, AGEs reduce osteoblast function and induce apoptosis thereby reducing bone formation (37).

In the second chapter of the study, we aimed at how extracellular pent-rich collagen-AGEs and free pent affect RANKL-induced OS.

Materials and Methods

Glycated collagen preparation

To prepare glycated collagen-I (col-AGEs), collagen-I (col-I) 3mg/mL (bovine skin collagen type I) (NIP-8901- 53) was incubated either with glucose (glu)/ fructose (fru)/ ribose (rib) for 1, 4, 7, and 10 days at 60 °C. Phosphate buffer (pH 7.4) was used to maintain the pH of the solution (soln). Final concentration (conc) of the col-I in the soln. was 0.6mg/mL, glu 200 mM, fru 200 mM, rib 100 mM, or as mentioned in the figures, phosphate buffer 0.05 mole/L. To prepare non-heated and heated col-I as negative controls, no glycating agent was added and MQ was used instead. The mixture was kept at 4 °C just after preparation in case of non-heated col-I and was incubated at 60 °C in case of heated col-I (38).

To prepare collagen peptide AGEs (col-pep-AGEs), col-pep powder (AFC-G, Nippi, Japan) was first dissolved in MQ to make the conc. 40 mg/mL. Henceforth, the procedure was the same as the col-AGE preparation method and the final conc. of col-pep in the reaction mixture was 8 mg/mL. After the incubation period, the reaction mixture was ultrafiltrated using centrifugal filter units 10K filter (Millipore, Darmstadt, Germany) and 3K filter (Merck Millipore Ltd, Tullagreen, Carrigtwohill, Ireland) for col-AGEs and col-pep-AGEs respectively to remove the unreacted glycating agent and phosphate buffer. Briefly, the filter was washed with 500 μl sterile MQ and centrifuged for 20 minutes (mins) at 14000 × g followed by discarding the flow through. Sample 500 μl was added at a time and centrifuged for 20 mins at 14000 × g. Flow through was discarded and the remaining mixture on the filter part was washed with 400 μl sterile MQ. Finally, the filter was inverted in a new tube, centrifuged shortly and ultrafiltrated samples were collected from the bottom of the tube. DC protein assay was performed to measure the final col-pep-AGE conc. col-AGEs and col-pep-AGEs were stored at 4 °C to use for the study.

Fluorescent AGEs measurement in the samples

Ultrafiltrated col-AGEs and col-pep-AGEs samples were used to measure fluorescence intensity. 150 µL of the reaction mixture was added to a 96-well clean black plate. As a reference for calibration of fluorescent materials Quinine sulfate solution (5 µg/mL) was used and fluorescence intensity was measured at excitation-emission (ex-em) 370-440 nm for fluorescent AGEs and 325-385 nm for pent using a Varioscan® Flash (Thermo Scientific, Waltham, MA) microplate reader.

Cell culture and reagents

Murine monocyte/macrophage RAW 264.7 (ATCC® TIB-71™) cell line was used for *in vitro* culture study and was bought from American Type Culture Collection (ATCC; Manassas, VA). Dulbecco's modified Eagle's medium (DMEM; Sigma-Aldrich, MO) with high glucose was used as cell culture media, and αMEM (Gibco, El Paso, TX) was used as differentiation media. 10% fetal bovine serum (FBS) (Nichirei Biosciences, Tokyo, Japan) was added to the media to provide nutrition to the cells. 100 units/mL penicillin, 100 µg/mL streptomycin, and 25 µg/mL amphotericin B (Gibco, El Paso, TX) were used as antibiotics and added to the media to protect the cells from any bacterial contamination. Cell culturing was done in a sterile condition and incubated at 37 °C and 5% CO_2 for different time periods (21, 25).

For the study to check the effect of free pent, commercially available standard pentosidine was used (PolyPep group, Strasbourg, France). Recombinant mouse (NSO derived) receptor activator of nuclear factor κappa B ligand (RANKL) (R&D systems, USA) was used to induce OS.

We received the third passage (P-3) cells from the company in a frozen state with cryopreservatives. Cells were thawed and cryopreservatives were removed by centrifugation. Then they were seeded on a 10 cm culture dish using DMEM with FBS and antibiotics. When they grew to 80% confluency, subculturing was done at a conc. of 5×10^5 cells/dish and was labeled as P-1. Cells were detached from the culture dish using a sterile cell scraper. To get enough cells for preparing cryovials for storage, subculturing was done till P-4. The liquid nitrogen vapor phase was used to store the cell containing cryovials as per the manufacturer's recommendation prepared from P-4 using

Cryopreservative Medium (Nippon Zenyaku Kogyo CO., Ltd, Fukushima, Japan). Cells from these cryovials were thawed, cultured, and sub-cultured for all the cell studies and labeled as P-0. From P-1 to P-21, cells were sub-cultured and used for the same studies from the same cryovial to compare lower passage and higher passage cells.

In vitro osteoclastogenesis

RAW264.7 cells were seeded at a density of 1×10^4 cells/well in a transparent 96-well plate and incubated for 24 hours in the proliferating media using DMEM-FBS-pen-str (DMEM +/+) followed by changing of media with αMEM-FBS-pen-str (αMEM +/+) (Gibco, El Paso, TX) with or without 100 ng/mL RANKL with or without samples as indicated in the figures. In case of col-AGEs or col-pep-AGEs, 200 mM glu, fru, and 100 mM rib were the final conc. of the glycating agents in the samples. 200 µg/mL col-AGE and 400 µg/mL col-pep-AGE or as mentioned in the figures were used for cell culture treatment. After 3 days, the medium was renewed, and TRAP activity was performed to check for *in vitro* OS as per manufacturers protocol after 5 days of cultures using a TRAP solution kit (Oriental Yeast Co., Tokyo, Japan). Briefly, culturing media was discarded, and cells were fixed with Acetone: Ethanol = 1:1 as a cell fixation buffer for 1 min. The fixative buffer was discarded, and the cells were allowed to dry for 30 mins at RT followed by adding the substrate solution and incubating for 45 mins. 1N NaOH was added to the cells as a stop soln. and colorimetric absorbance was taken at 405 nm using a Varioscan® Flash (Thermo Scientific, Waltham, MA) microplate reader after the yellow coloration of the soln. (25).

TRAP staining

To check the cell size, shape, and nuclei, TRAP staining was performed using a TRAP staining kit (387A-1KT, Sigma-Aldrich, USA) as per the manufacturer's protocol. Briefly, RAW 264.7 cells were seeded at a conc. of 1×10^4 cells/well in a 96-well transparent plate in DMEM +/+ and incubated for 24 hours followed by changing the media with αMEM +/+ with or without 100 ng/mL RANKL and with or without samples as indicated in figures. Media was renewed after 3 days. After 5 days, media

were discarded, and cells were fixed using 10% formalin neutral buffer soln. (Wako Pure Chemical Industries Ltd.) for 30 seconds followed by 3 times washing with MQ. Then, cells were stained using the TRAP staining kit and incubated at 37 °C for 1 hour. After the incubation period, stained cells were washed with MQ 3 times and incubated with hematoxylin (Sigma-Aldrich) for 20 mins to stain the nucleus. After 20 mins, cells were washed again with MQ 3 times for 5 mins each. A light microscope (Olympus CKX 41, Tokyo, Japan) was used to count the nuclei, and cells, and to capture the image. Multinucleated cells having ≥3 nuclei were regarded as osteoclast cells (25).

Evaluation of cell viability

Cell viability was evaluated using cell counting kit-8 (Dojindo, Kumamoto, Japan). RAW264.7 cells were seeded on 96-well plates at the density of 1×10^4 cells/well and were treated the same as mentioned above for 5 days. After 5 days, a 10% volume of WST-8 soln. was added to the culture medium, and the cells were incubated for 1 hour. Absorbance at 450 nm was then measured using a Varioscan® Flash microplate reader (25, 39). Sensolyte cell viability and proliferation assay kit (Anaspec) was used to check the effect of col-pep-AGEs and free pent on cell viability according to the manufacturer's protocol. A 15% volume of kit solution was added to the culture medium and incubated for 1 hour. After that absorbance was taken at ex-em 530-590 nm using the same microplate reader.

Isolation of total RNA and RT-PCR

RAW 264.7 cells were seeded at a conc. of 1×10^5 cells/mL conc. in a transparent 24-well plate or 96-well plate. After 24 hours, cells were treated with or without 100 ng/mL RANKL and with or without samples as mentioned in the figures. RNA was extracted after 6 hours or 24 hours or 3 days of media changing in the case of early marker gene expression study as indicated in the figures. Media was renewed after 3 days and a total of 5 days in differentiation media, RNA was extracted for checking maturation marker gene expression. As per the manufacturer’s protocol, total RNA was extracted using the Isogen II reagent (Nippon Gene, Toyama, Japan). cDNA was prepared using Applied Biosystems 2720 Thermal cycler. Five hundred ng or 250 ng of RNase-free DNase-treated

total RNA and PrimeScriptTM RT Master Mix (Takara Bio Inc., Japan) were used for this reverse transcription. Real-time quantitative PCR (RT-PCR) was done following the manufacturer's protocol using Thunderbird^{TM} SYBR qPCR mix (Toyobo Co., Ltd., Osaka, Japan) and used gene-specific primers. For amplification of the reactions, AB Applied Biosystems StepOnePlus Real-Time PCR system was used. An initial hold step (95°C for 1 min) and 40 cycles of PCR (95°C for 15 seconds, 60°C for 60 seconds), followed by a dissociation curve. 18S or GAPDH: glyceraldehyde-3-phosphate dehydrogenase was used for normalizing the mRNA expression as shown in the figures. The comparative CT method was followed to determine the difference in the target gene expression. Primers used for the study are listed below:

primer	**Forward**	**Reverse**
NFATc1	TCC AAA GTC ATT TTC GTG GA	CTT TGC TTC CAT CTC CCA GA
MMP9	CTG GAC AGC CAG ACA CTA AAG	CTC GCG GCA AGT CTT CAG AG
RAGE	ACT ACC GAG TCC GAG TCT ACC	GTA GCT TCC CTC AGA CAC ACA
TRAF6	GAA GAG GTC ATG GAC GCC AA	CGG GTA GAG ACT TCA CAG CG
ItgB3	TTA CCC CGT GGA CAT CTA CTA	AGT CTT CCA TCC AGG GCA ATA
c-Fos	CGG GTT TCA ACG CCG ACT A	TTG GCA CTA GAG ACG GAC AGA
18s	AGG AAT TGA CGG AAG GGC ACC A	GTG CAG CCC CGG ACA TCT AAG
MITF-E	CCA GAT ACA CAG ACA GTC ACA GAG	GCT GGC GTA GCA AGA TGC GTG A
CtSK	TGG ACT GTG TGA CTG AGA ATT ATG G	CCG TTC TGC TGC ACG TAT TG
TRAP	GCC AAA GAG ATC GCC AGA AC	GAA GTA GAA ATT GTC CCC CAG AGA
Atp6v	ACG GTG ATG TCA CAG CAG ACG T	CCT CTG GAT AGA GCC TGC CGC A
DC-stamp	GAA GTA GAA ATT GTC CCC CGA GA	GGA CTG GAA ACC AGA AAT GAA
OC-stamp	ATG AGG ACC ATC AGG GCA GCC ACG	GGA GAA GCT GGG TCA GTA GTT CGT
Itgav	GGA CTG GAA ACC AGA AAT GAA	CAA GGC CAG CAT TTA CAG TG

GAPDH	AGG TCG GTC TGA ACG GAT TTG	TGT AGA CCA TGT AGT TGA GGT CA

Protein Extraction and Western Blot Analysis

Cells from different passages were seeded in a 6-well plate at a conc. of 2×10^5 cells/well. RIPA buffer containing 50 mM Tris-HCl, 150 mM NaCl, 0.1% SDS, and 1% Triton X-100 with complete protease inhibitor (Wako Pure Chemical Industries, Osaka, Japan) was used to lyse the cells. To measure the protein conc. of cell lysate BCA assay was performed. 12% sodium dodecyl sulfate-polyacrylamide gel electrophoresis (SDS-PAGE) gel was used for the electrophoresis of the cell lysates. The protein was transferred on a Polyvinylidene difluoride (PVDF) membrane and to block it, 5% skim milk in TBS-T was used as a blocking buffer. Immunoblotting of the membranes with primary antibodies was done. The primary antibodies used for the western blotting are as follows:- anti-pentosidine (#KH012, Medicinal Chemistry Pharmaceutical, Co., Ltd., 1:1000, o/n), anti-CML (#MAB3247, R&D systems, 1:1000, o/n), anti-AGEs (#ab23722, abcam, 1:1000, o/n), anti-RAGE (#ab37647, abcam, 1:5000, o/n), anti-β-actin (#A5441, Sigma-Aldrich, St. Louis, MO, 1:5000, 1 h). Membranes were washed with TBS-T and incubated with secondary antibody, goat anti-rabbit IgG-HRP secondary antibody (#sc-2004, Santa Cruz Biotechnology, Dallas, TX, 1:10000) or goat anti-mouse IgG-HRP secondary antibody (#7076P2, Cell signaling technology, 1:10000) in blocking buffer for 1 hour. After the incubation, membranes were washed again, and the chemiluminescence horseradish peroxidase (HRP) substrate (Millpore Corporation, USA) was used to visualize the antigen–antibody complexes along with the detection system as per the manufacturer's recommendation. Each figure in the result represents at least three independent experiments. β-actin was used to normalize the data and ImageJ was used to measure the intensity of the protein bands.

Fluorescence scanning and intensity measurement

Cells were seeded in a 6-well plate at a density of 2×10^5 cells/well. Cells were lysed using RIPA buffer containing 50 mM Tris-HCl, 150 mM NaCl, 0.1% SDS, and 1% Triton X-100 with complete protease inhibitor (Wako Pure Chemical Industries, Osaka, Japan). The conc. of cell lysate was measured by the BCA assay method. 100 µL of 80 µg/mL cell lysate/well was added in a 96-well

black plate and fluorescent intensity was measured at ex-em 325-385 nm and 370-440 nm using a fluorometric microplate reader. For fluorescence scanning, excitation was done at 325 and 370 nm, and the emission from 360-600 and 400-650 nm was measured respectively.

Immunofluorescence assay

RAW 264.7 cells were seeded in a 96-well black wall and clear bottom plate at a conc. of 1×10^4 cells/well and incubated for 24 hours followed by changing the media with or without 100 ng/mL RANKL and with or without samples as mentioned in the figures. Media was renewed after 3 days and after 5 days of culture, the immunofluorescent assay was done. 4% formaldehyde was used to fix the cells at room temperature for 15 mins. Blocking was done with 3% BSA in PBST for 1 hour. After 1 hour, cells were incubated at 4°C overnight with the primary antibody in blocking buffer against RAGE (#ab37647, Abcam, 1:1000). Next day, cells were washed with PBST for 3 times followed by incubation with Donkey anti-rabbit IgG secondary antibody conjugated with PE (sc-3745, Santa Cruz Biotechnology, Inc., Dallas, Texas) and Phalloidin-iFlour 488 reagent (#ab176753, Abcam, 1:1000) in blocking buffer at RT. The plate was wrapped in foil in the dark for 2 hours and then washed 3 times with PBST. Later, cells were incubated with DAPI (#135-1303, Bio-Rad, 1:1000) in MQ and kept in the dark for 20 mins. Lastly, cells were washed 3 times with MQ. A fluorescence microscope (Olympus IX71, Tokyo, Japan) was used to capture representative images. ImageJ was used to process and analyze the images.

For pathway study, cells were seeded at a conc. of 1×10^4 cells/well in a 96-well clear bottom black wall plate. After the attachment of the cells to the plates, they were starved overnight using the media DMEM and antibiotics only, with no FBS. The next day, the media was changed with or without RANKL and with or without samples for 10/20 mins as mentioned in the figures. After the mentioned time treatment, media was discarded, and cells were fixed with 4% formaldehyde for 15 mins at RT followed by washing with MQ 3 times. 0.2% Triton X-100 in 3% BSA in PBST was added 100 µl/well to the cells for 10 mins to increase permeability and washed 3 times with PBS. Primary antibodies rabbit mAb for NFκB (D14E12), pERK (T208), pSAPK/JNK (T183/Y185), p38 (T180), and AKT

(PAN) (C67E7) were prepared in 3% BSA in PBST as per manufacturer's instructions and added 100 µl/well to the cells and incubated overnight at 4°C. The next day, primary antibodies were removed, and cells were washed with PBST 3 times for 5 mins for each wash. Alexa Flour 594 Rabbit IgG (H+L) Secondary Antibody (Invitrogen, USA) was prepared in 3% BSA in PBST and added to the cells 80 µl/well and kept at RT wrapped in aluminum foil for 120 mins followed by washing with PBST 3 times in the dark. Later, NucBlue ™ Fixed Cell Ready Probes ™ Reagent (DAPI) (#R37606, Thermo Fisher Scientific, 2 drops/ml) in PBS was prepared and added to the cells at 80 µl/well and incubated for 15 mins in the dark. Finally, cells were washed with MQ 3 times and were observed for fluorescence using an immunofluorescent microscope. Images were processed and analyzed using ImageJ and cell profiler.

HPLC analysis

For pent and intermediates *i.e.*, 3-DG, GO, and MGO measurement, the reverse-phase high-performance liquid chromatography (HPLC) method was used. Measurement conditions on HPLC method were used are as follows: - for pent; column: US-C18, 150 × 4.6 mm ID, 5 µm; eluent A: 100 mmol/L citric acid / ACN = 99.5 / 0.5, eluent B: 100% ACN; flow rate: 1.0 mL/min; fluorescence detection: ex-em 325-385 nm; and sample injection volume: 20 µL. Briefly, glycated col-pep samples were diluted 2X by using MQ, 0.4mM $NaBH_4$ was added to the samples followed by adding 6N HCl. This mixture was hydrolyzed for 18 hours at 105ºC using a hot plate and later evaporated. Evaporated samples were re-dissolved using eluent A. For intermediates; column: UK-phenyl, 75 × 3 mm ID, 3 µm; eluent A: 50mM phosphoric acid, eluent B: 100% ACN, flow rate: 1mL/min, column temp: 40°C, Fluorescence detection: ex-em 271-503 nm, and sample injection volume: 20μL. Briefly, glycated col-pep samples were diluted 3X using MQ. 6% perchloric acid was added to the diluted samples and centrifuged at 12000 rpm for 10 mins. Later, sodium bicarbonate and DAN were added to the sample mixture and HPLC was performed.

Ca^{2+} influx

RAW264.7 cells were seeded at a conc. of 1×10^4 cells/well in a sterile clear bottom black 96-well plate. The next day, cells were starved, and media were changed with DMEM without FBS but with antibiotics. The following day, a Ca^{2+} signaling assay was performed. Fluo 4 NW Calcium Assay kit (Thermo Fisher Scientific, USA) was used to check Ca^{2+} influx, and the assay was done according to the manufacturer's instructions. Briefly, 1 vial of probenecid was dissolved using 1 mL assay buffer, and 250 mM stock solution was prepared. 1X dye loading soln. was prepared using 100 µl of this 250 mM stock soln. and 10 mL assay buffer. Starving media were removed, and 1X dye loading soln. was added 100 µl/well to the cells. Then the plate was incubated at 37°C, 5% CO_2 for 30 mins, and at RT for 30 mins. Afterward, media were changed with or without RANKL and with or without 200 μg/mL col-AGEs. Media were prepared using the assay buffer provided with the kit. $CaCl_2$ was used as the positive control. Fluorescence was taken using the fluorometric plate reader.

Statistical analysis

Data were expressed as mean ± standard error of the mean (SEM) using GraphPad Prism 8 (GraphPad Software, Inc., San Diego, CA, USA). All statistical analyses were performed using either the Tukey-Kramer test for intergroup comparison using Excel add-ins or one-way ANOVA using GraphPad Prism 8 for intergroup comparison in all the experiments. Differences were considered significant at a significance level of 5%.

Results

Chapter 1: Role of intracellular AGEs on osteoclastogenesis

Intracellular fluorescent AGE formation in cells of different passages

Cells were collected from different passages and cell lysate was prepared. An equal amount of cell lysate was used to check intracellular fluorescent AGE formation and accumulation using a fluorometric microplate reader. Most of the fluorescent AGEs yield fluorescence at excitation/emission (ex/em) 370/440 nm. Being a fluorescent AGE, pent has its own range of exerting fluorescence and that is ex/em 325/385 nm, however, there are some other unidentified AGEs that also exert fluorescence at this ex/em wavelength which we have found in our other study. The data showed that fluorescent AGEs-derived fluorescence intensity at ex-em 370-440 nm was reduced in P-5 to P-7, increased from P-9 to P-11, reduced from P-13 to P-17, and increased again in P-19 followed by a decrease in P-21 (Figure 1-A). In the case of ex-em 325-385 nm, fluorescence intensity was decreased in P-5 to P-7 compared to P-1, increased in P-11 to P-13, decreased in P-15 to P-17, and increased again in P-19 followed by a decrease in P-21 than P-1 (Figure 1-B). In both cases, continuous increase and decrease in fluorescence intensity were observed suggesting continuous formation and accumulation of AGEs and the possible ability of cells to excrete the produced intracellular AGEs from the cell body. Moreover, scanning was done at ex/em 370/400–650 nm (Figure 1-C) and 325/360–600 nm (Figure 1-D) to confirm the range of our ex-em wavelength and to check whether there is any peak other than the range and no peak was found outside the range.

Intracellular AGE formation in cells of different passages

After checking intracellular fluorescent AGE formation by the fluorometric plate reader, western blotting was performed to check intracellular AGE formation at the protein level (Figure 2-A). Specific antibodies were used against intracellular total AGEs, pent, and CML. Total AGE formation was not changed over passaging of the cells (Figure 2-B). The pent formation was reduced in P-5 and showed an increasing trend from P-6 till P-11, started decreasing in P-13 to P-15, increased again in

P-17 to P-19 followed by decreeing in P-21 compared to P-1which is almost similar to the fluorometric plate reader data (Figure 2-C). CML formation was decreased in P-5 and P-15 compared to P-1. All other passages showed an incrementor trend compared to P-1 (Figure 2-D). RAGE expression was also checked and found almost no change over passaging in the case of RAGE 38 kDa expression except for P-17 and P-19 where it was highest (Figure 2-E). RAGE 34 kDa was found to be increased except for P-11, P-17, and P-19 compared to P-1 and was highest in P-5 and P-6 (Figure 2-F). Western blot data suggest an increased formation and accumulation of intracellular pent and CML during the process of cell subculture.

Role of passaging on osteoclastogenic differentiation

Cells from different passages were treated with RANKL and were checked for multinucleated OC formation by doing TRAP staining. Cells having ≥3 nuclei and cells having ≥10 nuclei were counted as multinucleated OC cells. Cells from P-3 to P-21 were checked by TRAP staining. Cells with ≥3 nuclei were found to be higher till P-7 which decreased significantly afterwards (Figure 3-A). In the case of Cells having ≥10 nuclei, it was higher till P-6 and decreased significantly from P-7 (Figure 3-B). The result from the TRAP staining data reveals the inverse relationship of passage number with multinucleated OC formation suggesting aging of cells has some negative role on OC differentiation (Figure 3-C).

Alteration in F-actin ring size with passaging

The F-actin ring is formed during the terminal differentiation or maturation of OC from the reorganization of a dot-like actin structure named podosomes and is crucial for bone resorption activity by OCs (40, 41). It is a special feature of OC and is formed by cell-cell fusion. Immunofluorescence staining was done to check the size and number of F-actin ring in cells of lower and higher passage. P-5 was taken as the lower passage and P-19 as the higher passage. Without RANKL, both in P-5 and P-19 neither OC nor F-actin ring were formed. However, with the RANKL treatment, the size of the F-actin ring was bigger in P-5 than in P-19 (Figure 4-A). F-actin ring numbers

were also higher in P-5 than in P-19. Reduced size and number of F-actin ring indicates reduced OS due to reduced cell-cell fusion (Figure 4-B). The data supports that OC differentiation was reduced in higher passage cells compared to lower passage cells.

Alteration in Osteoclastogenic gene expression with passaging

Cells from P-5 and P-19 were taken to check osteoclastogenic gene expression at the mRNA level. Maturation marker genes *mTRAP*, *mAtp6v*, *mMMP9*, and *mCtsK* were checked after 5 days of treatment with or without RANKL. All the maturation marker gene expressions except for *mAtp6v* showed an inhibitory trend in P-19 compared to P-5 (Figure 5-A-D). The early maturation marker gene *mNFATc1* expression was checked after 6 hours of treatment with or without RANKL and found to be exerted an inhibitory trend in P-19 compared to P-5 (Figure 5-E). Reduction of gene expression was not significant, but the RT-PCR data supports reduced OS in higher passage compared to lower passage cells.

Correlation study

The correlation study revealed that fluorescent AGEs derived intensity at ex-em 325-385 nm and 370-440 nm have a highly positive correlation with increasing passage number. Pent, CML, and total AGE formation also exerted the same trend. RAGE 34 kDa expression and multinucleated (both ≥3 nuclei and ≥10 nuclei) cell formation exerted a highly negative correlation with increasing passage number (Figure 6).

Multinucleated cell (≥3 nuclei) formation showed a strong negative correlation with intracellular pent and fluorescent AGE formation. Multinucleated giant cell (≥10 nuclei) formation showed a strong positive correlation with RAGE 34 kDa expression. CML formation with pent formation and pent formation with both fluorescent AGE 325-385 and 370-440 formations had a strong positive correlation. RAGE 34 kDa expression had a strong inverse correlation with pent and CML formation. Moreover, fluorescent AGE 325-385 formation showed a strong positive correlation with fluorescent AGE 370-440 formation (Figure 7).

Discussion

For *in vitro* cell culture studies, cell lines have always been a prime concern. RAW 264.7 cells is a monocyte/macrophage cell lineage and is being used for more than 20 years as osteoclast precursors because of its extensive availability; easy cell culturing and sub-culturing technique with homogenous nature; and no such difference in characteristics, functional and developmental processes, gene expression and signaling among isolated *in vivo* formed osteoclasts; primary precursor cell linage derived osteoclast; and osteoclast differentiated from RAW 264.7 cell (42)**.** RAW 264.7 cells have gained popularity over other primary precursor cells like bone marrow macrophage (43), peripheral blood monocytes (44), and splenocytes (45). Passaging is a crucial part of cell culture study and several studies have reported their effects on cell phenotypes, functions, gene expressions, and metabolomics using different cell lines *i.e.,* U87, OECs, HT29 (46), HUVEC (47), MCF7 (48), PC12 (49), D1 (50), MC3T3-E1 (51) including RAW 264.7 cells. Moreover, their effect on the reproducibility of data is also an important issue in cell culture studies. Since there is no report regarding the effect of passaging on intracellular AGE formation and osteoclastogenic differentiation, in this part of the study, my focus was to find out the effect.

Intracellular AGEs cause phenotypic changes in cells; hence, it was hypothesized that continuous passaging may induce intracellular AGE formation or accumulation as the cells are supplemented with a medium containing high glucose.

RAW 264.7 cells were sub-cultured consecutively 21 times and were labeled as P-1 to P-21. Fluorescence AGEs derived intensity at both ex-em 370-440 nm and 325-385 nm, we could see that compared to lower passage numbers, the intensity was higher in higher passage numbers which were minimum in P-5 to P-7 in both cases. The graph did not follow a uniform increase or decrease pattern but rather a frequent up-down trend. This suggests that the glycation reaction between the sugar and cellular protein is continuously producing AGEs which are accumulated intracellularly and excreted by cells as well. However, we could not confirm the excretion because when we tried to use the supernatant for the western blot, the background was high due to the presence of FBS from the media. Western blot performed using the cell lysate revealed and support the same trend of up-down pattern

in the case of pent and CML production. Pent and CML are among well-known AGEs that are associated with the prevalence of osteoporotic bone fracture and inflammation (7, 10, 12, 52–57) and serve as biomarkers for age-related macular degeneration (55) and type-2 diabetic retinopathy (58). Total AGE production and RAGE 38 kDa expression were not altered but RAGE 34 kDa expression was found to be decreased with passaging. RAGE can bind with extracellular HMGB1 apart from AGEs and induce OS and function, hence is an important factor for OS (59). F-actin ring formation was disrupted, and bone resorption was reduced in RAGE-deficient OC (60). Decreased RAGE expression with passaging could be responsible for reduced OS in our study.

Later, we performed TRAP staining to check osteoclast differentiation from RAW 264.7 cells. From the TRAP staining images, it is clearly visible that bigger cell formation decreased with passaging. Cells having ≥3 nuclei and ≥10 nuclei were counted, and the value was used to make a graph and found that giant cell formation decreased significantly after P-7 and P-6 respectively suggesting an association between fluorescent AGEs and osteoclastogenic differentiation with passaging of cells mimicking cellular aging. However, it has been reported that skeletal aging is influenced by human marrow cells and their products by increasing osteoclast differentiation (61) and decreasing osteoblast differentiation (62).

From the above-mentioned data, we found that relatively fluorescent AGE was minimum in P-5 and maximum in P-19, the same trend was observed for pent and CML as well. On the other hand, OS showed an opposite trend in these passages. So, P-5 and P-19 were chosen to study the molecular mechanism. Immunofluorescence was done to check the morphological status of the cells. F-actin structure formation is important for the initiation of bone resorption. It is a dense belt-like ring structure that forms surrounding the resorptive cavity. Immunofluorescent images clearly revealed that the F-actin ring size in P-5 is bigger than in P-19 which suggests that both multinucleated giant OC formation and cell activity are decreasing in higher passages as the ring size is an indicator of cell fusion. *mTRAP*, *mCtsk*, *mMMP-9*, and *mAtp6v* are the genes that are expressed by mature and active OC. All the gene expressions except for mAtp6v were lowered in higher passage suggesting reduced OS. *mNFATc1* is called the master regulator for OS as it induces the expression of OC activating genes (63) which was also decreased in higher passage cells.

All the above-mentioned data suggest an unavoidable role of intracellular AGEs that accumulate with repetitive cell subculturing and their significant effect on the differentiation capacity of RAW 264.7 cells. Hence for our further studies, we chose to use early passages that are from P-3 to P-6 cells. Data from this chapter has been published in the Pubmed indexed journal named international journal of molecular sciences (64).

Chapter 2: Role of extracellular AGEs on osteoclastogenesis

Results

Part 1: Effect of collagen-AGEs on osteoclastogenesis

Fluorescent AGE formation in glycated col-I depends on the glycating agent

Col-I was incubated with different glycating agents for different time periods of different conc. as mentioned in the materials methods section and figures. Col-I glycated by glucose/ fructose/ ribose will be termed hereafter as col-glu, col-fru, and col-rib respectively. Fluorescent AGE yielding fluorescence intensity at ex-em 370-440 nm was checked using a fluorometric plate reader and found that col-rib exerted the highest fluorescence followed by col-fru, col-glu, and heated col (no glycating agent). The data indicate that fluorescent AGE formation was highest in the col-rib group than in other groups. The intensity increased dose and time-dependently except for col-rib 400 mM where the intensity was reduced on day 10 compared to day 7 possibly due to saturation and re-reactivity of ribose with the produced AGEs. Fluorescent AGE formation was almost similar in the col-rib day 1 and col-glu day 10 group, hence, 1-day incubated samples were used to proceed the experiments (Figure 8-A).

Pent was measured in the samples by HPLC analysis. Our focus was to check the effect of pent rich col-AGEs on OS to find out whether increased pent in osteoporotic patient is a cause or not, different conc. of the glycating agent were used to glycate col-I as mentioned in the figures. No pent was formed in the heated col and col-glu group. Col-fru produced a little amount which was not a considerable amount. Col-rib produced the highest amount of pent and at 100 mM conc. of rib, it was maximum. With increasing conc. of rib, pent formation decreased (Figure 8-B). Henceforth, for cell culture study, 200 mM glu and fru, and 100 mM rib were used to prepare col-AGE to treat the cells.

Induction of osteoclastogenic differentiation by Col-AGE without causing cell death

Cells were treated with or without RANKL and 200 µg/mL col-AGE. TRAP activity was performed to check OS. RANKL was taken as a positive control of OS and the data was expressed as % of RANKL. RANKL induced OS significantly compared to MEM. Col-glu, col-fru, and col-rib stimulated RANKL-induced OS significantly compared to RANKL only. Heated col (no glycating agent) did not induce RANKL-induced OS (Figure 9-A).

WST-8 assay was done to check cell viability using the same above-mentioned experimental conditions. In the RANKL group, cell viability seemed to be decreased which is because of entering the cells into the differentiation phase rather than the proliferative phase. None of the col-AGE groups caused the death of the cells (Figure 9-B).

TRAP staining data revealed stimulated RANKL-induce OS with no cell death by col-glu, col-fru, and col-rib as we found from TRAP activity and WST-8 (Figure 9-C).

Effect of col-AGEs on the formation of F-actin ring, RAGE expression, and HMGB1 translocation

Immunofluorescent images clearly show that the size of the F-actin ring was induced by col-AGEs compared to RANKL and heated col. DAPI represents a stained nucleus and phalloidin represents cytoplasm (Figure 10-A).

Zhou et al. reported that HMGB1-RAGE interaction plays an important role in cytoskeletal reorganization for F-actin ring formation and translocation of HMGB1 from the nucleus to cytoplasm stimulates RANKL-induced OS both *in vitro* and *in vivo* (59). So, we checked RAGE expression and HMGB1 colocalization by immunofluorescence assay. HMGB1 colocalized with F-actin ring in all the condition (Figure 10-B) and RAGE expression was not altered by any group (Figure 10-C) which also support the stimulatory role of col-AGE on OS without any dependency on the source of the glycating agent.

Role of col-AGEs on osteoclastogenic gene expression

Different genes are responsible and are expressed in RANKL-induced OS at different phases of the process. *NFATc1* and *c-Fos* are the master regulator and are early osteoclastogenic markers; *TRAF-6* is important to activate downstream signaling pathways; *MITF-E*, *DC-stamp*, and *OC-stamp* are responsible for the fusion of cells to produce multinucleated OC; *Itgav*, *ItgB3*, *ATP6v*, *MMP-9* are responsible for osteoclastogenic activity; *TRAP*, *Ctsk* are the maturation marker, RAGE is the receptor for AGEs. These genes were checked by RT-PCR at different time points from 6 hours to 5 days after the treatment with RANKL and col-AGEs as mentioned in the figures.

mNFATc1 expression was induced by RANKL and col-AGE compared to αMEM, however, only col-rib induced it 1.5-fold more than RANKL only group (Figure 11-A). *mc-Fos* expression was induced in all RANKL-containing groups compared to α MEM, but no col-AGE group stimulated the expression compared to RANKL only, however, a stimulatory trend was observed by col-fru and col-rib (Figure 11-B). *mMITF-E* expression was induced by RANKL-containing groups compared to αMEM, and col-fru significantly stimulated the expression compared to RANKL only (Figure 11-C). *mItgav* expression induced by RANKL-containing groups compared to αMEM and col-AGE group did not exert any effect on the expression compared to RANKL only (Figure 11-D). *mTRAF-6* expression was induced by RANKL-containing groups compared to αMEM till 24 hours and declined significantly thereafter. Col-AGE did not affect the expression compared to RANKL only (Figure 11-E—G). *mDC-stamp* and *mOC-stamp* expression were significantly induced by RANKL-containing groups compared to αMEM. Col-glu and col-fru stimulated *mDC-stamp* expression but none of them altered *mOC-stamp* expression compared to RANKL only (Figure 11-H, I). *mItgB3* expression was not affected by RANKL-containing groups compared to αMEM, however, after 3 days, it exerted a slight incrementor trend (Figure 11-J—L). RANKL-containing groups did not affect RAGE expression compared to αMEM, but col-AGE significantly stimulated RAGE expression after 1 day which became non-significant after 3 days and almost similar after 5 days compared to RANKL only (Figure M—P). *mAtp6v*, *mMMP-9*, *mCtsk*, and *mTRAP* expression were significantly induced by

RANKL-containing groups compared to αMEM and col-AGE did not affect their expression except for *mCtsk* which was significantly inhibited by col-rib (Figure 11-Q—T).

Effect of col-AGEs on Ca^{2+} influx

Ca^{2+} acts as a second messenger and is crucial for OS. RANKL-containing group induced Ca^{2+} influx significantly compared to no RANKL. Col-AGEs significantly stimulated and heated col significantly inhibited Ca^{2+} influx compared to RANKL only (Figure 12).

Activation of different pathways depending on the glycating agent by col-AGEs

The binding of RANKL with its receptor RANK recruits TRAF-6 protein and activates several signaling pathways including NF-κB, AKT, pERK, p38, pJNK. These pathways were checked using an immunofluorescence assay. The data revealed that AKT activation was reduced by col-AGEs (Figure 13-A), p38 activation was reduced by col-rib (Figure 13-B), activation of NF-κB p65 and nuclear translocation was significantly enhanced by col-rib (Figure 13-C), pERK activation and nuclear translocation were induced by col-fru and col-rib but reduced by col-glu (Figure 13-D), pJNK activation was reduced by col-AGEs (Figure 13-E).

Part 2: Effect of collagen-peptide-AGEs on osteoclastogenesis

Fluorescent AGE and intermediates formation in glycated col-pep

From the glycation of collagen-I study, it was revealed that different glycating agents produce variable amounts of pent in glycated col-I but all of them stimulated RANKL-induced TRAP activity to an almost similar extent, we hypothesized that different glycating agents may have some contribution to this occurrence by producing different AGEs. So, we tried to measure the intermediates produced in the samples. The same conditions and the same protocol were used to glycate collagen peptides.

Fluorescent AGE-derived fluorescence intensity at ex-em 370-440 nm by plate reader showed that col-rib yielded the highest intensity followed by col-fru and col-glu time-dependently which is the same as col-AGEs (Figure 14-A). Both 1-day and 10 days incubated samples were used to measure pent by HPLC and found that in 1-day incubated samples, only col-pep-rib produced a significant amount of pent. In 10 days of incubated samples, col-pep-fru produced a considerable amount of pent but way lesser than col-pep-rib (Figure 14-B). Intermediate of AGEs were checked by HPLC in 1-day incubated samples. 3-DG was produced in col-pep-fru in the highest amount followed by col-pep-glu but not in col-pep-rib or only non-heated and heated col-pep (Figure 14-C). MGO was produced in the highest amount in col-pep-rib followed by col-pep-fru but not in col-pep-glu or other conditions (Figure 14-D). GO was produced in all 3 col-pep-AGE but lowest in col-pep-glu and highest in col-pep-rib (Figure 14-E).

Stimulation of RANKL-induced TRAP activity by col-pep-AGEs without any alteration on cell viability

At the same experimental conditions as the col-AGE study, TRAP activity was performed to check the effect of col-pep-AGEs on OS. One day and 10 days incubated samples were used at 200 μg/mL concentration to treat the cells along with RANKL as mentioned in the figures. All the samples exerted a similar incrementor trend in inducing RANKL-induced OS (Figure 15-A). Later two different concentrations of col-pep-rib were taken as mentioned in the figures and found that at 400

μg/mL conc. of 1-day incubated col-pep-rib significantly stimulated RANKL-induced OS (Figure 15-B). Nevertheless, no samples at any concentration caused any cell death (Figure 15-C).

Part 3: Effect of free pentosidine on osteoclastogenesis

Inhibition of RANKL-induced OS and stimulation of cell viability by free pentosidine

Commercially available standard free (not bound to any protein) pent was used at different conc. as mentioned in the figures with the same experimental design. RANKL-containing conditions significantly stimulated OS compared to no RANKL condition. Lower concentrations of pent did not affect TRAP activity until 100 ng/mL from where it started to significantly inhibit RANKL-induced OS (Figure 16-A).

Cell viability assay was done to find out any effect of free pent and found that no conc. caused cell death, rather at higher conc. ($\geq$100 ng/mL) cell viability increased, suggesting a shift from a differential state to a proliferative state (Figure 16-B).

Later, for all the experiments, 200 ng/mL of free pent was used to treat the cells to study the mechanism of inhibition.

TRAP staining data revealed small OC in free pent-treated cells (Figure 16-C) and fewer dead cells (Figure 16-D).

HMGB1 and RAGE expression were checked by immunofluorescence staining and found to be reduced by free pent (Figure 17-A, B)

Reduction of Osteoclastogenic gene expressions by free pentosidine

RT-PCR was done to check the mRNA expression of different genes after treating the cells with or without RANKL and free pent for different time periods as mentioned in the figures. Early marker gene *mNFATc1* and *mc-Fos* expression were not altered by free pent (Figure 18-A, B). *mTRAF-6* expression was slightly reduced by free pent along with fusion gene *mMITF-E* expression (Figure 18-C, D). However, other fusion gene *mDC-stamp* and *mOC-stamp* expressions were not altered by free pent (Figure 18-E, F). Maturation marker gene *mTRAP* and *mCtsk* were not altered but activity marker genes *mMMP-9* and *mAtp6v* were slightly reduced by free pent (Figure 18-G—J). *mRAGE* expression showed a decreasing trend after 5 days of treatment with free pent (Figure 18-K—N).

Alteration of downstream signaling pathways by free pentosidine

To check the effect of free pent on activating different signaling cascades, cells were treated for different time periods as mentioned in the figures. Secondary Ab only was used in some of them to check non-specific binding. The data showed that free pent increased Akt, pERK, p65, and pJNK activation, and on the other hand, p38 activation was reduced (Figure 19-A—E).

Discussion

Excessive generation of aldehydes in the body from reducing sugars, lipids, and alcohol result in the production of excess AGEs and cause glycative stress. Glycative stress has been linked with the early onset of diabetes and its complication and the development of diseases like cataracts (65), osteoporosis (31, 66–70), dementia (71), and skin aging (72). Osteoporosis is a common metabolic disorder characterized by weak bone due to low bone mass and reduced bone quality. Osteoporosis is associated with higher AGEs levels (57) and a higher urinary level of pent is associated with the prevalence of vertebral fracture in diabetic patients with old age which is not dependent on bone mass or other risk factors (73). However, it has not been clearly reported whether the higher pent level is the causal factor or an incidental factor. AGEs cause an abnormal cross-linking in the collagen protein of bone and decrease its elasticity resulting in poor bone strength and quality (7, 74). In this study, we wanted to check the effect of pent-rich col-AGE as col-bound pent (col-pent) and free pent on *in vitro* osteoclastogenic model.

Our data revealed that col-rib produced the highest amount of pent and all 3 groups significantly stimulated RANKL-induced OS. Irrespective of the significant difference in pent amount among 3 groups, there was no difference in the OS stimulation suggesting either no direct role of col-pent on OS or this stimulatory effect is not dose-dependent. However, we tried to find out the molecular mechanism and if there were any differences. F-actin ring size was bigger in all 3 groups suggesting they are inducing fusion which is not dependent on the glycating agent that was used. HMGB1 is a nuclear protein. Upon RANKL stimulation, it translocates into the cytoplasm, co-localizes with the F-actin ring, secretes into extracellular space, and binds with cell surface receptor RAGE of neighboring cells to trigger cell-cell fusion, and plays an important role in OS (59). Immunofluorescence data indicated that HMGB1 translocated to cytoplasm and collocated along the F-actin ring in a similar manner in all col-AGE groups. RAGE expression was similar in all conditions but *mRAGE* expression was found to be stimulated after 24 hours treatment of cells with col-AGEs suggesting possible involvement of RAGE-col-AGE interaction. NFATc1 plays a vital role in inducing and activating several osteoclastic genes (63) and is called the master regulator of OS. NFATc1-deficient embryonic

stem cells were unable to differentiate into OC in response to RANKL (75). *mNFATc1* expression was stimulated by col-rib. *mMITF-E* and *mItgB3* expression were significantly stimulated by col-fru. *mDC-stamp* expression was stimulated by col-fru and col-rib. mRNA expression data suggest that different gene expressions were affected by different glycating agent-derived col-AGE at different points of time to induce OS. The RANKL-RANK signaling stimulates Ca^{2+} signaling by activating phospholipase c(PLC)λ (76) which in turn induces activation of NFATc1 in the nucleus. Ca^{2+} influx was stimulated by col-AGEs derived from glu, fru, and rib compared to the control group RANKL only. The data support the stimulation of RANKL-induced OS by col-AGEs and suggest that Ca^{2+} signaling-induced OS is independent of the glycating agent. RANKL-RANK interaction activates downstream signaling cascades to induce OS. These pathways are multifunctional and are associated with osteoclast survival, proliferation, differentiation, and activity depending on the signal-inducing ligand/ receptor/ protein. Immunofluorescent data showed that AKT and pJNK activation was reduced by col-AGEs. p38 activation was reduced by col-rib. Activation of NF-κB p65 and nuclear translocation was significantly enhanced by col-rib. ERK activation and nuclear translocation were induced by col-fru and col-rib but reduced by col-glu.

From the above-mentioned data, we found different glycating agent-derived col-AGEs are simulating RANKL-induced OS by activating different sets of genes and different signaling pathways, henceforth, we hypothesized the involvement of different AGE precursors. At a molecular level, glycation reaction produces chemical compounds that can be divided into intermediates which are very reactive compared to more stable AGEs. MGO, GO, and 3-DG are dicarbonyl compounds with very high reactivity. Along with pent, their amount of production was different in glycated col-pep samples derived from different glycating agents which could be a reason to activate different signaling pathways. MGO was found to inhibit osteoblast cell differentiation from human bone marrow-derived stromal cells (BMSCs) and inhibit collagen metabolism (77) as well as MGO prominently inhibited RANKL-induced TRAP activity (78). In another study using both animal and RAW 264.7 cells, MGO was found to induce OS by increasing *Ctsk*, *Oscar*, *TRACP5* gene expression and c-JNK pathway activation (79). Kitamura *et. al.,* reported that glyoxal-derived AGEs reduced collagen flexibility and thus bone strength using the goldfish scale (80). 3-DG is responsible for several biological activities

like cellular toxicity, and suppression of cell proliferation (81). Taken together, it can be said that intermediates and AGE production depend on the glycating agent, and their function and mechanism of action depends on the intermediates and AGEs produced.

Lastly, the role of free pent on OS was checked and found to be reduced significantly at higher conc. along with significantly induced cell viability. *TRAF6*, *MITF-E*, *RAGE*, *MMP9*, and *Ctsk* were lowered at the mRNA level supporting reduced OS. AKT, pERK, and pJNK signaling pathways were stimulated, suggesting the possible effect on proliferation supporting induced cell viability. p38 stimulation activates MITF and regulates OS positively (82). Free pent inhibited p38 activation and *mMITF-E* expression suggest a possible pathway of the inhibitory effect on OS. However, more molecular studies are required to confirm that. NFκB p65 activation was also induced by free pent suggesting its possible role in inflammation. In relation to this finding, the pent level in serum correlates positively with C-reactive protein, interleukin-6, and erythrocyte sedimentation which are considered an inflammatory marker in patients with rheumatoid arthritis (83). OS is a complex process regulated by several different pathways. The same signaling pathways could be used to induce or suppress OS based on which ligand-receptor interaction activated that.

Decisively, Pent-rich col-AGEs have no dose-dependent role in inducing *in* vitro RANKL-induced OS suggesting that a small amount of pent can stimulate OS significantly to resorb the col-pent and the inhibitory role of free pent could be a feedback inhibition of col-AGEs-induced OS. However, why pent level increases in osteoporotic diseases are yet to be found out.

Research Limitation

Our study has several limitations such as we could not use pure collagen bound pent as it is not commercially available. That is why, we had to prepare a pent-rich collagen glycation model using different glycating agents of different conc. However, there was a significant difference in the pent amount being produced in the samples, so we can speculate that in the pent-rich sample, the effect was exerted by collagen bound pent. We could not measure the protein conc. of col-AGE as no classical protein assay method was suitable for glycated col-I. We theoretically calculated protein conc. based on the total protein incubated and the final volume recovered after ultrafiltration. Moreover, we were unable to use pathway inhibitors to confirm the pathway activated due to high cell death caused by the inhibitors.

Conclusion

Our results show that both intracellular and extracellular AGEs alter OS *in vitro*. It suggests that the reduction of aldehyde production in the body and prevention of AGE formation by improving a lifestyle that alleviates glycative stress is important for bone metabolism and homeostasis.

Conflicts of Interest

There are no conflicts of interest.

References

1. Odetti, P., Rossi, S., Monacelli, F., Poggi, A., Cirnigliaro, M., Federici, M., and Federici, A. (2005) Advanced glycation end products and bone loss during aging. *Ann. N. Y. Acad. Sci.* **1043**, 710–717
2. Aragno, M., and Mastrocola, R. (2017) Dietary Sugars and Endogenous Formation of Advanced Glycation Endproducts: Emerging Mechanisms of Disease. *Nutr. 2017, Vol. 9, Page 385*. **9**, 385
3. Uribarri, J., Cai, W., Peppa, M., Goodman, S., Ferrucci, L., Striker, G., and Vlassara, H. (2007) Circulating Glycotoxins and Dietary Advanced Glycation Endproducts: Two Links to Inflammatory Response, Oxidative Stress, and Aging. *J. Gerontol. A. Biol. Sci. Med. Sci.* **62**, 427
4. Yagi, M., Isshiki, K., Takabe, W., Ishizaki, K., and Yonei, Y. (2018) Glycative Stress Research. *Glycative Stress Res.* **5**, 119–128
5. Yagi, M., and Yonei, Y. (2018) Glycative stress and anti-aging: 10. Glycative stress and liver disease. *Glycative Stress Res.* **5**, 177–180
6. Yagi, M., and Yonei, Y. (2018) Glycative stress and anti-aging: 9. Glycative stress and schizophrenia. *Glycative Stress Res.* . **5**, 147–150
7. Saito, M., and Marumo, K. (2015) New treatment strategy against osteoporosis: Advanced glycation end products as a factor for poor bone quality. *Glycative Stress Res.* **2**, 1–14
8. Lin, H. K., Hu, Y. C., Yang, L., Altuwaijri, S., Chen, Y. T., Kang, H. Y., and Chang, C. (2003) Suppression Versus Induction of Androgen Receptor Functions by the Phosphatidylinositol 3-Kinase/Akt Pathway in Prostate Cancer LNCaP Cells with Different Passage Numbers. *J. Biol. Chem.* **278**, 50902–50907
9. Sareen, N., Sequiera, G. L., Chaudhary, R., Abu-El-Rub, E., Chowdhury, S. R.,

Sharma, V., Surendran, A., Moudgil, M., Fernyhough, P., Ravandi, A., and Dhingra, S. (2018) Early passaging of mesenchymal stem cells does not instigate significant modifications in their immunological behavior. *Stem Cell Res. Ther.* **9**, 1–11

10. Franke, S., Sommer, M., Rüster, C., Bondeva, T., Marticke, J., Hofmann, G., Hein, G., and Wolf, G. (2009) Advanced glycation end products induce cell cycle arrest and proinflammatory changes in osteoarthritic fibroblast-like synovial cells. *Arthritis Res. Ther.* 10.1186/ar2807
11. Li, C., Chang, Y., Li, Y., Chen, S., Chen, Y., Ye, N., Dai, D., and Sun, Y. (2017) Advanced glycation end products promote the proliferation and migration of primary rat vascular smooth muscle cells via the upregulation of BAG3. *Int. J. Mol. Med.* **39**, 1242–1254
12. Gao, Y., Wake, H., Morioka, Y., Liu, K., Teshigawara, K., Shibuya, M., Zhou, J., Mori, S., Takahashi, H., and Nishibori, M. (2017) Phagocytosis of Advanced Glycation End Products (AGEs) in Macrophages Induces Cell Apoptosis. *Oxid. Med. Cell. Longev.* 10.1155/2017/8419035
13. Haridas, P., McGovern, J. A., Kashyap, A. S., McElwain, D. L. S., and Simpson, M. J. (2016) Standard melanoma-associated markers do not identify the MM127 metastatic melanoma cell line. *Sci. Reports 2016 61*. **6**, 1–6
14. Schneider, E. L., and Mitsui, Y. (1976) The relationship between in vitro cellular aging and in vivo human age. *Proc. Natl. Acad. Sci.* **73**, 3584–3588
15. Passage Number Effects in Cell Lines | ATCC [online] https://www.atcc.org/resources/technical-documents/passage-number-effects-in-cell-lines (Accessed May 12, 2023)
16. Hayflick, L. (1965) The limited in vitro lifetime of human diploid cell strains. *Exp. Cell Res.* **37**, 614–636

17. Foster, S. A., and Galloway, D. A. (1996) Human papillomavirus type 16 E7 alleviates a proliferation block in early passage human mammary epithelial cells. *Oncogene*. **12**, 1773–1779

18. Rubin, H. (1997) Cell aging in vivo and in vitro. *Mech. Ageing Dev.* 10.1016/s0047-6374(97)00067-5

19. Bonab, M. M., Alimoghaddam, K., Talebian, F., Ghaffari, S. H., Ghavamzadeh, A., and Nikbin, B. (2006) Aging of mesenchymal stem cell in vitro. *BMC Cell Biol.* **7**, 1–7

20. Collin-Osdoby, P., and Osdoby, P. (2012) RANKL-Mediated Osteoclast Formation from Murine RAW 264.7 cells BT - Bone Research Protocols. in *Bone Research Protocols* (Helfrich, M. H., and Ralston, S. H. eds), pp. 187–202, Humana Press, Totowa, NJ, **816**, 187–202

21. Mamun-Or-Rashid A. N. M., Takabe Wakako, Yagi Masayuki, and Yonei Yoshikazu (2017) RANKL regulates RAW264.7 cell osteoclastogenesis in a manner independent of M-CSF, dependent on FBS, media content and cell density. *Glycative Stress Res.* **4**, 040–052

22. Mamun-Or-Rashid, A. N. M., Takabe, W., Yagi, M., and Yonei, Y. (2019) Melatonin and astareal modulate RANKL-induced TRAP activity in RAW264.7 cells in opposite fashion. *Glycative Stress Res.* **6**, 135–141

23. Mamun-Or-Rashid, A. N. M., Takabe, W., Yagi, M., and Yonei, Y. (2017) Glycated-proteins modulate RANKL-induced osteoclastogenesis in RAW264.7 cells. *Glycative Stress Res.* **4**, 232–239

24. Mamun-Or-Rashid, A. N. M., Takabe, W., Yagi, M., and Yonei, Y. (2017) Glycated-HSA inhibits osteoclastogenesis in RAW264.7 cells depending on the glycating agents via downregulating RANKL-signaling. *Glycative Stress Res.* **4**, 217–231

25. Sato, K., Yagi, M., Umehara, H., and Yonei, Y. (2014) Establishment of a model for

evaluating tumor necrosis factor-α production by cultured RAW264.7 in response to glycation stress. *Glycative Stress Res.* **1**, 1–7

26. Donato, R. (2007) RAGE: A Single Receptor for Several Ligands and Different Cellular Responses: The Case of Certain S100 Proteins. *Curr. Mol. Med.* **7**, 711–724
27. Raggatt, L. J., and Partridge, N. C. (2010) Cellular and molecular mechanisms of bone remodeling. *J. Biol. Chem.* **285**, 25103–25108
28. Young, M. F., Kerr, J. M., Ibaraki, K., Heegaard, A. M., and Robey, P. G. (1992) Structure, expression, and regulation of the major noncollagenous matrix proteins of bone. *Clin. Orthop. Relat. Res.* 10.1097/00003086-199208000-00042
29. Osteoporosis prevention, diagnosis, and therapy (2001) *JAMA*. **285**, 785–795
30. Reznikov, N., Shahar, R., and Weiner, S. (2014) Bone hierarchical structure in three dimensions. *Acta Biomater.* **10**, 3815–3826
31. Saito, M., and Marumo, K. (2010) Collagen cross-links as a determinant of bone quality: A possible explanation for bone fragility in aging, osteoporosis, and diabetes mellitus. *Osteoporos. Int.* **21**, 195–214
32. Saito, M., Kida, Y., Nishizawa, T., Arakawa, S., Okabe, H., Seki, A., and Marumo, K. (2015) Effects of 18-month treatment with bazedoxifene on enzymatic immature and mature cross-links and non-enzymatic advanced glycation end products, mineralization, and trabecular microarchitecture of vertebra in ovariectomized monkeys. *Bone*. **81**, 573–580
33. Yoshihara, K., Nakamura, K., Kanai, M., Nagayama, Y., Takahashi, S., Saito, N., and Nagata, M. (1998) Determination of urinary and serum pentosidine and its application to elder patients. *Biol. Pharm. Bull.* **21**, 1005–1008
34. Tamaki, J., Kouda, K., Fujita, Y., Iki, M., Yura, A., Miura, M., Sato, Y., Okamoto, N., and Kurumatani, N. (2018) Ratio of endogenous secretory receptor for advanced

glycation end products to pentosidine predicts fractures in men. *J. Clin. Endocrinol. Metab.* **103**, 85–94

35. Tanaka, S., Kuroda, T., Saito, M., and Shiraki, M. (2011) Urinary pentosidine improves risk classification using fracture risk assessment tools for postmenopausal women. *J. Bone Miner. Res.* **26**, 2778–2784

36. Mitome, J., Yamamoto, H., Saito, M., Yokoyama, K., Marumo, K., and Hosoya, T. (2011) Nonenzymatic cross-linking pentosidine increase in bone collagen and are associated with disorders of bone mineralization in dialysis patients. *Calcif. Tissue Int.* **88**, 521–529

37. Sanguineti, R., Storace, D., Monacelli, F., Federici, A., and Odetti, P. (2008) Pentosidine effects on human osteoblasts in vitro. *Ann. N. Y. Acad. Sci.* **1126**, 166–172

38. Hori, M., Yagi, M., Nomoto, K., Ichijo, R., Shimode, A., Kitano, T., and Yonei, Y. (2012) Experimental models for advanced glycation end product formation using albumin, collagen, elastin, keratin and proteoglycan. *Anti-Aging Med.* **9**, 125–134

39. Sato, K., Takabe, W., Yagi, M., Yonei, Y., Takabe, W., and Yonei, Y. (2015) Inhibitory effect of plant extract on tumor necrosis factor-α formation from carboxymethyllysine stimulated macrophages Koichi. *Glycative Stress Res.* **2**, 191–196

40. Jurdic, P., Saltel, F., Chabadel, A., and Destaing, O. (2006) Podosome and sealing zone: Specificity of the osteoclast model. *Eur. J. Cell Biol.* **85**, 195–202

41. Boyce, B. F., Yoneda, T., Lowe, C., Soriano, P., and Mundy, G. R. (1992) Requirement of pp60c-src expression for osteoclasts to form ruffled borders and resorb bone in mice. *J. Clin. Invest.* **90**, 1622–1627

42. Collin-Osdoby, P., and Osdoby, P. (2012) RANKL-mediated osteoclast formation from murine RAW 264.7 cells. *Methods Mol. Biol.* **816**, 187–202

43. Povolny, B., and MY, L. (1993) The role of recombinant human M-CSF, IL-3, GM-CSF and calcitriol in clonal development of osteoclast precursors in primate bone marrow - PubMed. *Exp. Hematol.* **21**, 532–537

44. Orcel, P., Bielakoff, J., and De Vernejoul, M. C. (1990) Formation of multinucleated cells with osteoclast precursor features in human cord monocytes cultures. *Anat. Rec.* **226**, 1–9

45. Reinke, D. C., Kogawa, M., Barratt, K. R., Morris, H. A., Anderson, P. H., and Atkins, G. J. (2016) Evidence for altered osteoclastogenesis in splenocyte cultures from Cyp27b1 knockout mice. *J. Steroid Biochem. Mol. Biol.* **164**, 353–360

46. Cao, J., Wu, X., Qin, X.-M., and Li, Z. (2021) Uncovering the Effect of Passage Number on HT29 Cell Line Based on the Cell Metabolomic Approach. *J. Proteome Res.* **20**, 1582−1590

47. Chennazhy, K. P., and Krishnan, L. K. (2005) Effect of passage number and matrix characteristics on differentiation of endothelial cells cultured for tissue engineering. *Biomaterials*. 10.1016/j.biomaterials.2005.02.024

48. Hamadneh, L., Al-Majawleh, M., Jarrar, Y., Shraim, S., Hasan, M., and Abu-Irmaileh, B. (2018) Culturing conditions highly affect DNA methylation and gene expression levels in MCF7 breast cancer cell line. *Vitr. Cell. Dev. Biol. - Anim.* **54**, 331–334

49. Kinarivala, N., Shah, K., Abbruscato, T. J., and Trippier, P. C. (2016) Passage Variation of PC12 Cells Results in Inconsistent Susceptibility to Externally Induced Apoptosis. *ACS Chem. Neurosci.* **8**, 82–88

50. Kwist, K., Bridges, W. C., and Burg, K. J. L. (2016) The effect of cell passage number on osteogenic and adipogenic characteristics of D1 cells. *Cytotechnology*. **68**, 1661–7

51. Peterson, W. J., Tachiki, K. H., and Yamaguchi, D. T. (2004) Serial passage of MC3T3-E1 cells down-regulates proliferation during osteogenesis in vitro. *Cell Prolif.*

37, 325–336

52. Nakano, M., Nakamura, Y., Suzuki, T., Miyazaki, A., Takahashi, J., Saito, M., and Shiraki, M. (2020) Pentosidine and carboxymethyl-lysine associate differently with prevalent osteoporotic vertebral fracture and various bone markers. *Sci. Rep.* **10**, 22090
53. Sanguineti, R., Puddu, A., Mach, F., Montecucco, F., and Viviani, G. L. (2014) Advanced glycation end products play adverse proinflammatory activities in osteoporosis. *Mediators Inflamm.* 10.1155/2014/975872
54. Rabbani, N., Xue, M., and Thornalley, P. J. (2021) Dicarbonyl stress, protein glycation and the unfolded protein response. *Glycoconj. J.* **38**, 331–340
55. Ni, J., Yuan, X., Gu, J., Yue, X., Gu, X., Nagaraj, R. H., and Crabb, J. W. (2009) Plasma protein pentosidine and carboxymethyllysine, biomarkers for age-related macular degeneration. *Mol. Cell. Proteomics*. **8**, 1921–1933
56. Barzilay, J. I., Bůžková, P., Zieman, S. J., Kizer, J. R., Djoussé, L., Ix, J. H., Tracy, R. P., Siscovick, D. S., Cauley, J. A., Mukamal, K. J., and Barzilay, J. (2014) Circulating levels of carboxy-methyl-lysine (CML) are associated with hip fracture risk: the cardiovascular health study HHS Public Access. *J Bone Min. Res.* . **29**, 1061–1066
57. Hein, G., Wiegand, R., Lehmann, G., Stein, G., and Franke, S. (2003) Advanced glycation end-products pentosidine and N -carboxymethyllysine are elevated in serum of patients with osteoporosis. *Rheumatology*. **42**, 1242–1246
58. Ghanem, A. A., Elewa, A., and Arafa, L. F. (2011) Pentosidine and N-carboxymethyl-lysine: biomarkers for type 2 diabetic retinopathy. *Eur. J. Ophthalmol.* **21**, 48–54
59. Zhou, Z., Han, J.-Y., Xi, C.-X., Xie, J.-X., Feng, X., Wang, C.-Y., Mei, L., and Xiong, W.-C. (2008) HMGB1 Regulates RANKL-Induced Osteoclastogenesis in a Manner Dependent on RAGE. *J. Bone Miner. Res.* **23**, 1084–1096
60. Zhou, Z., Immel, D., Xi, C. X., Bierhaus, A., Feng, X., Mei, L., Nawroth, P., Stern, D.

M., and Xiong, W. C. (2006) Regulation of osteoclast function and bone mass by RAGE. *J. Exp. Med.* **203**, 1067–1080

61. Chung, P. L., Zhou, S., Eslami, B., Shen, L., Leboff, M. S., and Glowacki, J. (2014) Effect of age on regulation of human osteoclast differentiation. *J. Cell. Biochem.* **115**, 1412–1419

62. Zhou, S., Greenberger, J. S., Epperly, M. W., Goff, J. P., Adler, C., Leboff, M. S., and Glowacki, J. (2008) Age-related intrinsic changes in human bone-marrow-derived mesenchymal stem cells and their differentiation to osteoblasts. *Aging Cell*. **7**, 335–343

63. Song, I., Kim, J. H., Kim, K., Jin, H. M., Youn, B. U., and Kim, N. (2009) Regulatory mechanism of NFATc1 in RANKL-induced osteoclast activation. *FEBS Lett.* **583**, 2435–2440

64. Lucy, T. T., Mamun-Or-rashid, A. N. M., Yagi, M., and Yonei, Y. (2022) Serial Passaging of RAW 264.7 Cells Modulates Intracellular AGE Formation and Downregulates RANKL-Induced In Vitro Osteoclastogenesis. *Int. J. Mol. Sci.* 10.3390/IJMS23042371

65. Uemura, T., Takeshita, S., and Yamada, M. (2017) The effectiveness of the peel extract of water chestnut (Trapa bispinosa Roxb.) in an α-crystallin glycation model with glyoxal. *Glycative Stress Res.* **4**, 104–108

66. Schwartz, A. V. (2003) Diabetes Mellitus: Does it Affect Bone? *Calcif. Tissue Int.* **73**, 515–519

67. Yamaguchi, T. (2010) Bone fragility in type 2 diabetes mellitus. *World J. Orthop.* **1**, 3–9

68. Karim, L., and Bouxsein, M. L. (2016) Effect of type 2 diabetes-related non-enzymatic glycation on bone biomechanical properties. *Bone*. **82**, 21–27

69. Hough, F. S., Pierroz, D. D., Cooper, C., and Ferrari, S. L. (2016) Mechanisms and

evaluation of bone fragility in type 1 diabetes mellitus. *Eur. J. Endocrinol.* 10.1530/EJE-15-0820

70. Kanazawa, I., and Sugimoto, T. (2017) The mechanism of bone fragility in diabetes mellitus. *Glycative Stress Res.* **4**, 266–274

71. Baric, N. (2014) Role of advanced glycation end products in Alzheimer's disease. *Glycative Stress Res.* **1**, 068–083

72. Yonei, Y., Takabe, W., and Yagi, M. (2015) Photoaging and Glycation of Elastin: Effect on Skin. *Glycative Stress Res.* **2**, 182–190

73. Schwartz, A. V., Garnero, P., Hillier, T. A., Sellmeyer, D. E., Strotmeyer, E. S., Feingold, K. R., Resnick, H. E., Tylavsky, F. A., Black, D. M., Cummings, S. R., Harris, T. B., and Bauer, D. C. (2009) Pentosidine and Increased Fracture Risk in Older Adults with Type 2 Diabetes. *J. Clin. Endocrinol. Metab.* **94**, 2380–2386

74. Sroga, G. E., Siddula, A., and Vashishth, D. (2015) Glycation of Human Cortical and Cancellous Bone Captures Differences in the Formation of Maillard Reaction Products between Glucose and Ribose. *PLoS One*. **10**, e0117240

75. Takayanagi, H., Kim, S., Koga, T., Nishina, H., Isshiki, M., Yoshida, H., Saiura, A., Isobe, M., Yokochi, T., Inoue, J. I., Wagner, E. F., Mak, T. W., Kodama, T., and Taniguchi, T. (2002) Induction and activation of the transcription factor NFATc1 (NFAT2) integrate RANKL signaling in terminal differentiation of osteoclasts. *Dev. Cell*. **3**, 889–901

76. Lieben, L., and Carmeliet, G. (2012) The involvement of TRP channels in bone homeostasis. *Front. Endocrinol. (Lausanne).* **3**, 99

77. Waqas, K., Muller, M., Koedam, M., el Kadi, Y., Zillikens, M. C., and van der Eerden, B. C. J. (2022) Methylglyoxal – an advanced glycation end products (AGEs) precursor – Inhibits differentiation of human MSC-derived osteoblasts in vitro independently of

receptor for AGEs (RAGE). *Bone*. **164**, 116526

78. Suh, K. S., Chon, S., Jung, W. W., and Choi, E. M. (2018) Effects of methylglyoxal on RANKL-induced osteoclast differentiation in RAW264.7 cells. *Chem. Biol. Interact.* **296**, 18–25

79. Lee, K. M., Lee, C. Y., Zhang, G., Lyu, A., and Yue, K. K. M. (2019) Methylglyoxal activates osteoclasts through JNK pathway leading to osteoporosis. *Chem. Biol. Interact.* **308**, 147–154

80. Kitamura, K. ichiro, Hirayama, J., Tabuchi, Y., Minami, T., Matsubara, H., Hattori, A., and Suzuki, N. (2021) Glyoxal-induced formation of advanced glycation end-products in type 1 collagen decreases both its strength and flexibility in vitro. *J. Diabetes Investig.* **12**, 1555–1559

81. Niwa, T. (1999) 3-Deoxyglucosone: Metabolism, analysis, biological activity, and clinical implication. *J. Chromatogr. B Biomed. Sci. Appl.* **731**, 23–36

82. Hotokezaka, H., Sakai, E., Kanaoka, K., Saito, K., Matsuo, K. -i., Kitaura, H., Yoshida, N., and Nakayama, K. (2002) U0126 and PD98059, specific inhibitors of MEK, accelerate differentiation of RAW264.7 cells into osteoclast-like cells. *J. Biol. Chem.* **277**, 47366–47372

83. Tilg, H., Wilmer, A., Vogel, W., Herold, M., Nölchen, B., Judmaier, G., and Huber, C. (1992) Serum levels of cytokines in chronic liver diseases. *Gastroenterology*. **103**, 264–274

Figures

A)

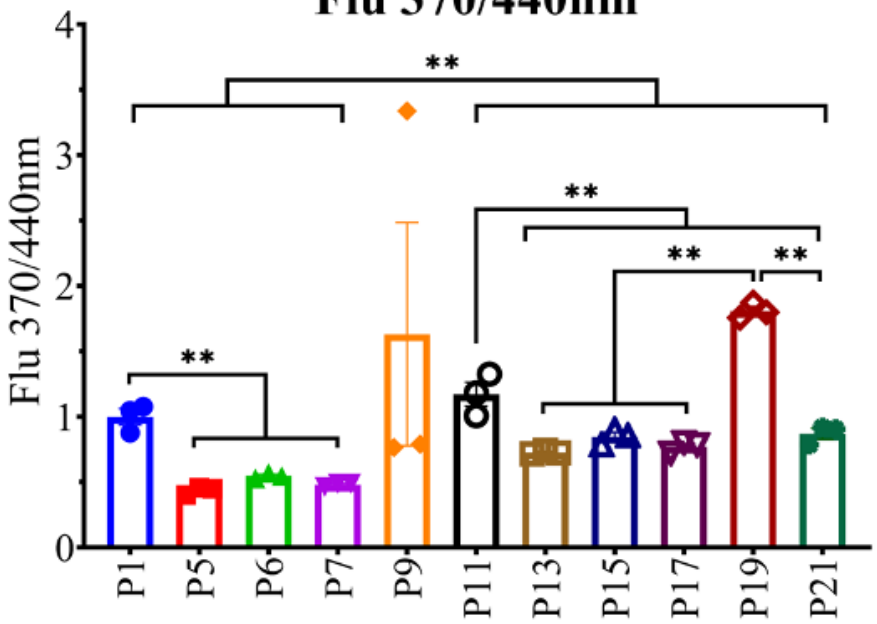
Flu 370/440nm
Flu 370/440nm
4
3
2
1
0
**
**
**
**
**
P1
P5
P6
P7
P9
P11
P13
P15
P17
P19
P21

B)

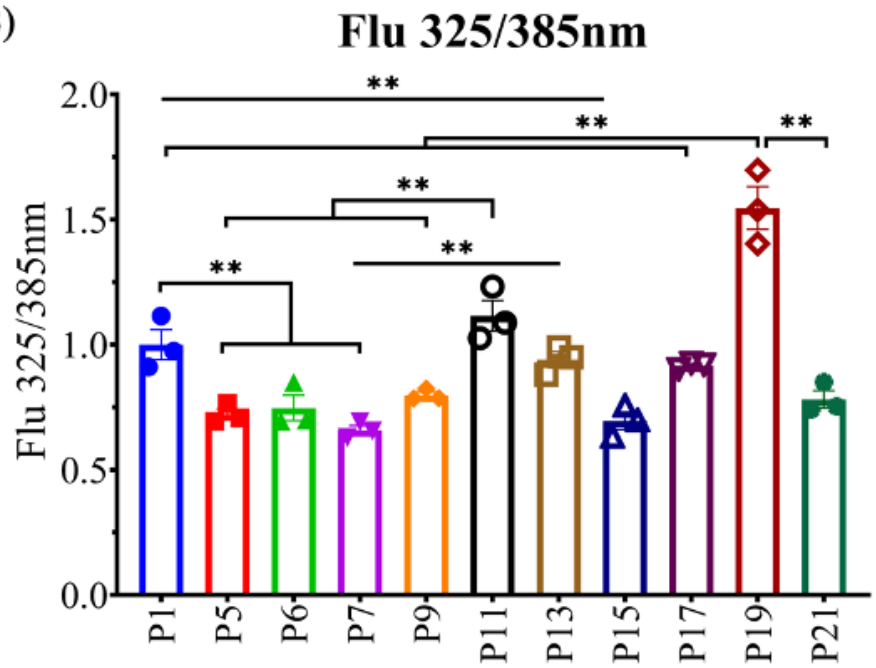
Flu 325/385nm
Flu 325/385nm
2.0
1.5
1.0
0.5
0.0
**
**
**
**
**
P1
P5
P6
P7
P9
P11
P13
P15
P17
P19
P21

C)

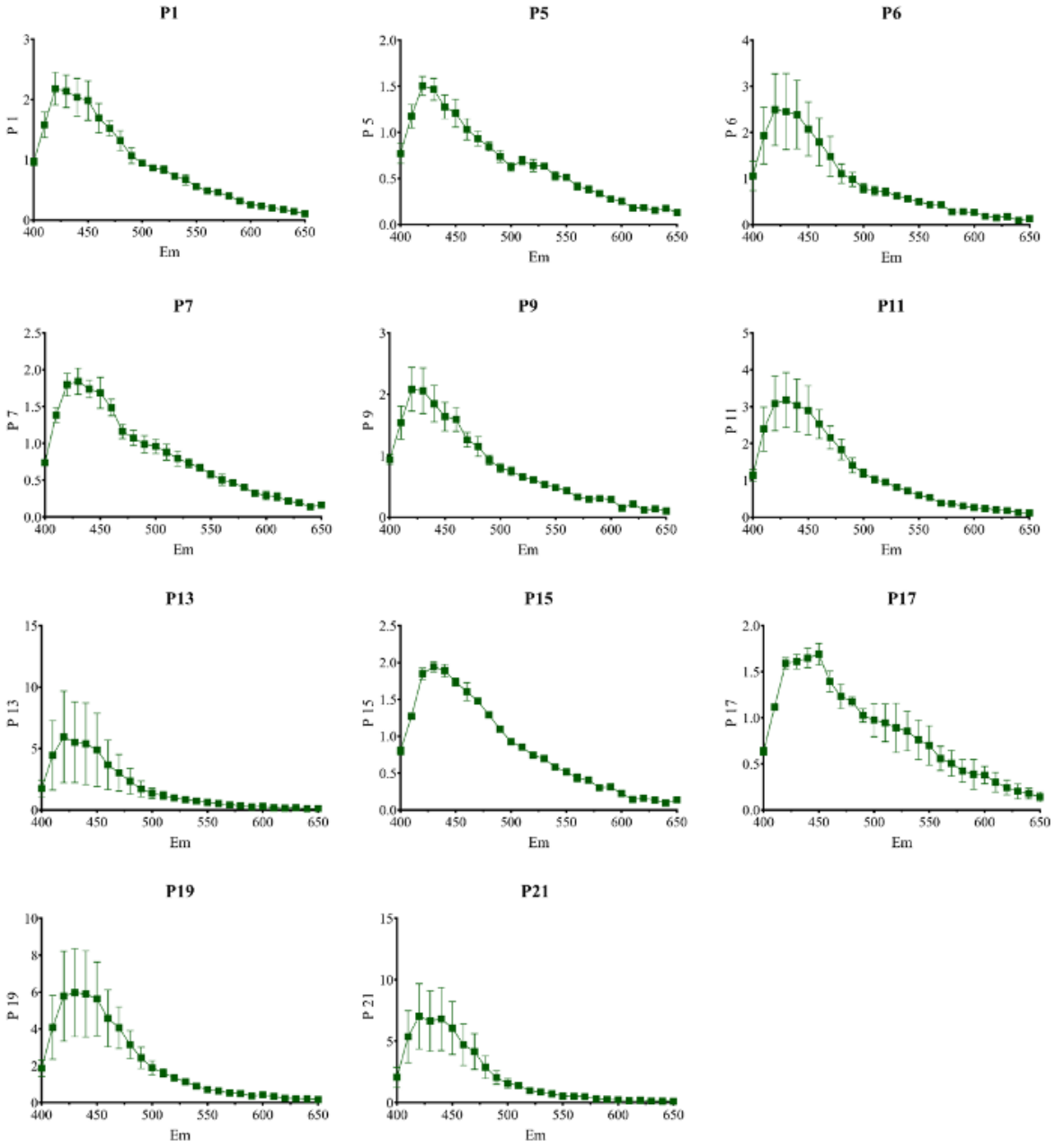
P1
P 1
Em
P5
P 5
Em
P6
P 6
Em
P7
P 7
Em
P9
P 9
Em
P11
P 11
Em
P13
P 13
Em
P15
P 15
Em
P17
P 17
Em
P19
P 19
Em
P21
P 21
Em

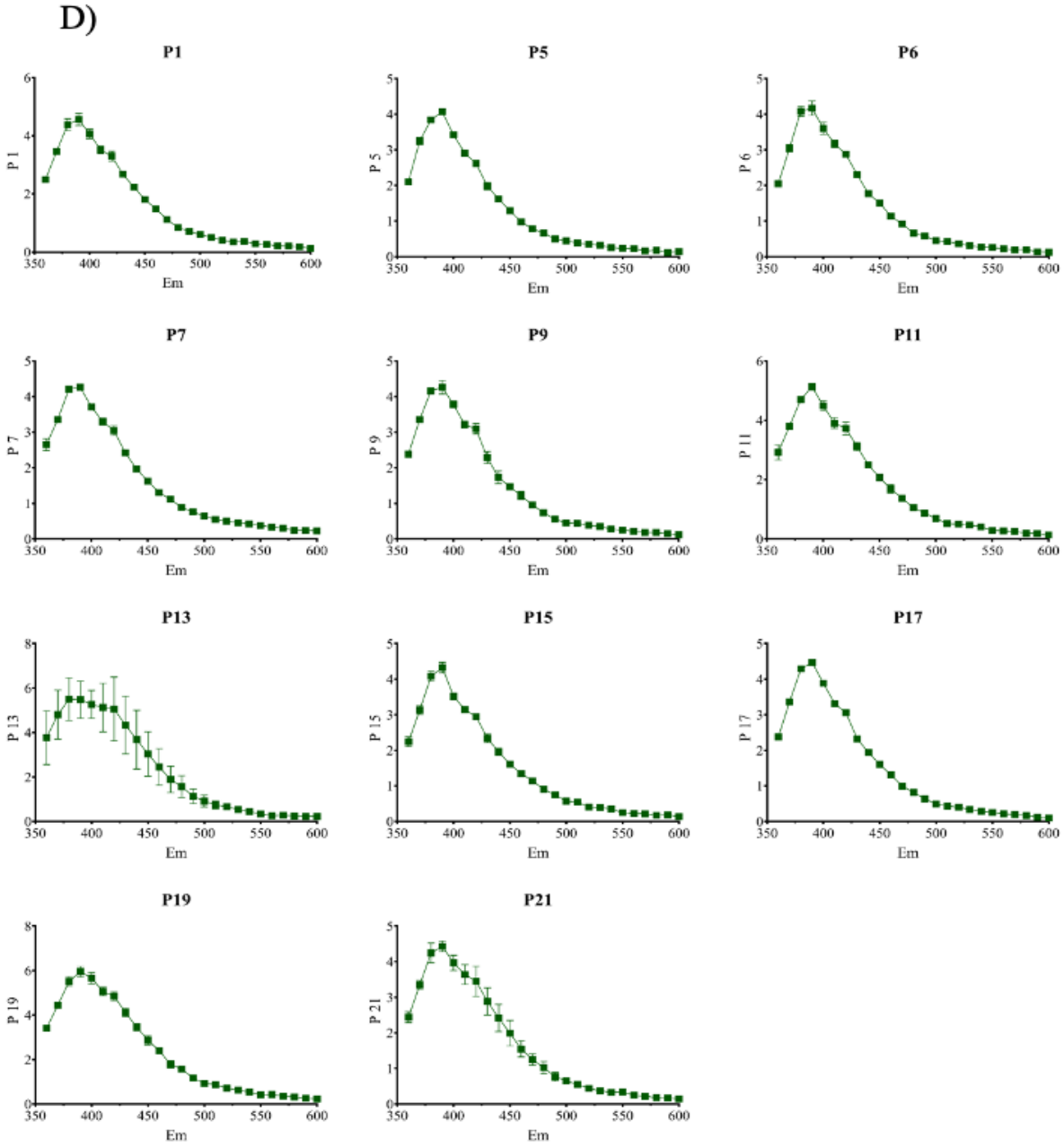

Figure 1: Intracellular fluorescent AGE formation in different passages. (A) fluorescent intensity at ex-em 370-440 nm, (B) fluorescent intensity at ex-em 325-385 nm, (C) fluorescence scanning at ex 370/em 400-650 nm (D) fluorescence scanning at ex 325/em 360-600 nm. All data are shown as means ± SEM, n=3. **p<0.01 by the Tukey-Kramer test. These data have been published in (64).

A)

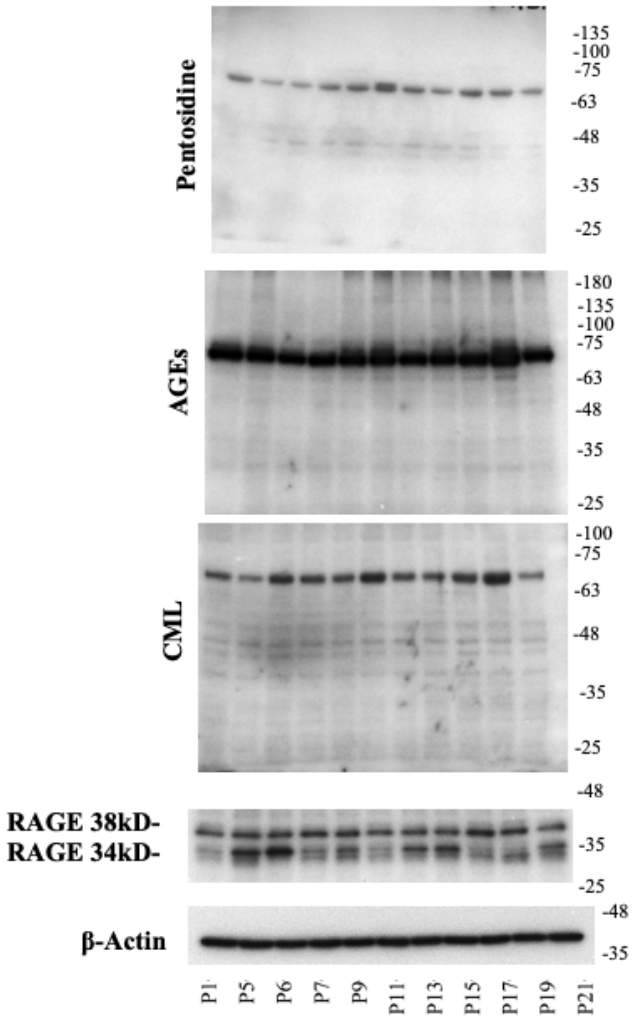
Pentosidine
-135
-100
-75
-63
-48
-35
-25
AGEs
-180
-135
-100
-75
-63
-48
-35
-25
CML
-100
-75
-63
-48
-35
-25
RAGE 38kD-
RAGE 34kD-
-48
-35
-25
β-Actin
-48
-35
P1
P5
P6
P7
P9
P11
P13
P15
P17
P19
P21

B)

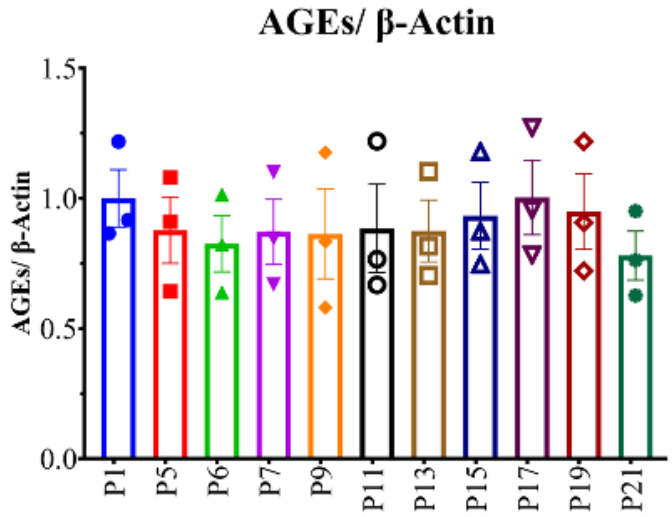
AGEs/ β-Actin
AGEs/ β-Actin
1.5
1.0
0.5
0.0
P1
P5
P6
P7
P9
P11
P13
P15
P17
P19
P21

C)

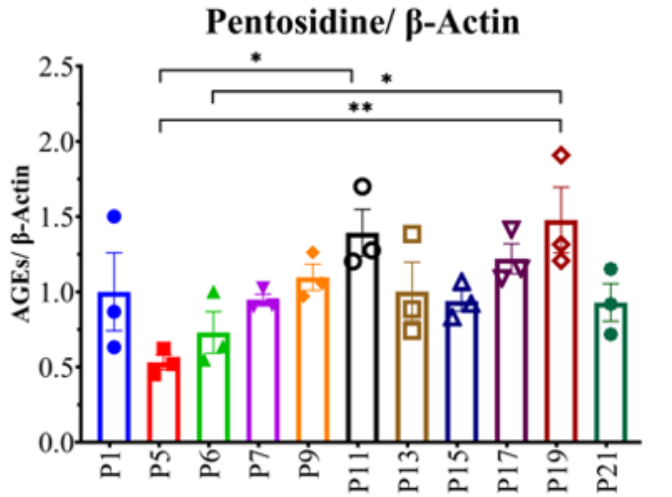
Pentosidine/ β-Actin
AGEs/ β-Actin
2.5
2.0
1.5
1.0
0.5
0.0
*
*
**
P1
P5
P6
P7
P9
P11
P13
P15
P17
P19
P21

D)

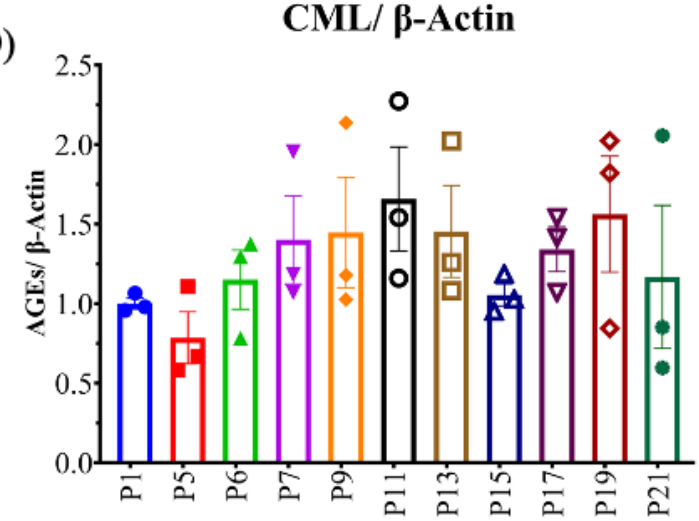
CML/ β-Actin
AGEs/ β-Actin
2.5
2.0
1.5
1.0
0.5
0.0
P1
P5
P6
P7
P9
P11
P13
P15
P17
P19
P21

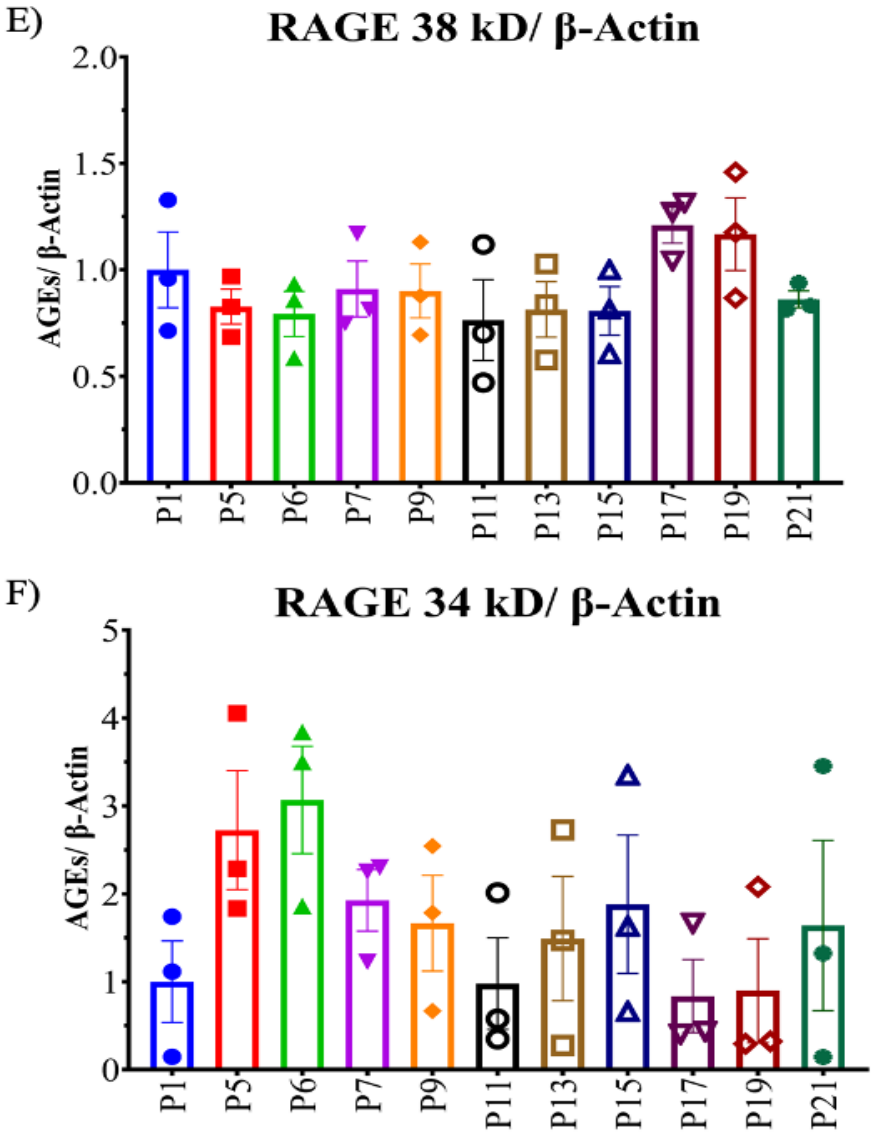

Figure 2: Intracellular AGE formation in different passages. (A) Western blot images for pentosidine, CML, AGEs, RAGE protein expression, and (B-F) band intensity were analyzed by ImageJ. Values are means±SEM, n=3 by Tukey-Kramer test, *p<0.05, ** p<0.01. These data have been published in (64).

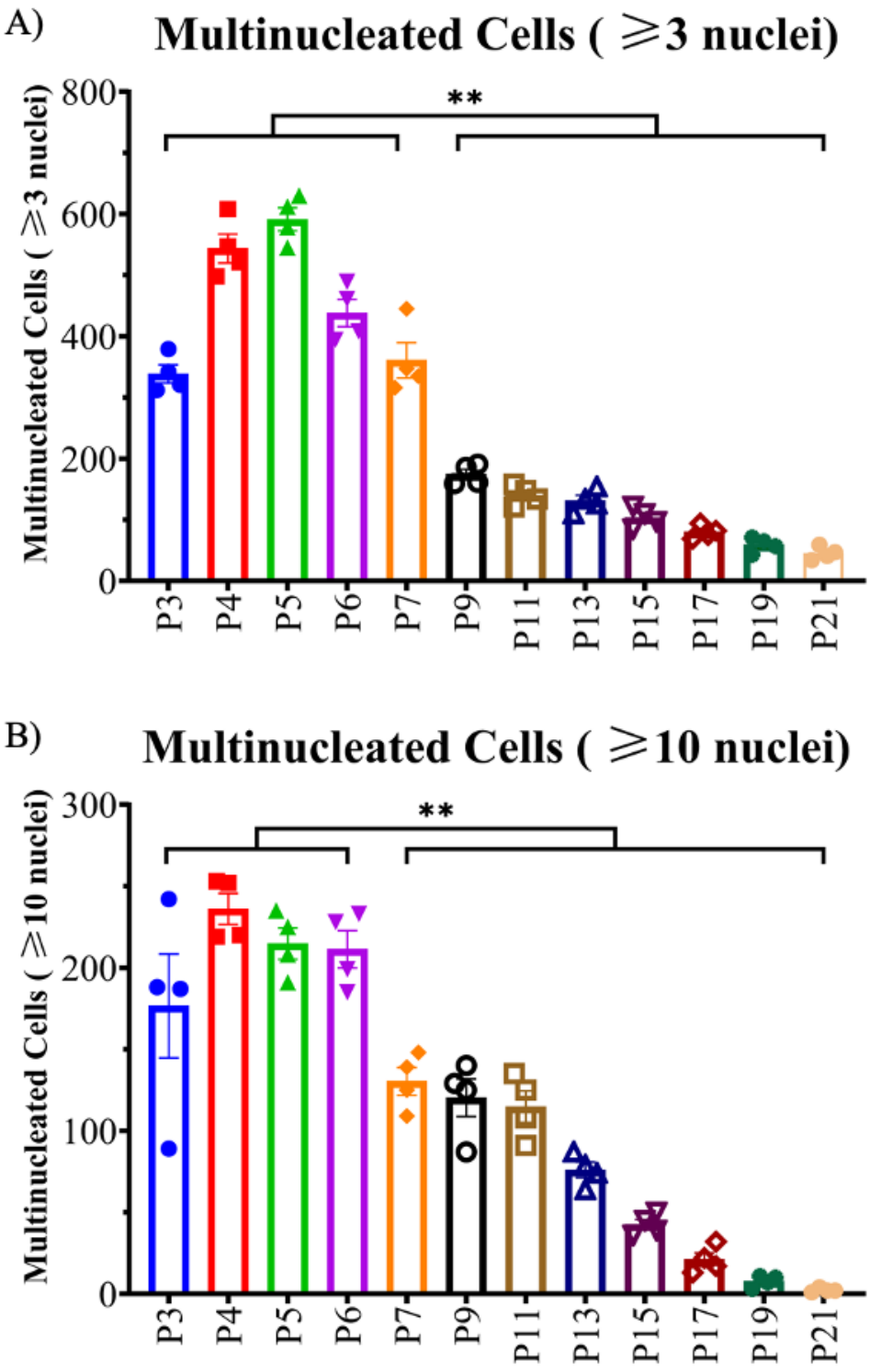
A)
Multinucleated Cells (⩾3 nuclei)
Multinucleated Cells (⩾3 nuclei)
800
600
400
200
0
**
P3
P4
P5
P6
P7
P9
P11
P13
P15
P17
P19
P21
B)
Multinucleated Cells (⩾10 nuclei)
Multinucleated Cells (⩾10 nuclei)
300
200
100
0
**
P3
P4
P5
P6
P7
P9
P11
P13
P15
P17
P19
P21

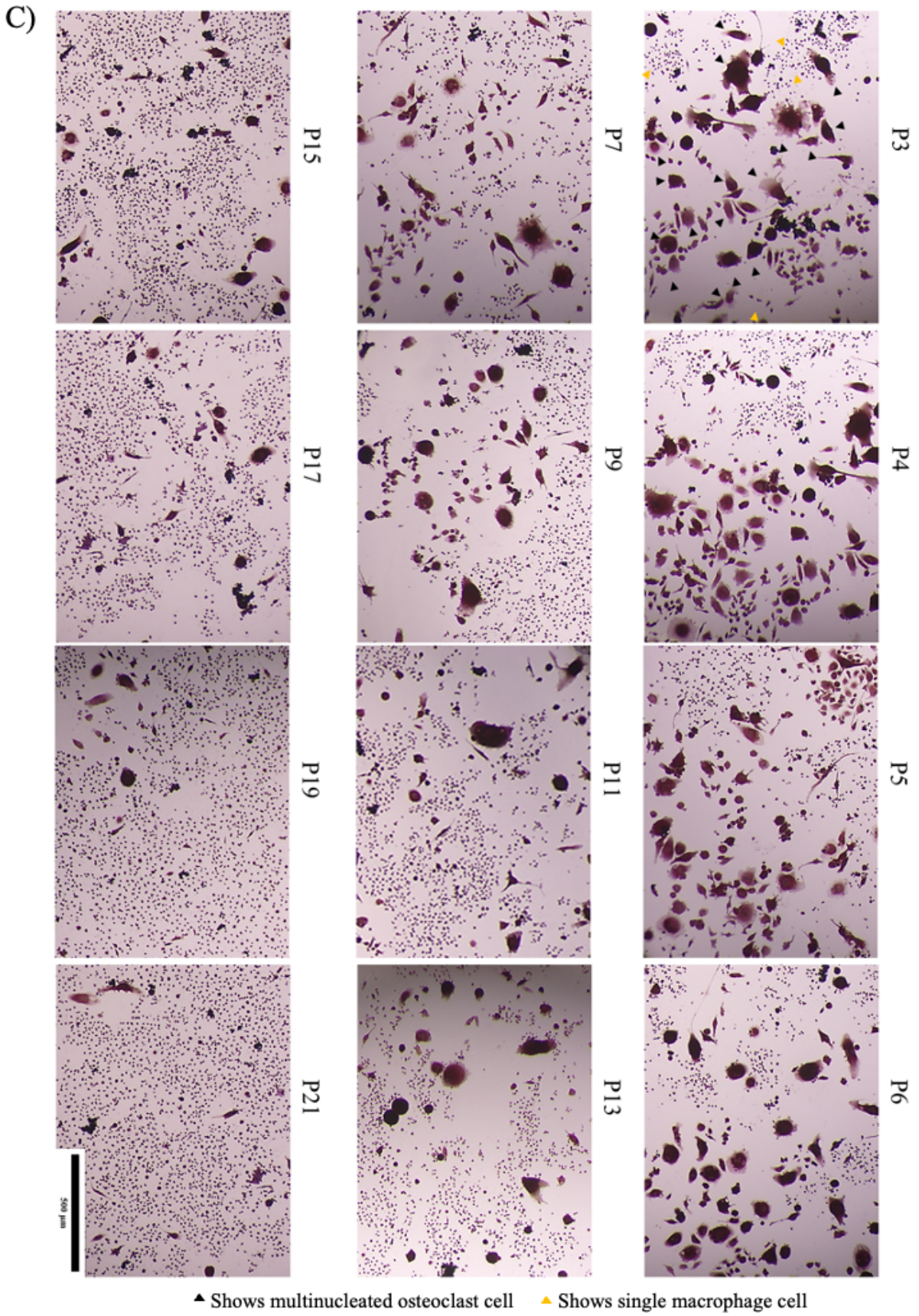

Figure 3:Multinucleated TRAP-positive cell formation in different passages. These data have been published in (64).

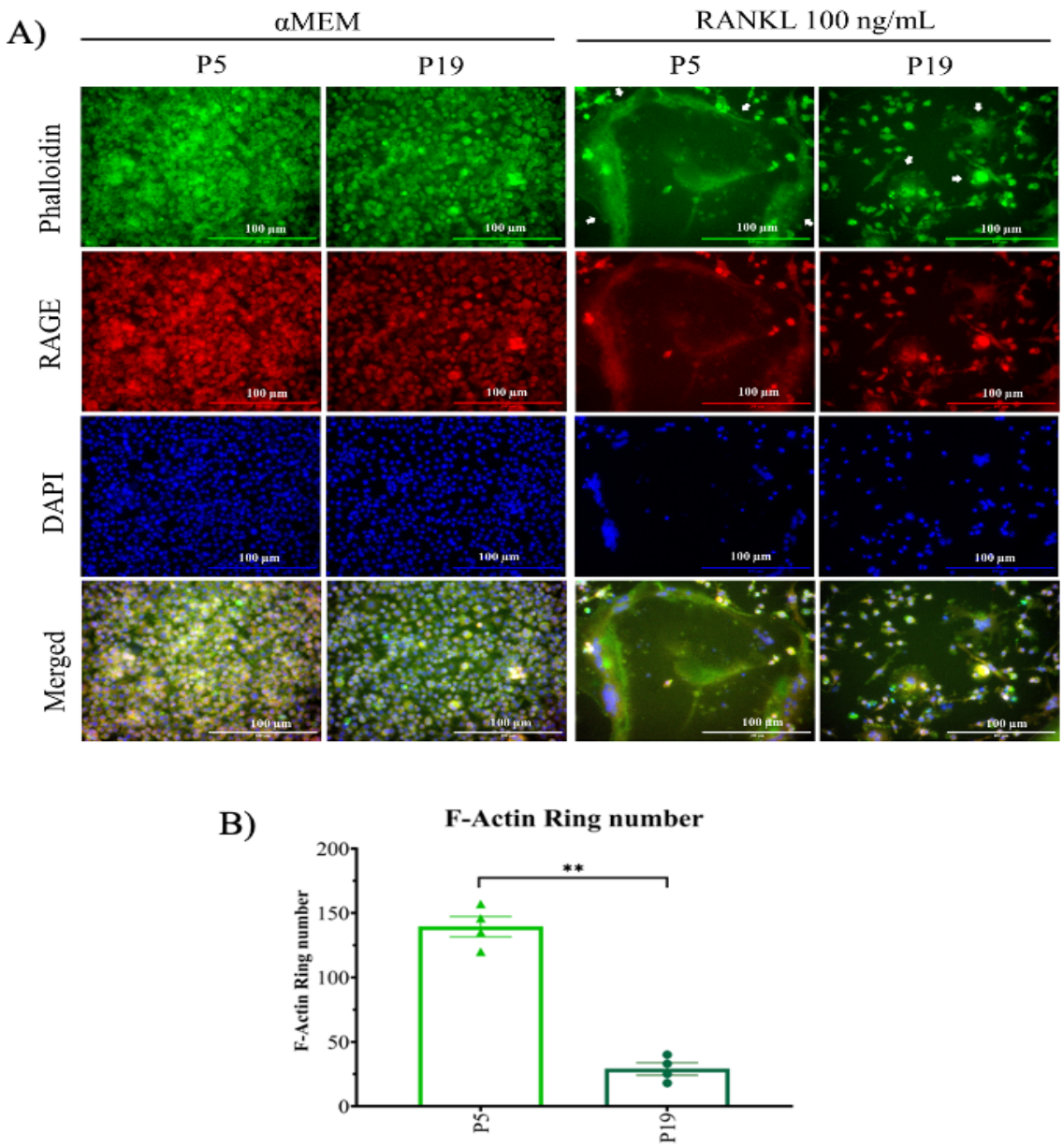

Figure 4: F-actin ring formation. Phalloidin to stain cytoplasm (green), antibody against RAGE (red), and DAPI to stain the nucleus (blue) were used. The scale bar represents 100 µm. Values are means±SEM, ** $p<0.01$. These data have been published in (64).

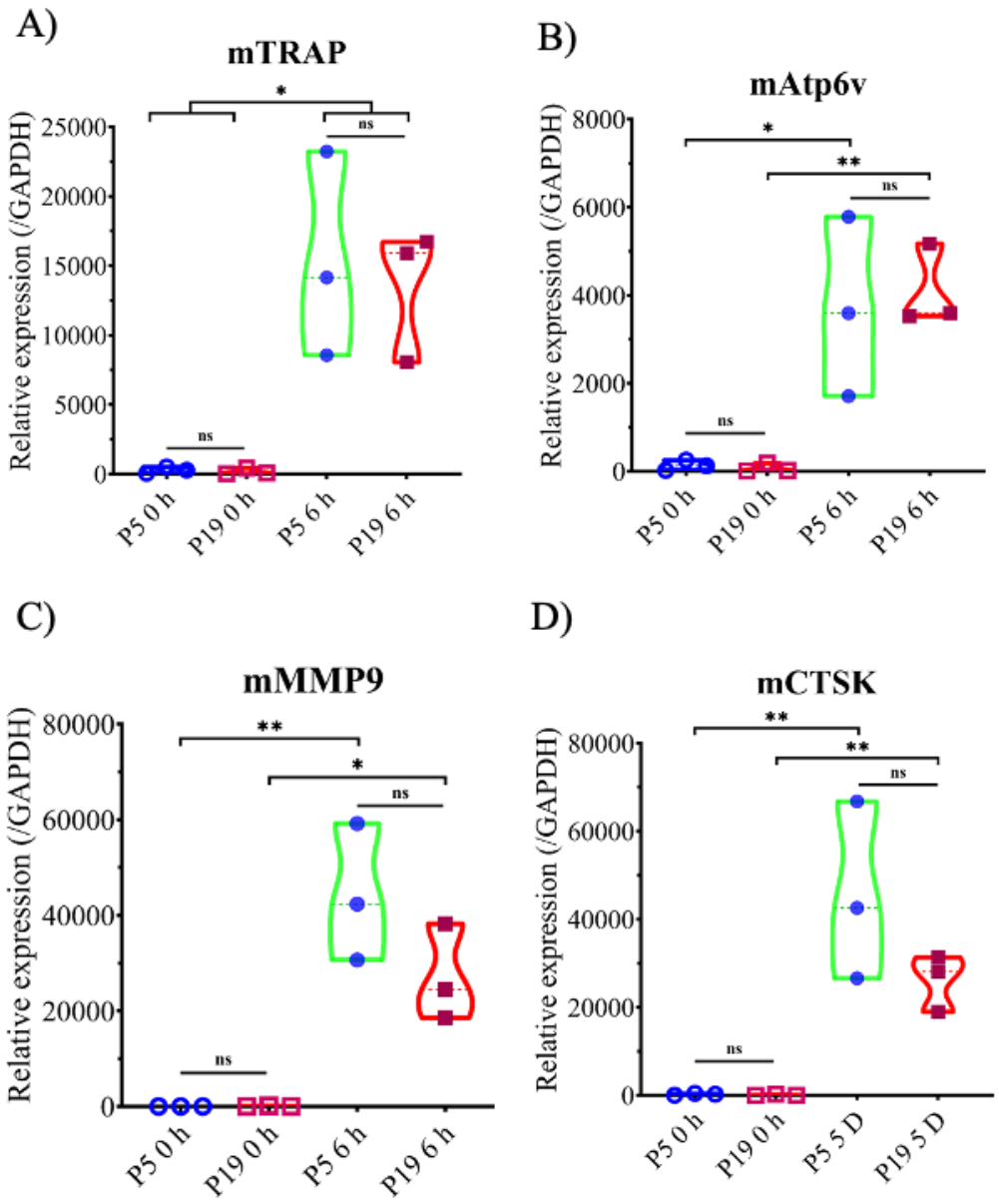
A)
mTRAP
Relative expression (/GAPDH)
25000
20000
15000
10000
5000
0
*
ns
ns
P5 0 h
P19 0 h
P5 6 h
P19 6 h
B)
mAtp6v
Relative expression (/GAPDH)
8000
6000
4000
2000
0
*
**
ns
ns
P5 0 h
P19 0 h
P5 6 h
P19 6 h
C)
mMMP9
Relative expression (/GAPDH)
80000
60000
40000
20000
0
**
*
ns
ns
P5 0 h
P19 0 h
P5 6 h
P19 6 h
D)
mCTSK
Relative expression (/GAPDH)
80000
60000
40000
20000
0
**
**
ns
ns
P5 0 h
P19 0 h
P5 5 D
P19 5 D

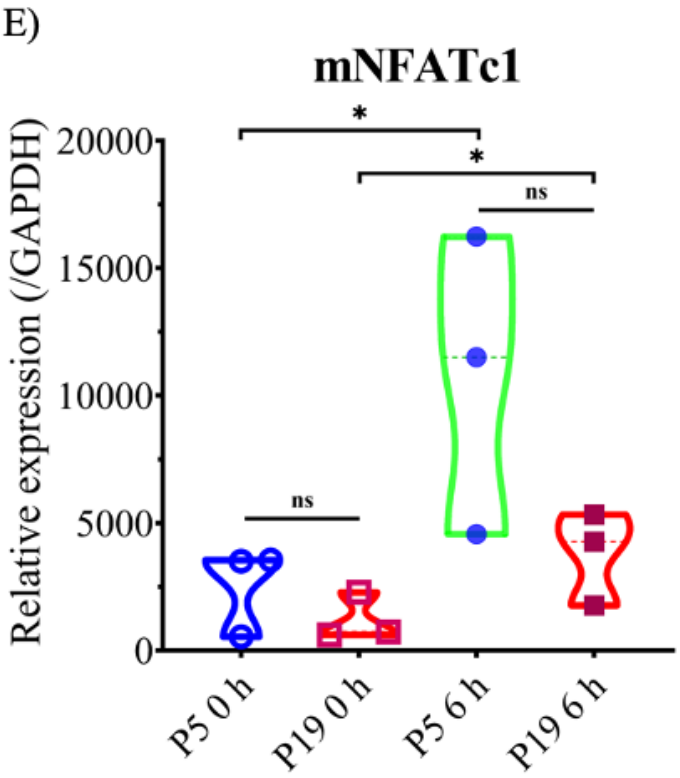

Figure 5: Osteoclastogenic gene expression. Values are means±SEM, *p<0.05, ** p<0.01, ns-non-significant. These data have been published in (64).

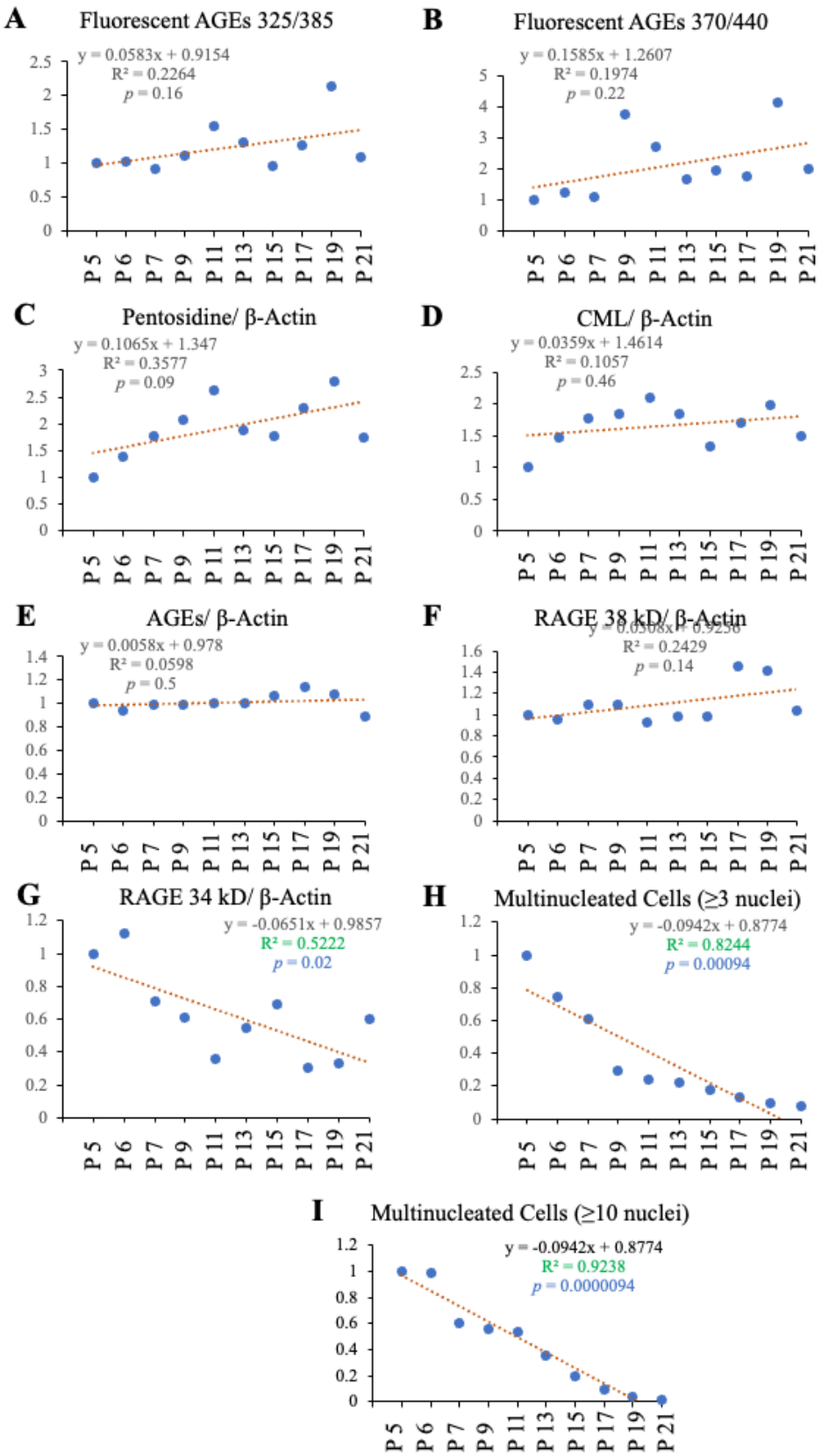

Figure 6: Correlation analysis of passage number with different features as mentioned in the figures. Higher R^2 and lower p-value (<0.05) indicate highly correlated statistically significant data. These data have been published in (64).

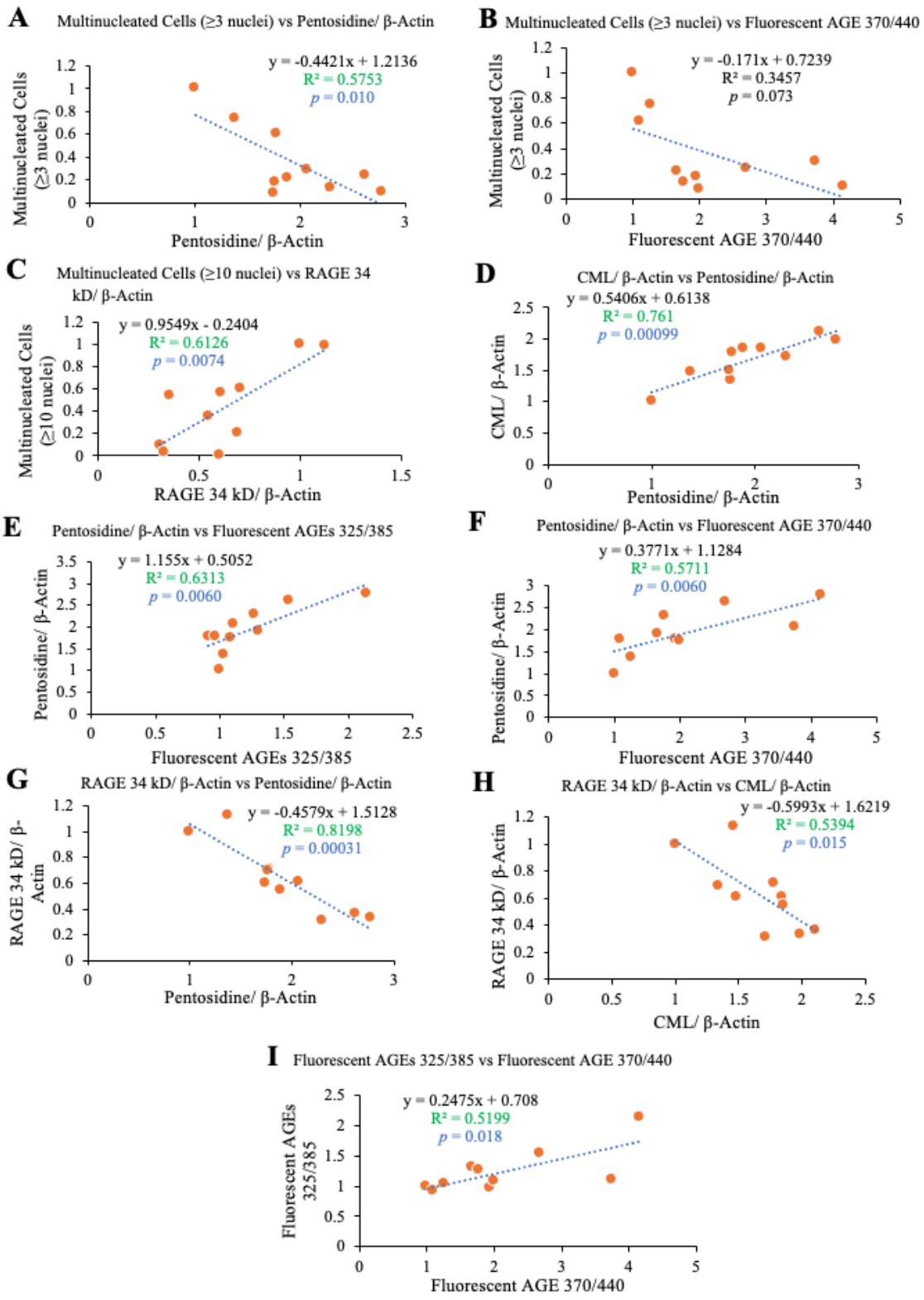

Figure 7: Correlation analysis of different features as mentioned in the figures. Higher R2 and lower p-value (<0.05) indicate highly correlated statistically significant data. These data have been published in (64).

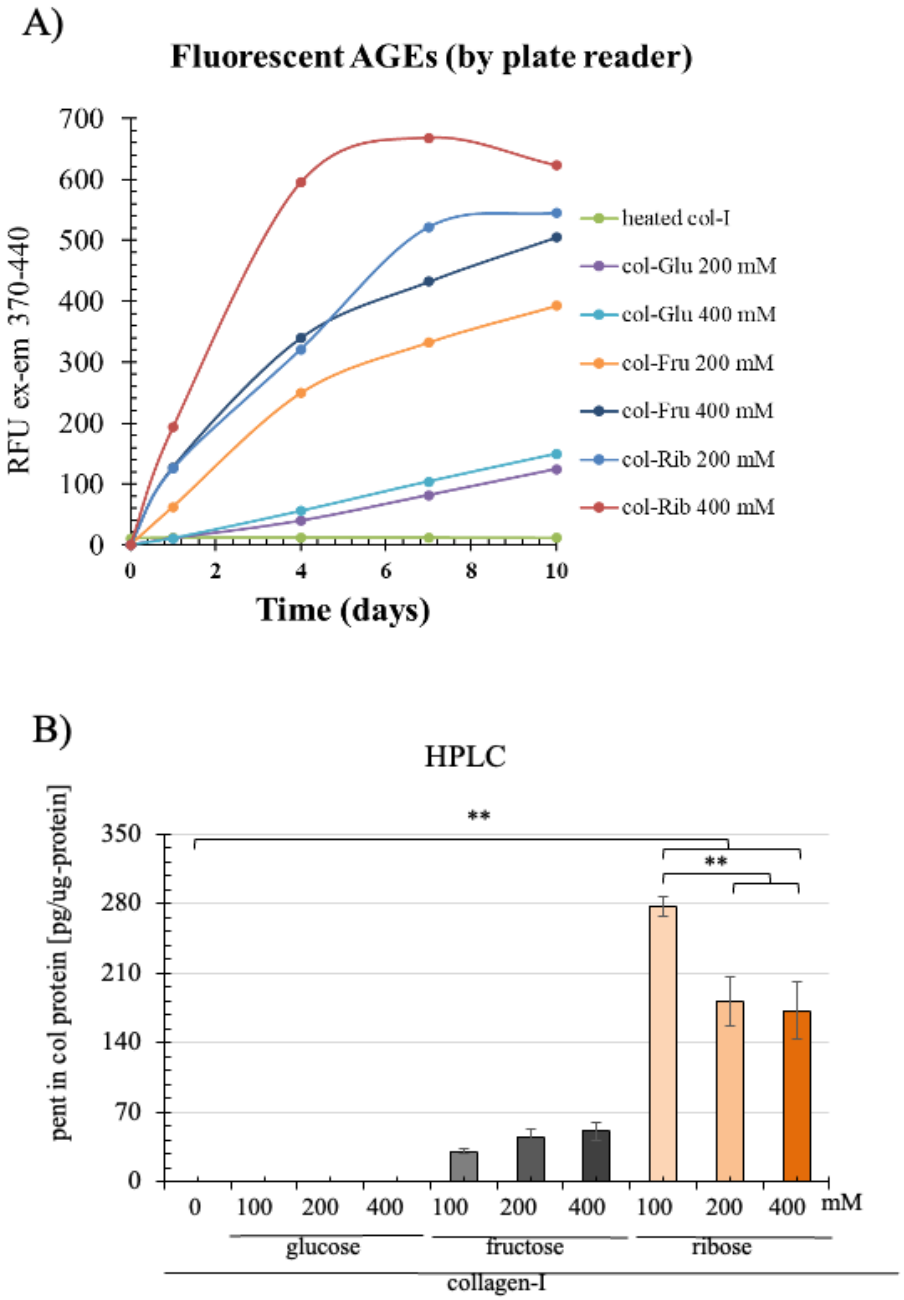

Figure 8: Fluorescent AGE formation in Glycated collagen protein. (A) fluorescent intensity at ex-em 370-440 nm using a fluorometric plate reader, (B) pentosidine measurement by HPLC analysis. Values are means±SEM, n=3 by Tukey-Kramer test, ** $p<0.01$.

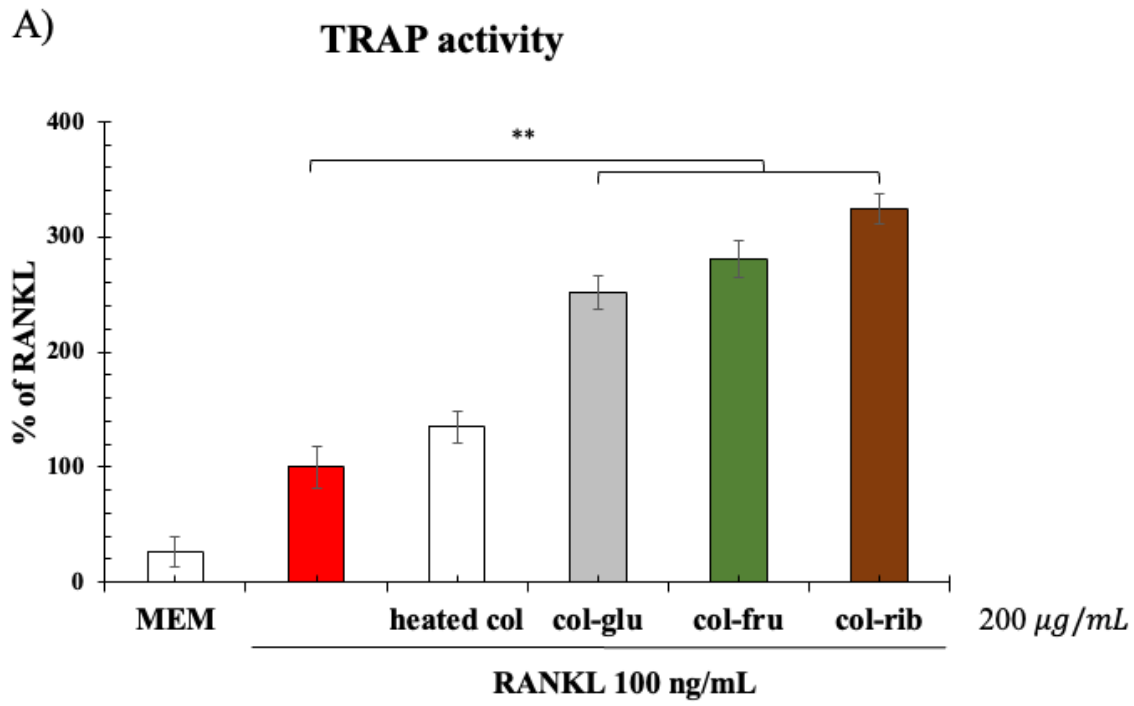
A)
TRAP activity
400
300
200
100
0
% of RANKL
**
MEM
heated col
col-glu
col-fru
col-rib
200 μg/mL
RANKL 100 ng/mL

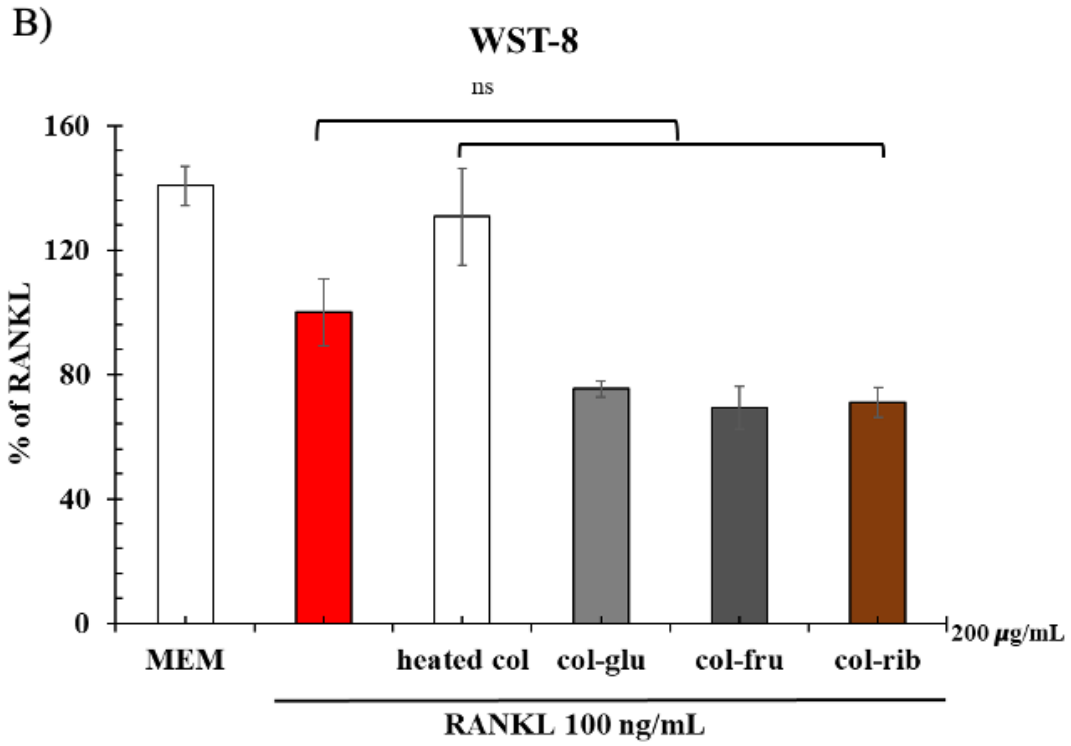
B)
WST-8
ns
160
120
80
40
0
% of RANKL
MEM
heated col
col-glu
col-fru
col-rib
200 μg/mL
RANKL 100 ng/mL

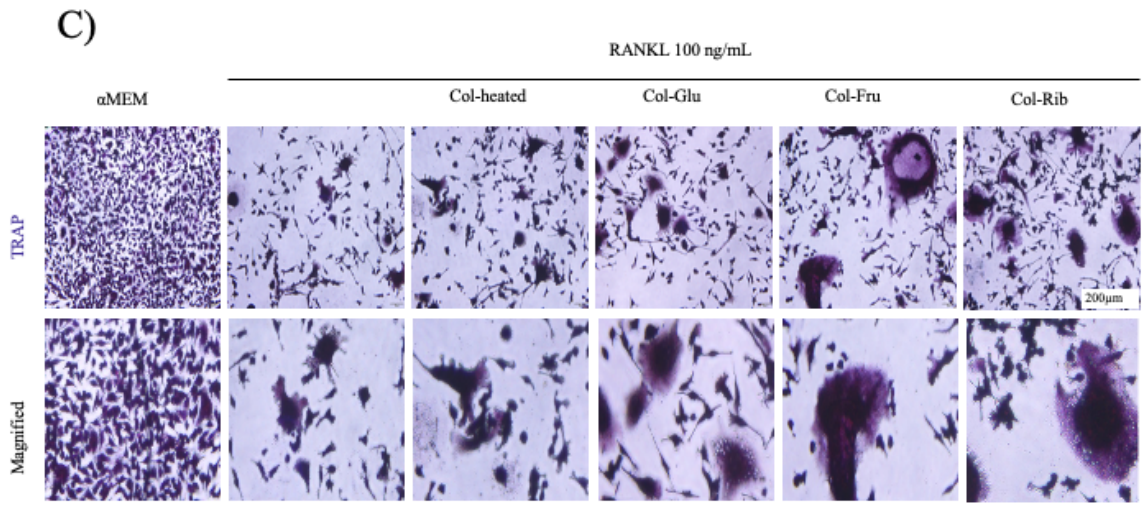

Figure 9: Effect of glycated collagen protein on osteoclast differentiation and cell viability. (A) Trap activity (B) WST-8 (C) TRAP staining. Values are means±SEM, n=3 by Tukey-Kramer test, ** $p<0.01$, ns-non-significant.

A)

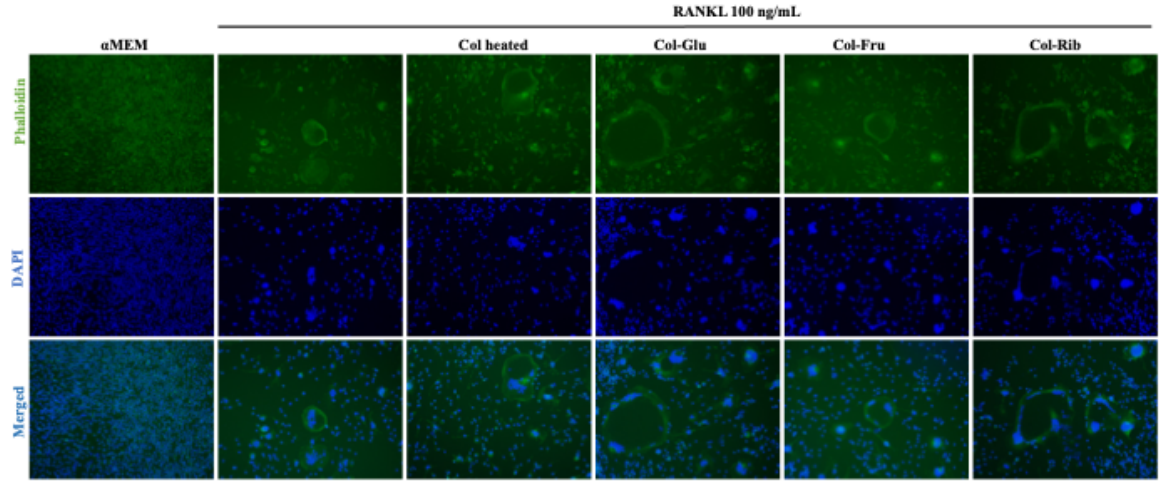
RANKL 100 ng/mL
αMEM
Col heated
Col-Glu
Col-Fru
Col-Rib
Phalloidin
DAPI
Merged

B)

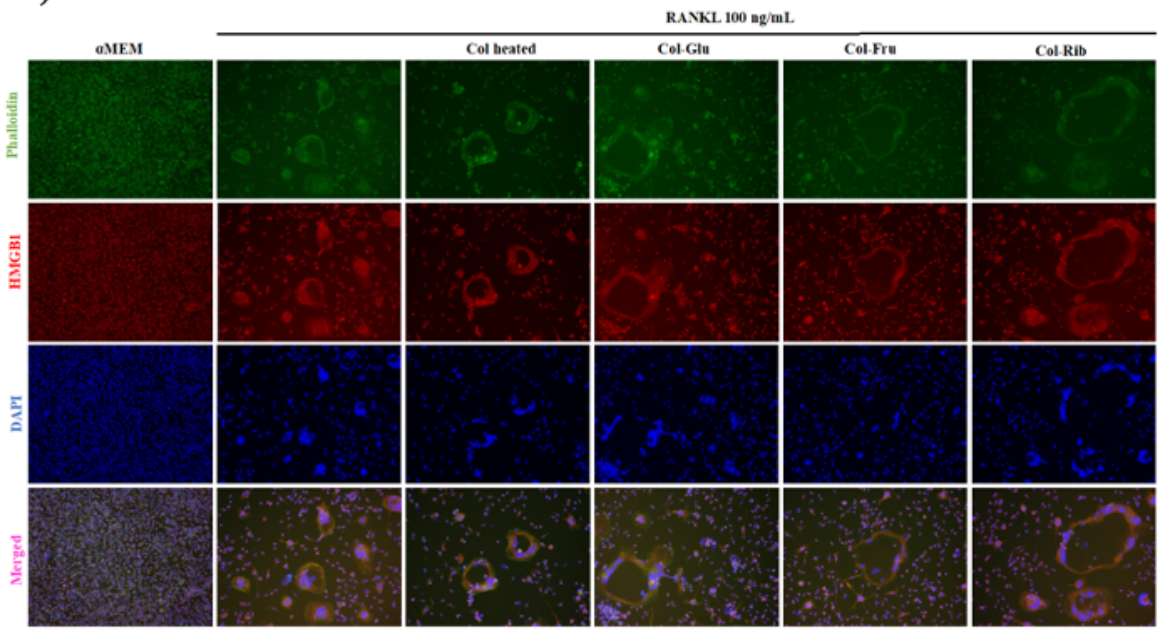
RANKL 100 ng/mL
αMEM
Col heated
Col-Glu
Col-Fru
Col-Rib
Phalloidin
HMGB1
DAPI
Merged

C)

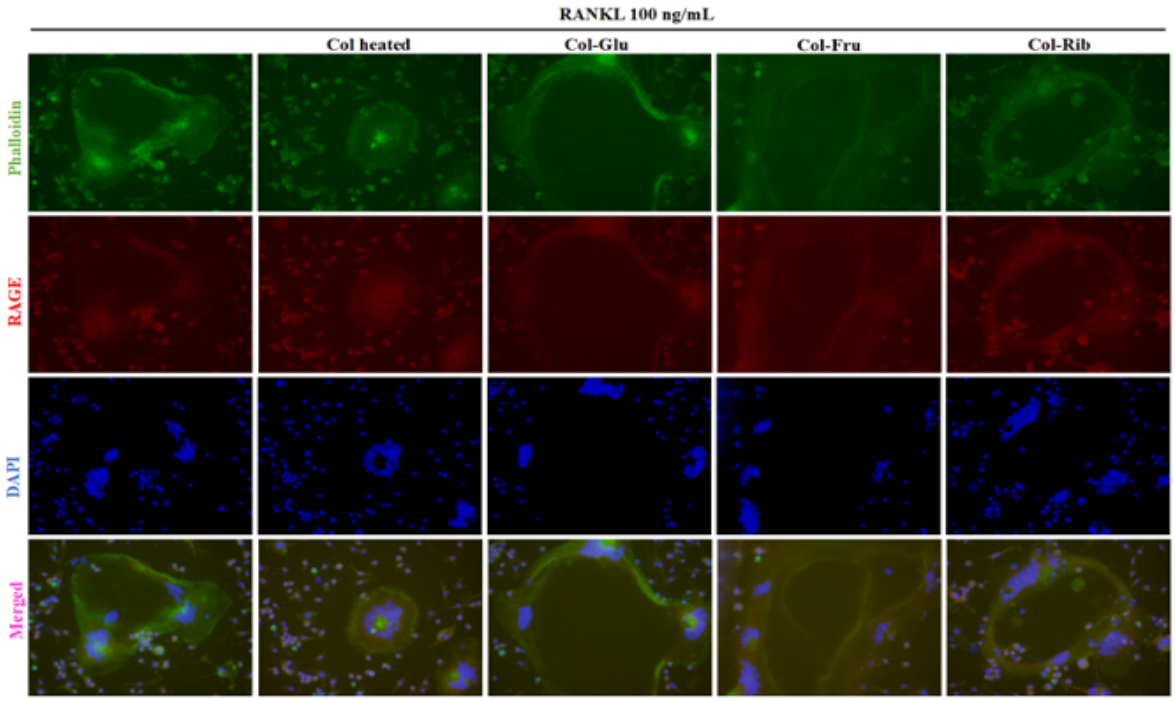

Figure 10: Effect of glycated collagen protein on f-actin ring formation, HMGB1 translocation, and RAGE expression. (A) f-actin ring formation, (B) HMGB1 translocation, and (C) RAGE expression. Microscopic images are shown at 10X magnification except for RAGE at 20X.

A)

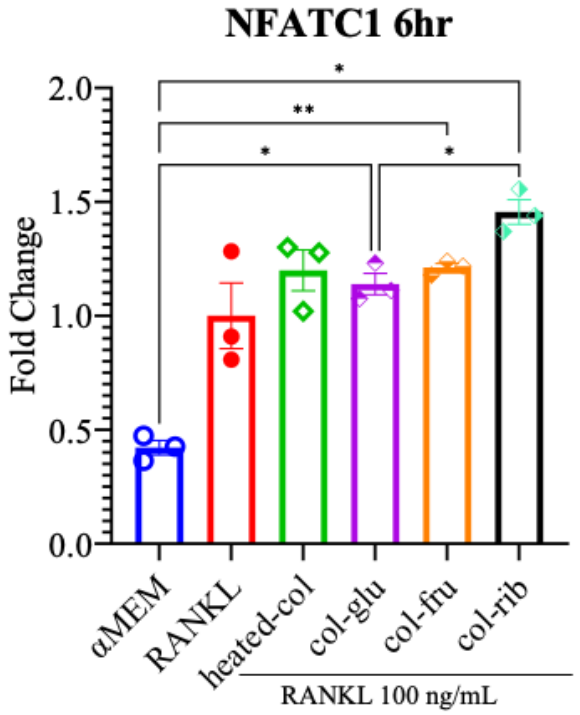
NFATC1 6hr
Fold Change
2.0
1.5
1.0
0.5
0.0
*
**
*
*
αMEM
RANKL
heated-col
col-glu
col-fru
col-rib
RANKL 100 ng/mL

B)

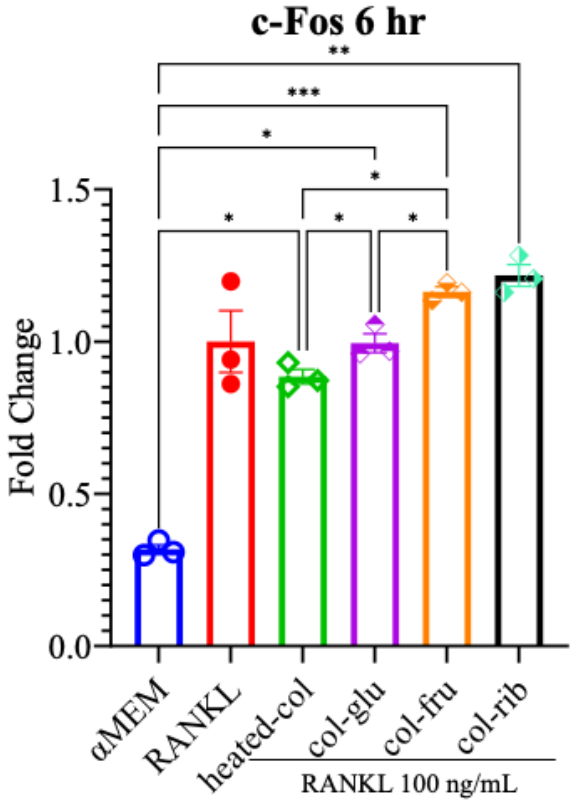
c-Fos 6 hr
Fold Change
1.5
1.0
0.5
0.0
**
***
*
*
*
*
*
αMEM
RANKL
heated-col
col-glu
col-fru
col-rib
RANKL 100 ng/mL

C)

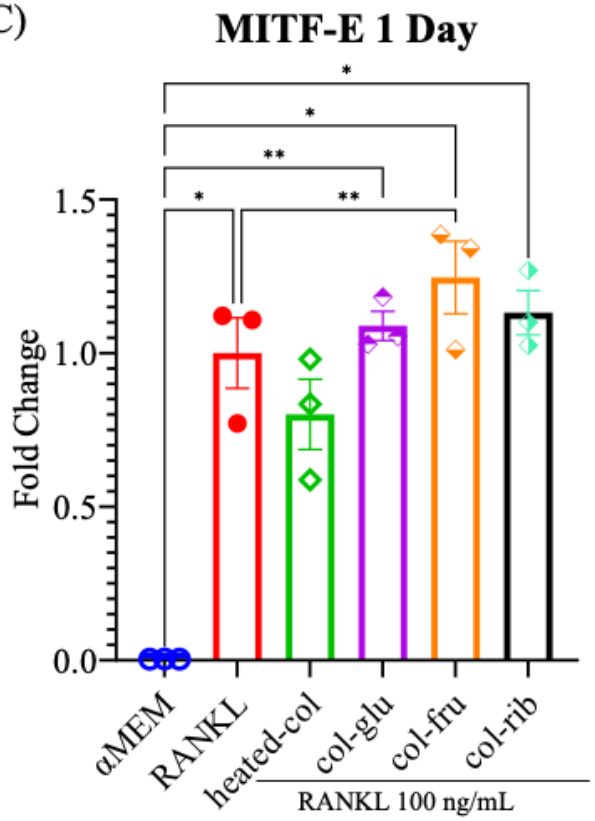
MITF-E 1 Day
Fold Change
1.5
1.0
0.5
0.0
*
*
**
*
**
αMEM
RANKL
heated-col
col-glu
col-fru
col-rib
RANKL 100 ng/mL

D)

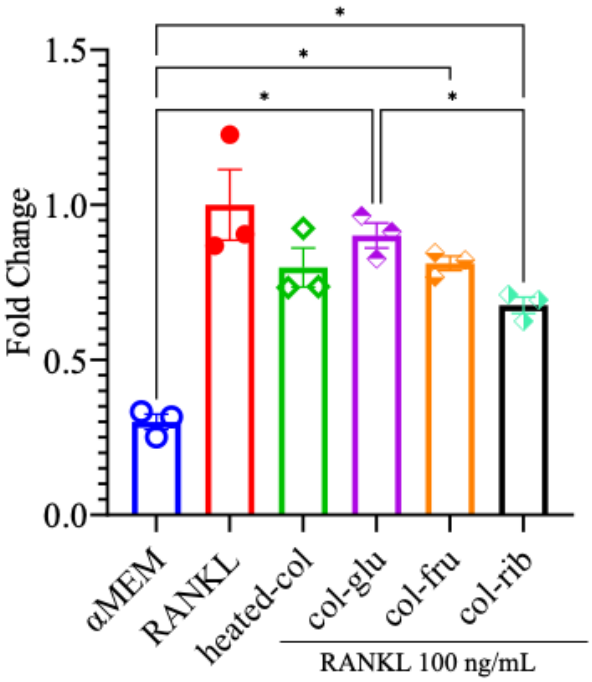
Itgav 3 Days
Fold Change
1.5
1.0
0.5
0.0
*
*
*
*
αMEM
RANKL
heated-col
col-glu
col-fru
col-rib
RANKL 100 ng/mL

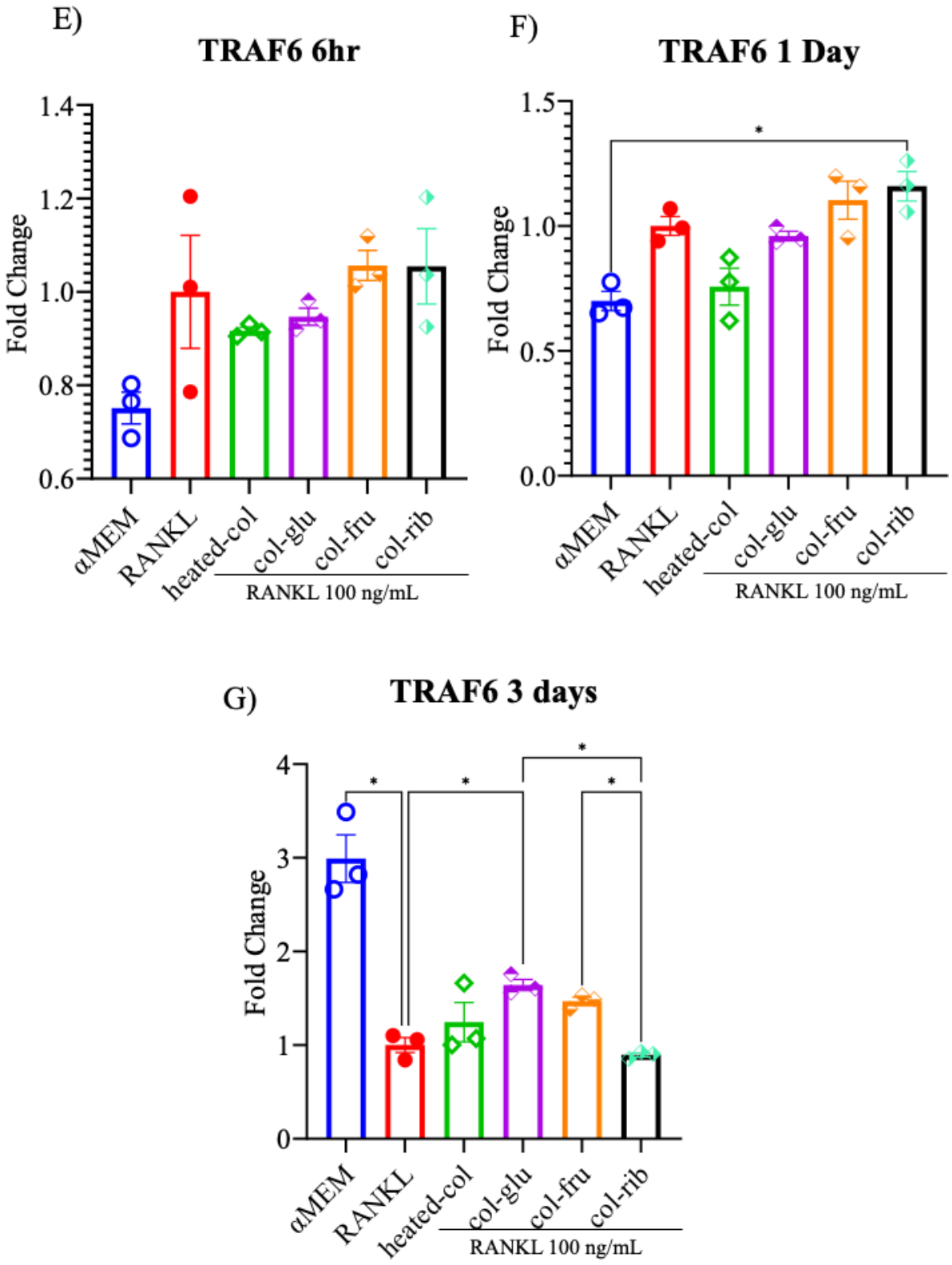
E)
TRAF6 6hr
Fold Change
1.4
1.2
1.0
0.8
0.6
αMEM
RANKL
heated-col
col-glu
col-fru
col-rib
RANKL 100 ng/mL
F)
TRAF6 1 Day
Fold Change
1.5
1.0
0.5
0.0
*
αMEM
RANKL
heated-col
col-glu
col-fru
col-rib
RANKL 100 ng/mL
G)
TRAF6 3 days
Fold Change
4
3
2
1
0
*
*
*
*
αMEM
RANKL
heated-col
col-glu
col-fru
col-rib
RANKL 100 ng/mL

H)

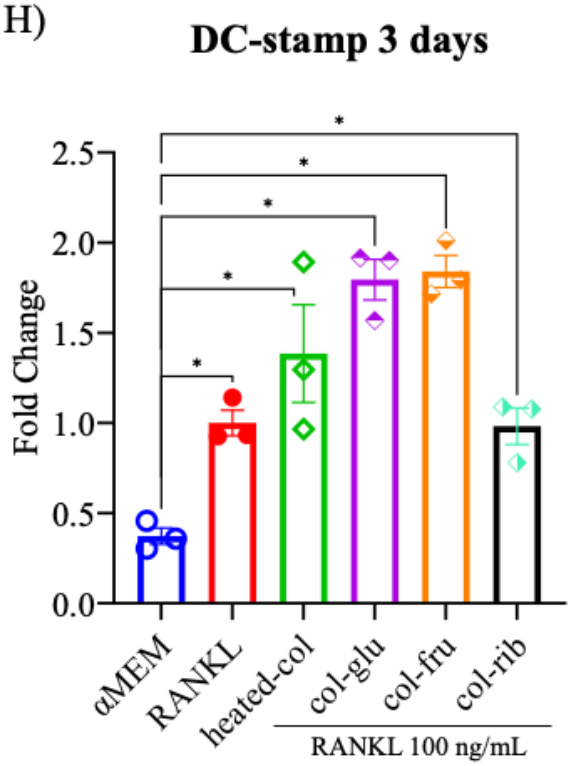
DC-stamp 3 days
Fold Change
2.5
2.0
1.5
1.0
0.5
0.0
*
*
*
*
*
αMEM
RANKL
heated-col
col-glu
col-fru
col-rib
RANKL 100 ng/mL

I)

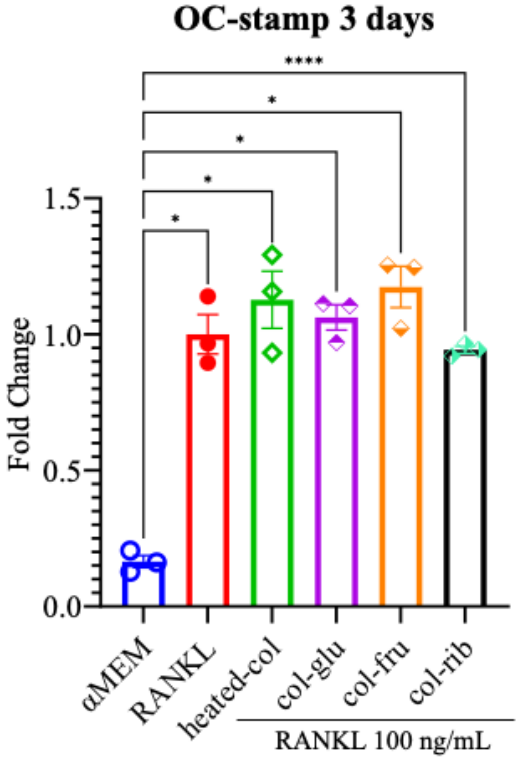
OC-stamp 3 days
Fold Change
1.5
1.0
0.5
0.0
****
*
*
*
*
αMEM
RANKL
heated-col
col-glu
col-fru
col-rib
RANKL 100 ng/mL

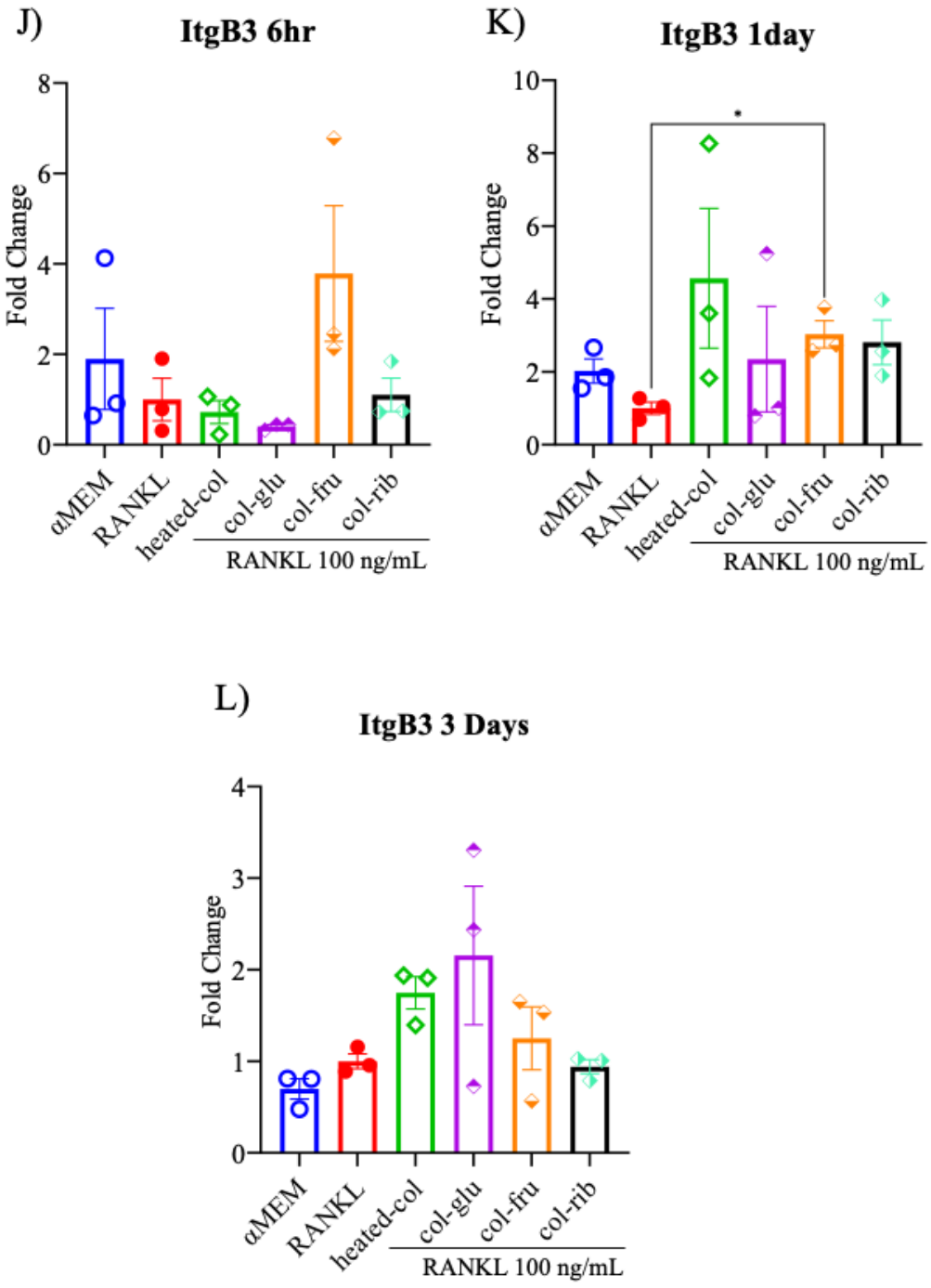
J)
ItgB3 6hr
Fold Change
8
6
4
2
0
αMEM
RANKL
heated-col
col-glu
col-fru
col-rib
RANKL 100 ng/mL
K)
ItgB3 1day
Fold Change
10
8
6
4
2
0
*
αMEM
RANKL
heated-col
col-glu
col-fru
col-rib
RANKL 100 ng/mL
L)
ItgB3 3 Days
Fold Change
4
3
2
1
0
αMEM
RANKL
heated-col
col-glu
col-fru
col-rib
RANKL 100 ng/mL

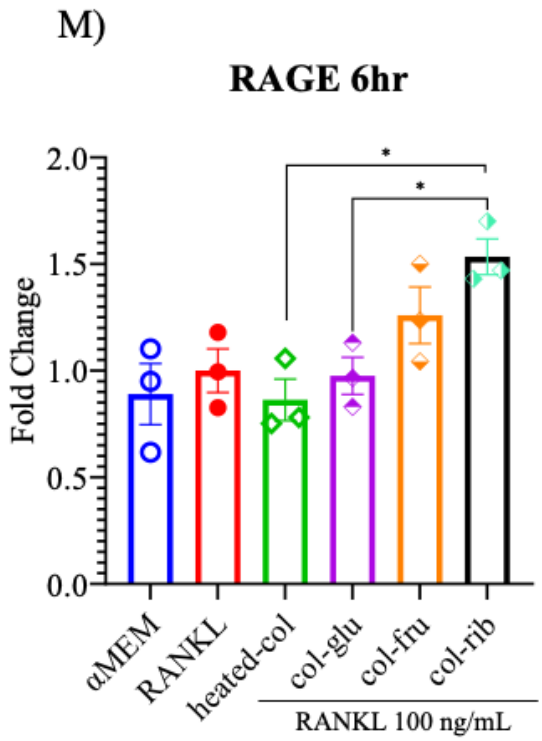
M)
RAGE 6hr
Fold Change
2.0
1.5
1.0
0.5
0.0
*
*
αMEM
RANKL
heated-col
col-glu
col-fru
col-rib
RANKL 100 ng/mL

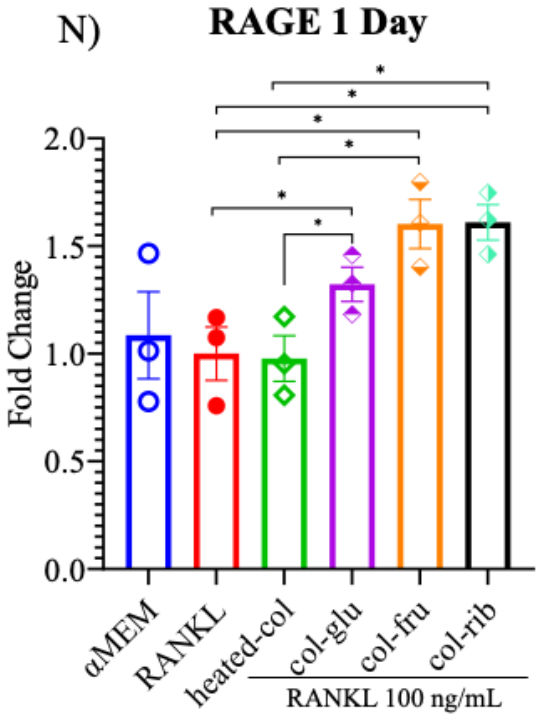
N)
RAGE 1 Day
Fold Change
2.0
1.5
1.0
0.5
0.0
*
*
*
*
*
*
αMEM
RANKL
heated-col
col-glu
col-fru
col-rib
RANKL 100 ng/mL

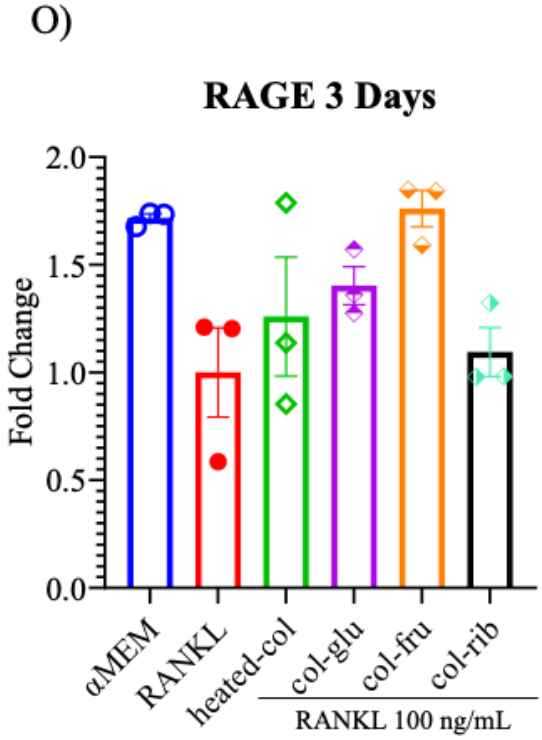
O)
RAGE 3 Days
Fold Change
2.0
1.5
1.0
0.5
0.0
αMEM
RANKL
heated-col
col-glu
col-fru
col-rib
RANKL 100 ng/mL

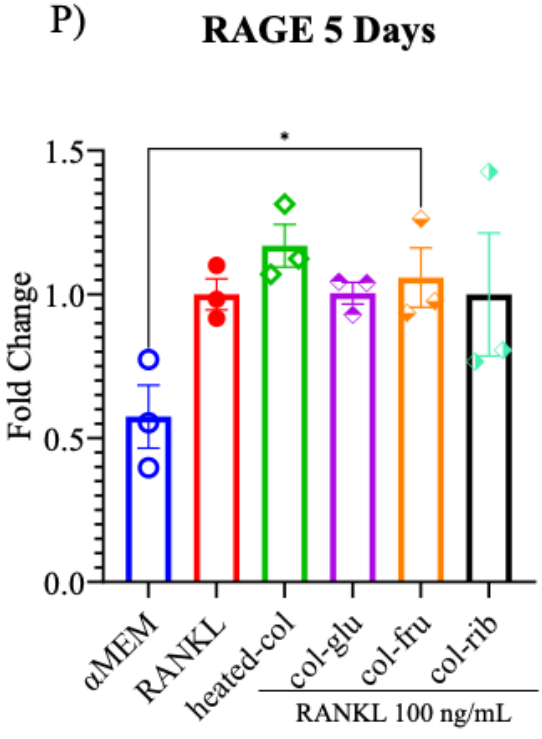
P)
RAGE 5 Days
Fold Change
1.5
1.0
0.5
0.0
*
αMEM
RANKL
heated-col
col-glu
col-fru
col-rib
RANKL 100 ng/mL

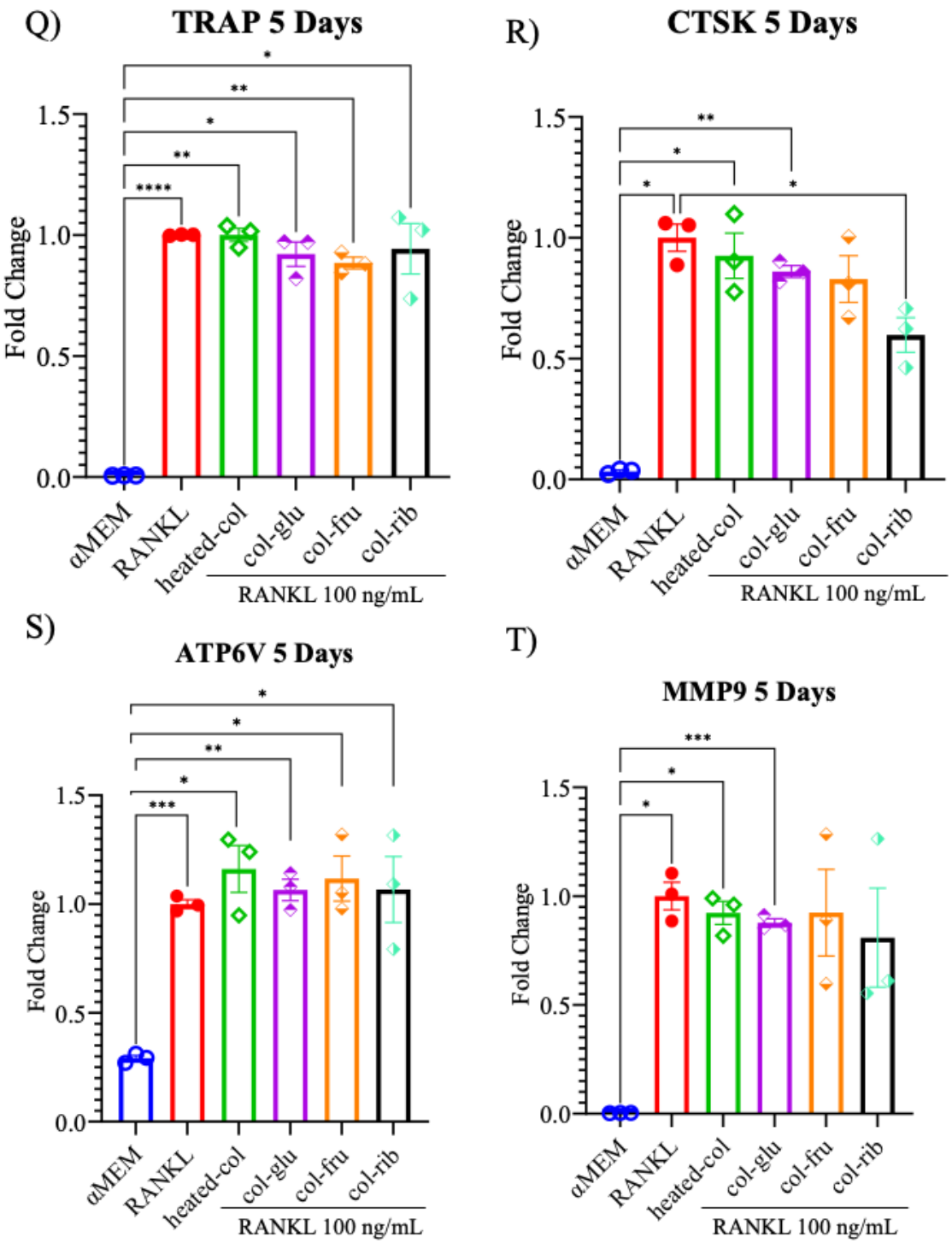

Figure 11: Effect of glycated collagen protein on osteoclastogenic gene expression. Values are means±SEM, *p<0.05, ** p<0.01, ***p<0.001, ****p<0.0001.

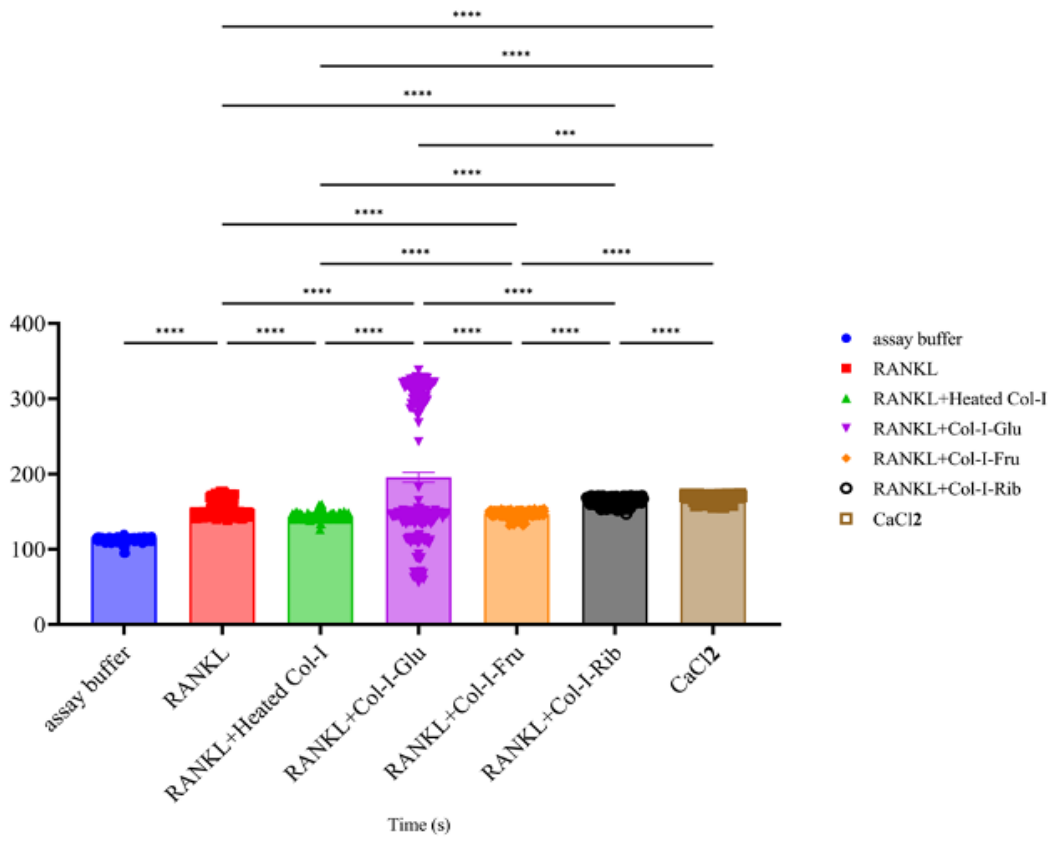

Figure 12: Effect of glycated collagen protein on Ca^{2+} influx. Values are means ± SEM, ***p<0.001, ****p<0.0001.

A)

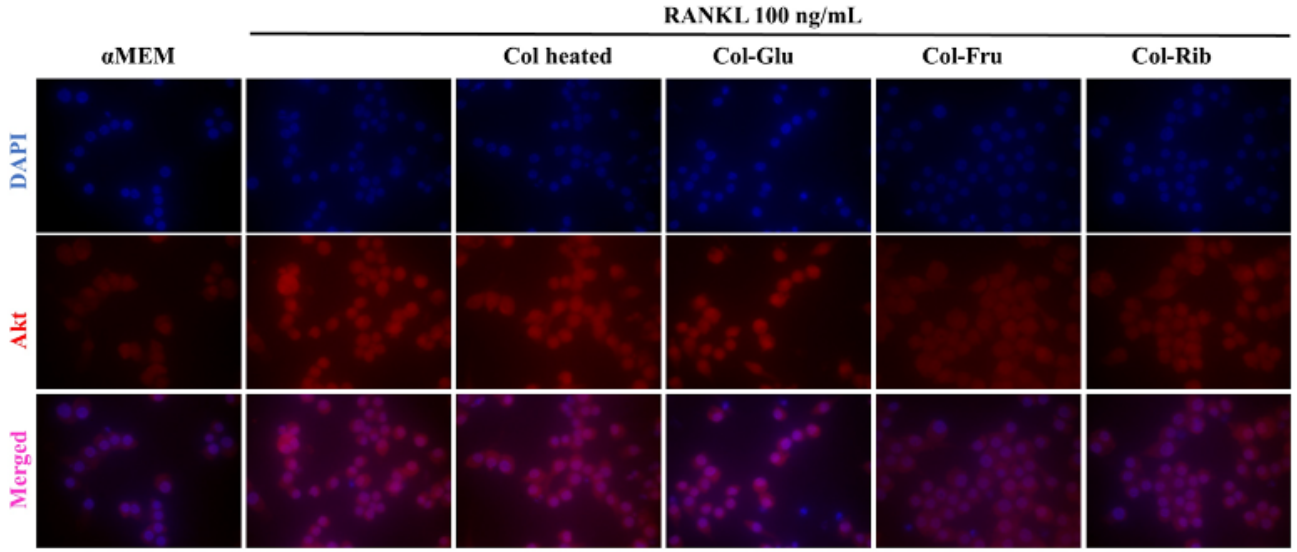
RANKL 100 ng/mL
αMEM
Col heated
Col-Glu
Col-Fru
Col-Rib
DAPI
Akt
Merged

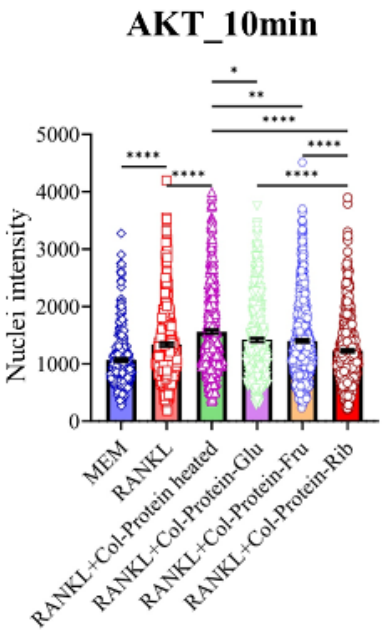
AKT_10min
Nuclei intensity
5000
4000
3000
2000
1000
0
*
**
****
****
****
****
****
MEM
RANKL
RANKL+Col-Protein heated
RANKL+Col-Protein-Glu
RANKL+Col-Protein-Fru
RANKL+Col-Protein-Rib

B)

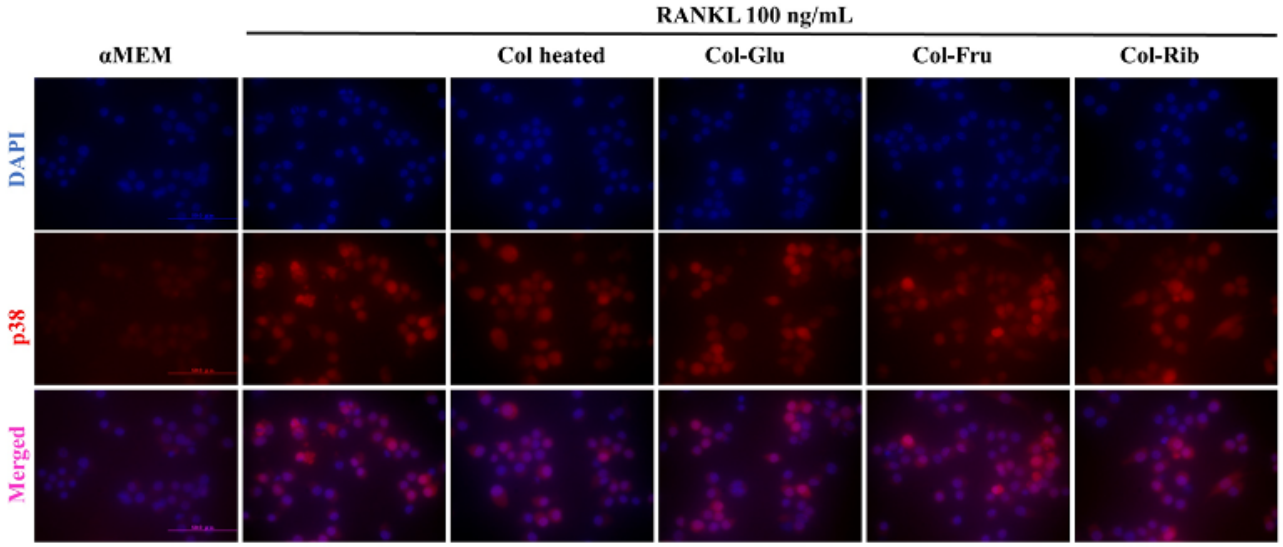
RANKL 100 ng/mL
αMEM
Col heated
Col-Glu
Col-Fru
Col-Rib
DAPI
p38
Merged

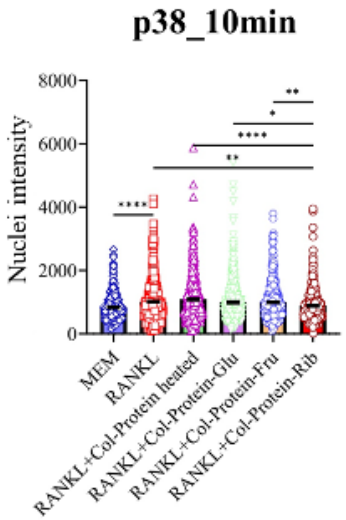
p38_10min
Nuclei intensity
8000
6000
4000
2000
0
****
**
****
*
**
MEM
RANKL
RANKL+Col-Protein heated
RANKL+Col-Protein-Glu
RANKL+Col-Protein-Fru
RANKL+Col-Protein-Rib

C)

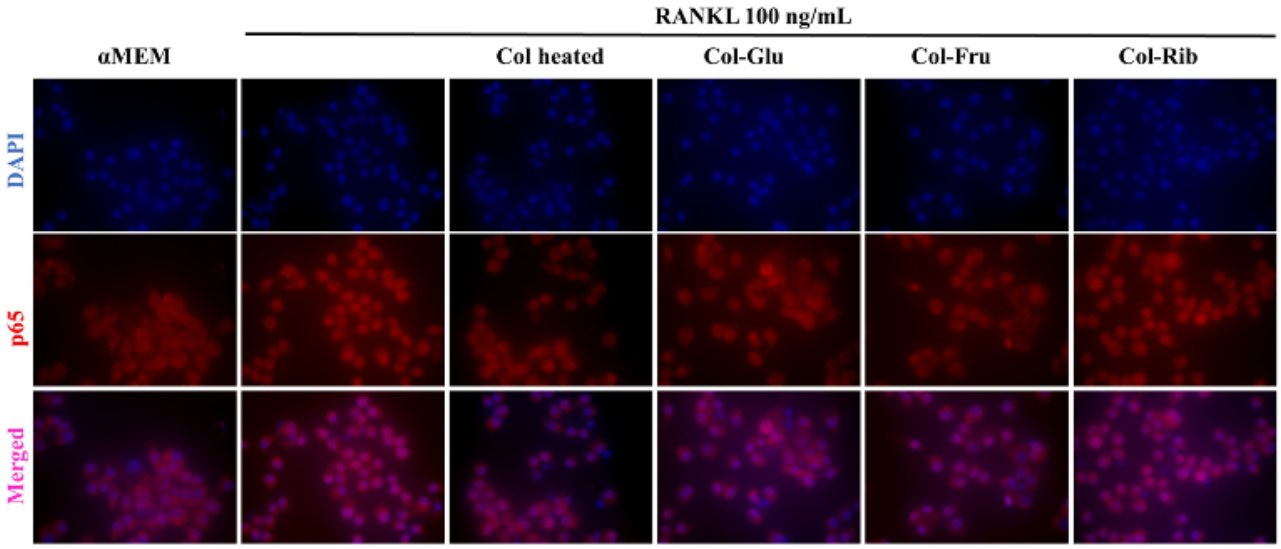
RANKL 100 ng/mL
αMEM
Col heated
Col-Glu
Col-Fru
Col-Rib
DAPI
p65
Merged

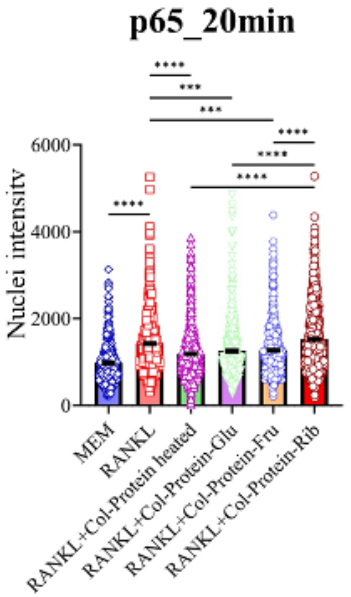
p65_20min
Nuclei intensity
6000
4000
2000
0
****
***
***
****
****
****
****
MEM
RANKL
RANKL+Col-Protein heated
RANKL+Col-Protein-Glu
RANKL+Col-Protein-Fru
RANKL+Col-Protein-Rib

D)

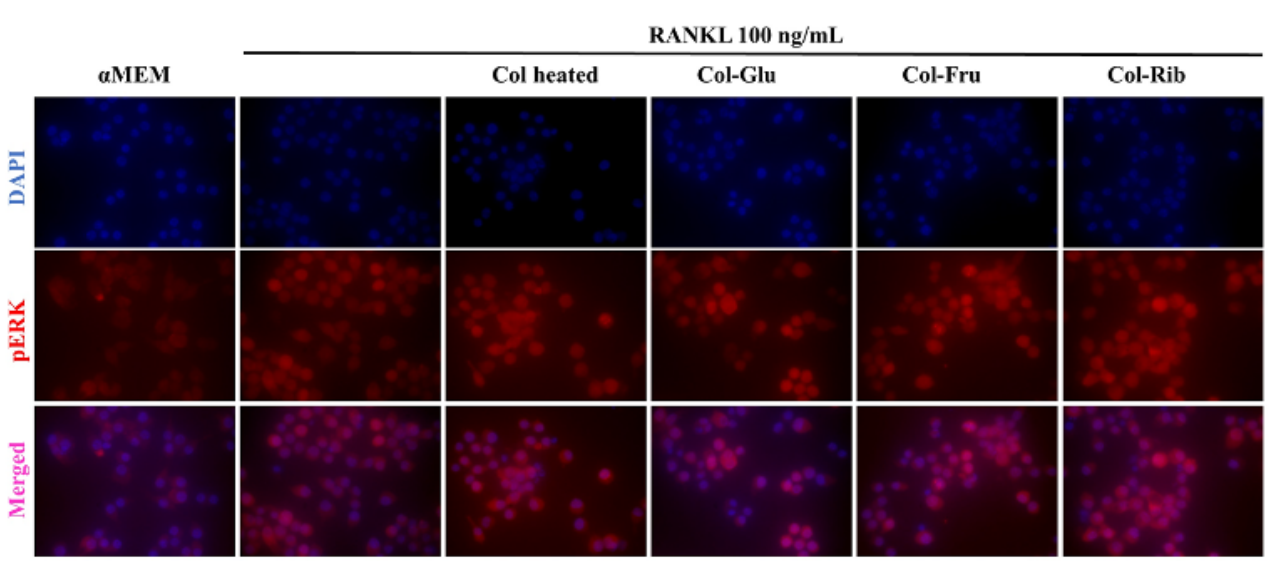
RANKL 100 ng/mL
αMEM
Col heated
Col-Glu
Col-Fru
Col-Rib
DAPI
pERK
Merged

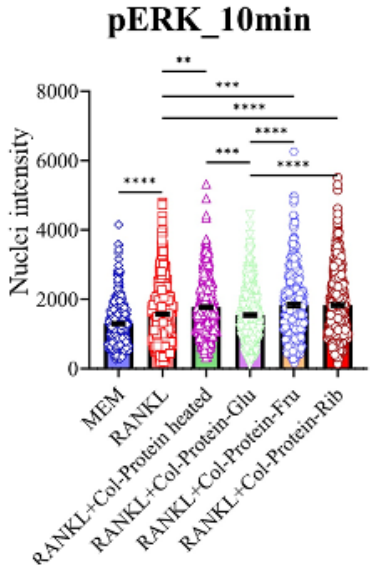
pERK_10min
Nuclei intensity
8000
6000
4000
2000
0
**
***
****
****
***
****
****
MEM
RANKL
RANKL+Col-Protein heated
RANKL+Col-Protein-Glu
RANKL+Col-Protein-Fru
RANKL+Col-Protein-Rib

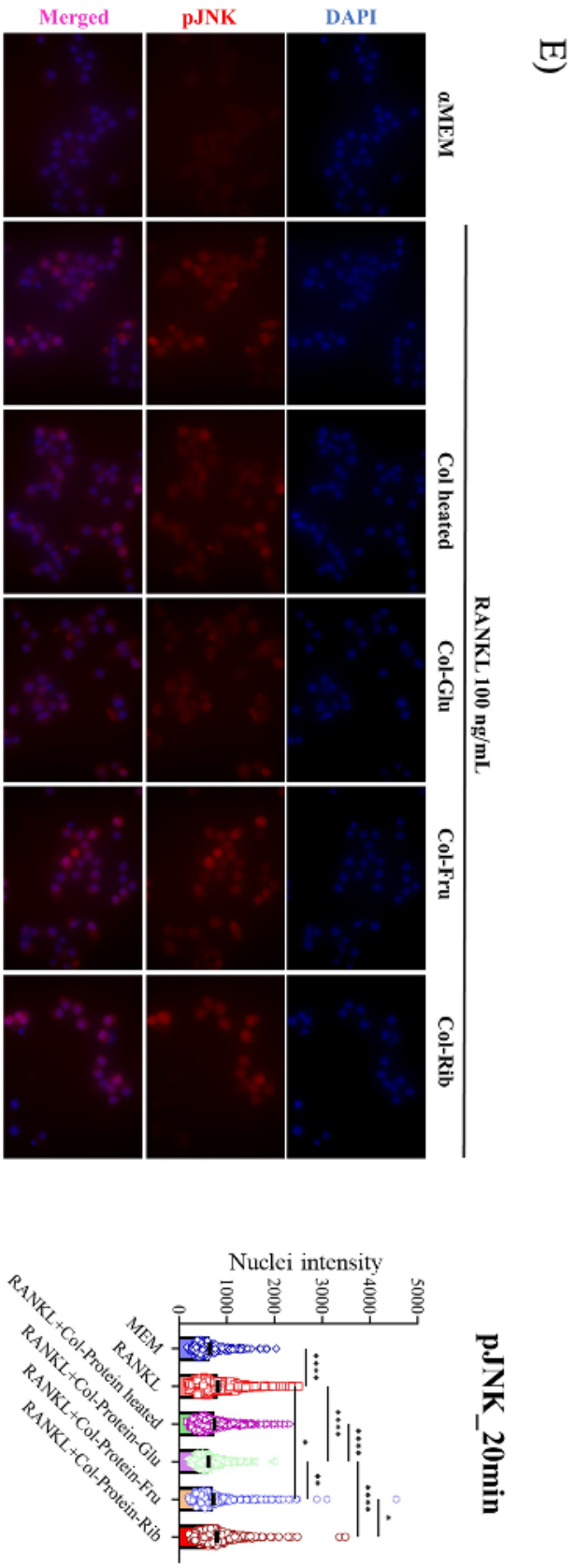

Figure 13: Effect of glycated collagen protein on pathway activation. Values are means±SEM, *p<0.05, ** p<0.01, ***p<0.001, ****p<0.0001.

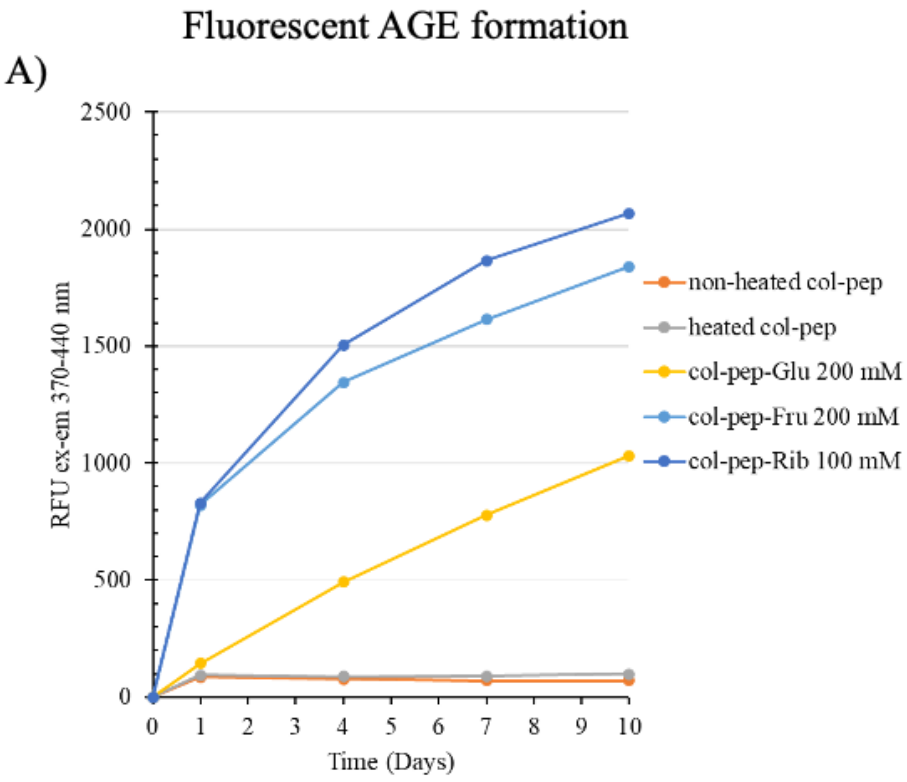
Fluorescent AGE formation
A)
RFU ex-em 370-440 nm
2500
2000
1500
1000
500
0
0 1 2 3 4 5 6 7 8 9 10
Time (Days)
non-heated col-pep
heated col-pep
col-pep-Glu 200 mM
col-pep-Fru 200 mM
col-pep-Rib 100 mM

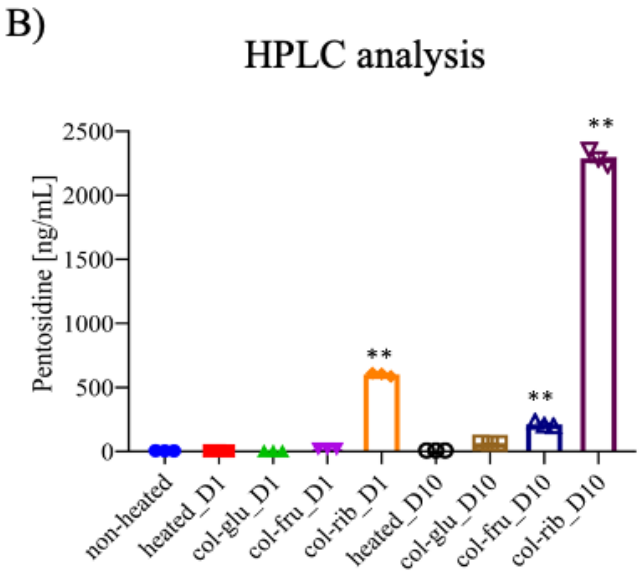
B)
HPLC analysis
Pentosidine [ng/mL]
2500
2000
1500
1000
500
0
**
**
**
non-heated
heated_D1
col-glu_D1
col-fru_D1
col-rib_D1
heated_D10
col-glu_D10
col-fru_D10
col-rib_D10

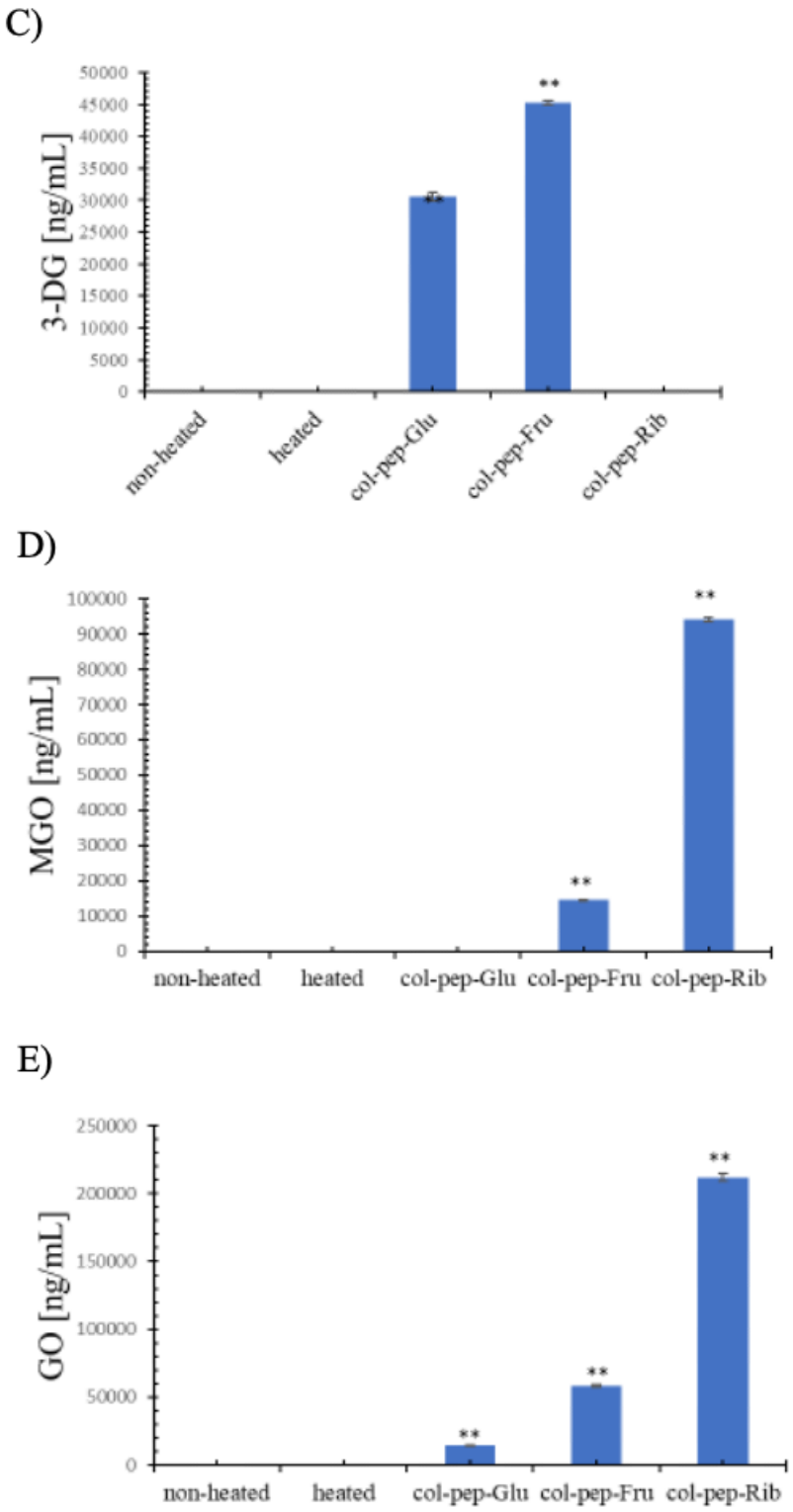

Figure 14: Formation of fluorescent AGEs and intermediates in glycated collagen peptide. (A) fluorescence intensity at ex-em 370-440 nm by fluorometric plate reader, (B) pentosidine, (C) 3-Deoxyglucosone [3-DG], (D) Methylglyoxal [MGO], and (E) Glyoxal [GO] measurement by HPLC analysis. Values are means±SEM, ** $p<0.01$.

A)

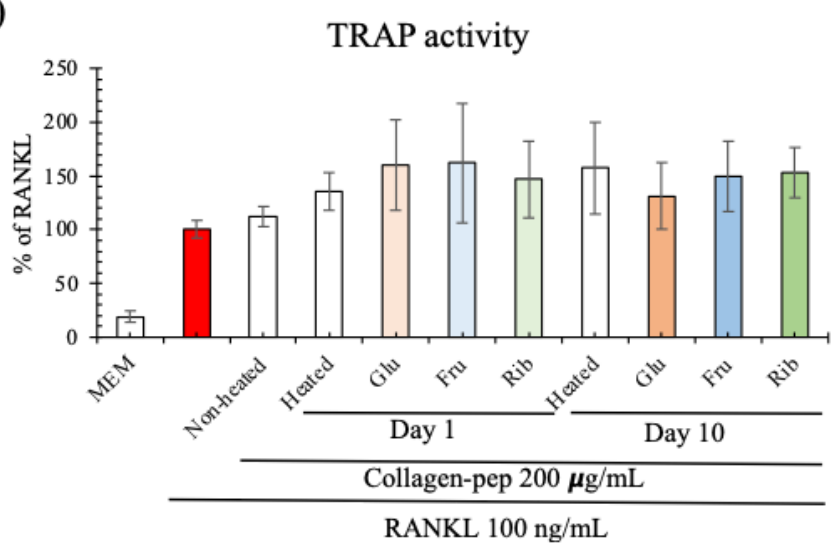
TRAP activity
% of RANKL
250
200
150
100
50
0
MEM
Non-heated
Heated
Glu
Fru
Rib
Heated
Glu
Fru
Rib
Day 1
Day 10
Collagen-pep 200 μg/mL
RANKL 100 ng/mL

B)

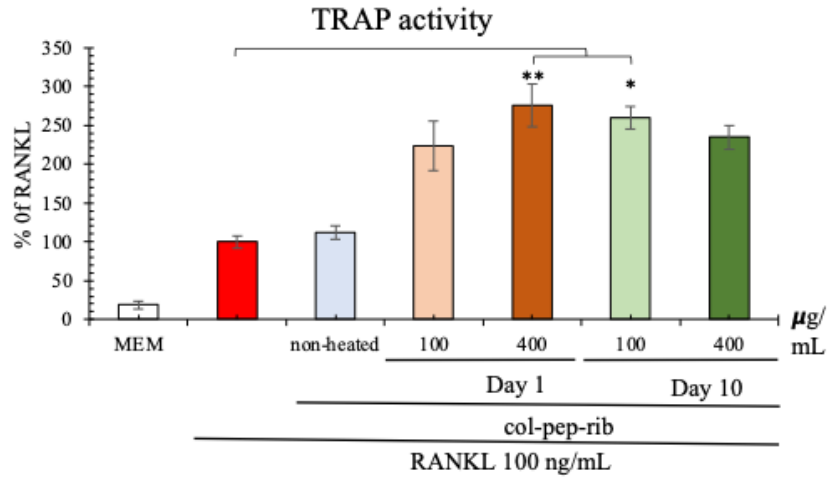
TRAP activity
% 0f RANKL
350
300
250
200
150
100
50
0
**
*
MEM
non-heated
100
400
100
400
μg/mL
Day 1
Day 10
col-pep-rib
RANKL 100 ng/mL

C)

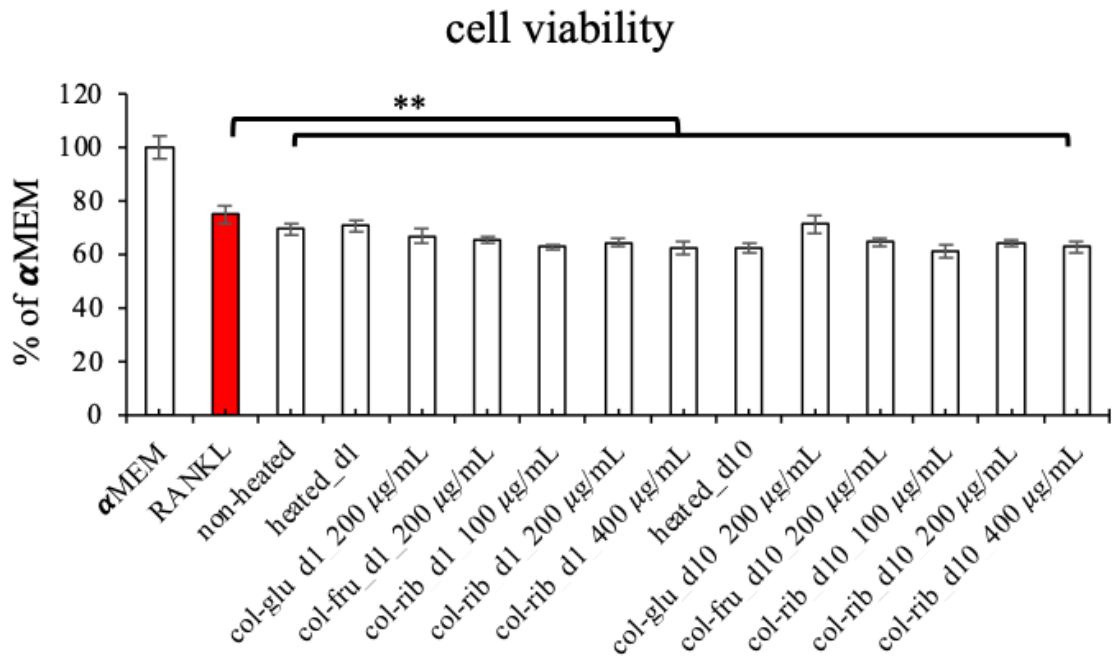

Figure 15: Effect of glycated collagen peptide on osteoclast differentiation and cell viability. (A-B) TRAP activity, (C) sensolyte assay for cell viability. Values are means±SEM, *p<0.05, ** p<0.01.

A)

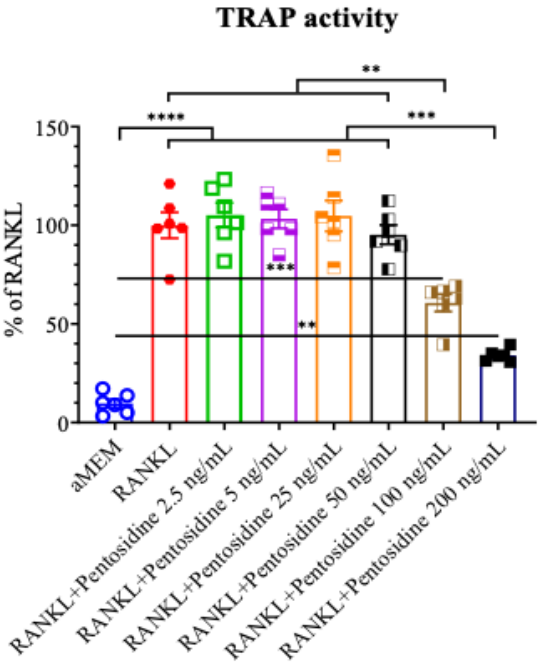
TRAP activity
% of RANKL
150
100
50
0
****
**
***
***
**
aMEM
RANKL
RANKL+Pentosidine 2.5 ng/mL
RANKL+Pentosidine 5 ng/mL
RANKL+Pentosidine 25 ng/mL
RANKL+Pentosidine 50 ng/mL
RANKL+Pentosidine 100 ng/mL
RANKL+Pentosidine 200 ng/mL

B)

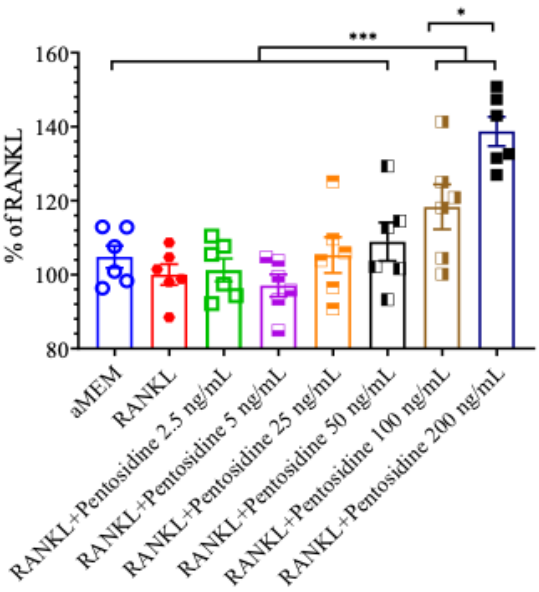
Cell viability
% of RANKL
160
140
120
100
80
***
*
aMEM
RANKL
RANKL+Pentosidine 2.5 ng/mL
RANKL+Pentosidine 5 ng/mL
RANKL+Pentosidine 25 ng/mL
RANKL+Pentosidine 50 ng/mL
RANKL+Pentosidine 100 ng/mL
RANKL+Pentosidine 200 ng/mL

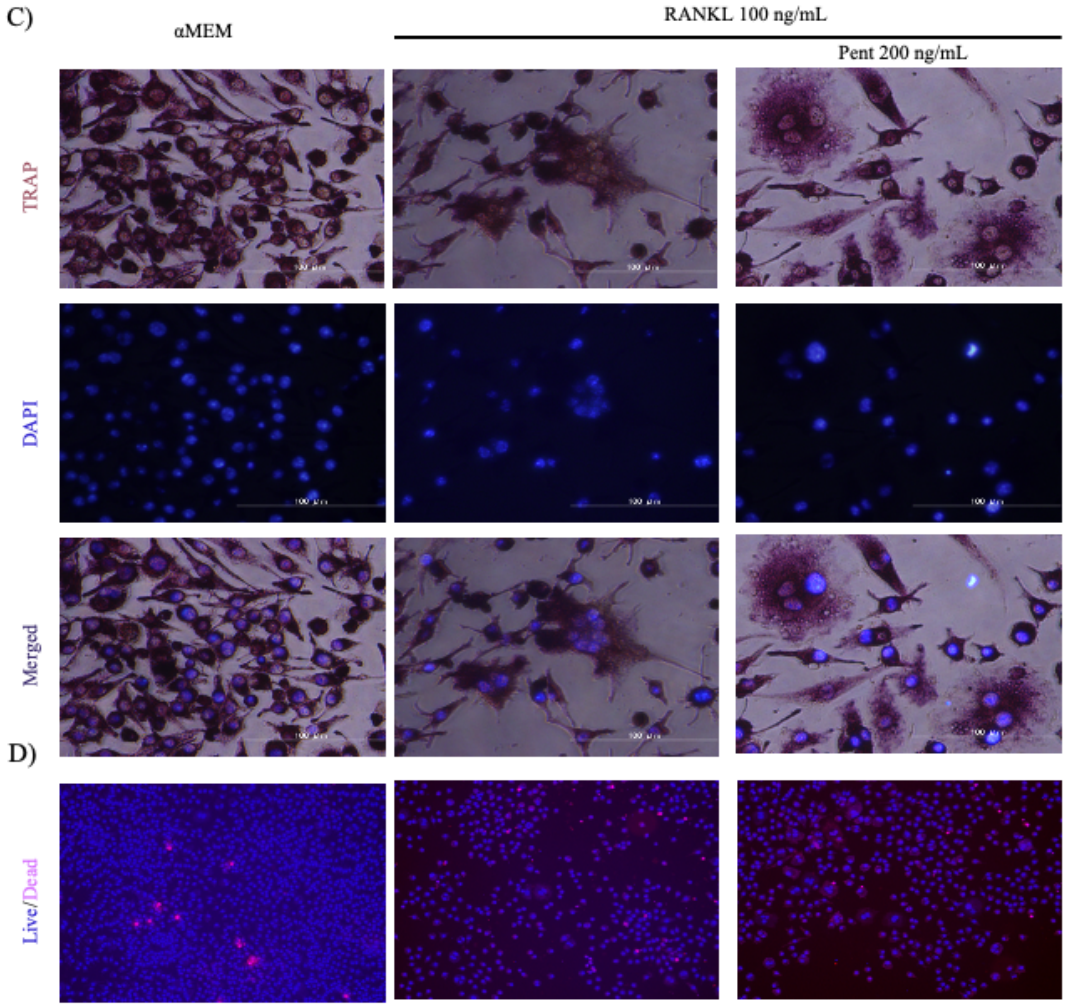

Figure 16: Role of free pentosidine on osteoclast differentiation and cell viability. (A) TRAP activity, (B) sensolyte assay for cell viability, (C)TRAP staining, (D) live/dead cells at 10X magnification. Values are means±SEM, *p<0.05, ** p<0.01, ***p<0.001, ****p<0.0001.

A)

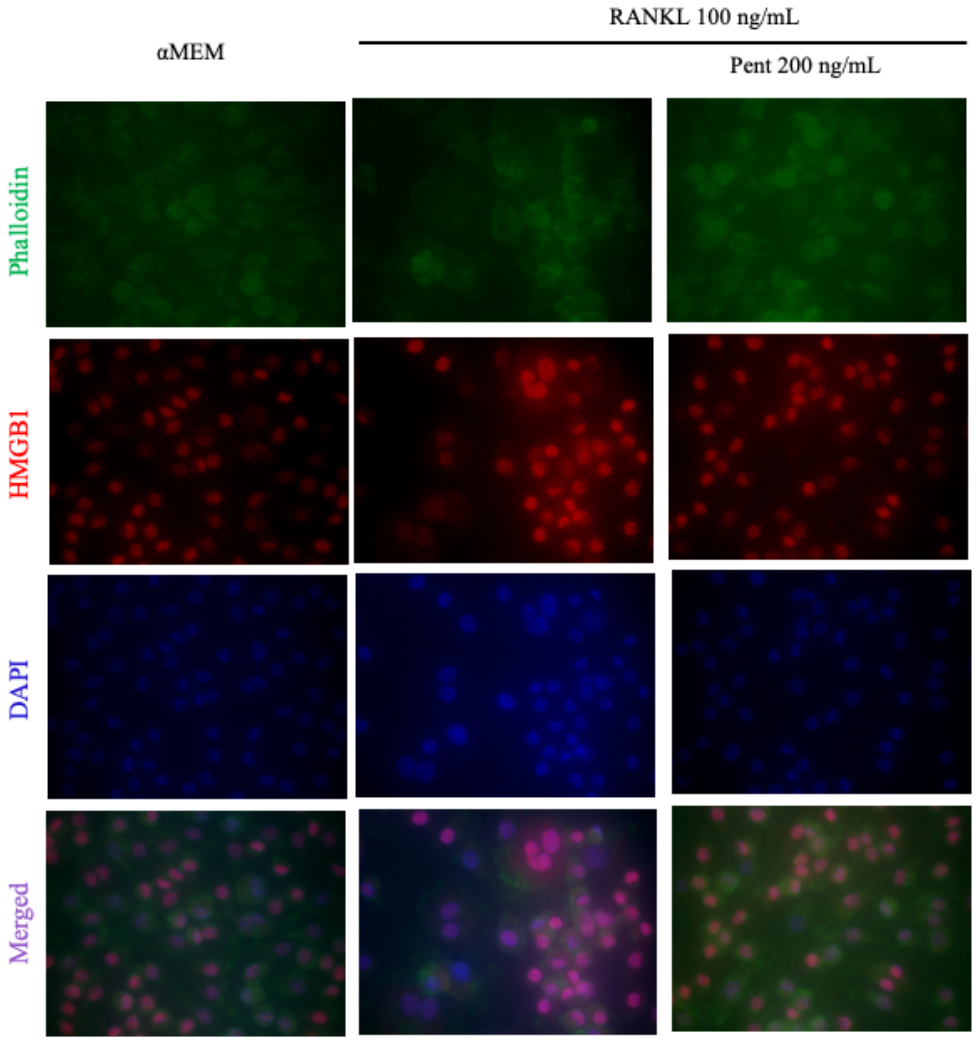
αMEM
RANKL 100 ng/mL
Pent 200 ng/mL
Phalloidin
HMGB1
DAPI
Merged

B)

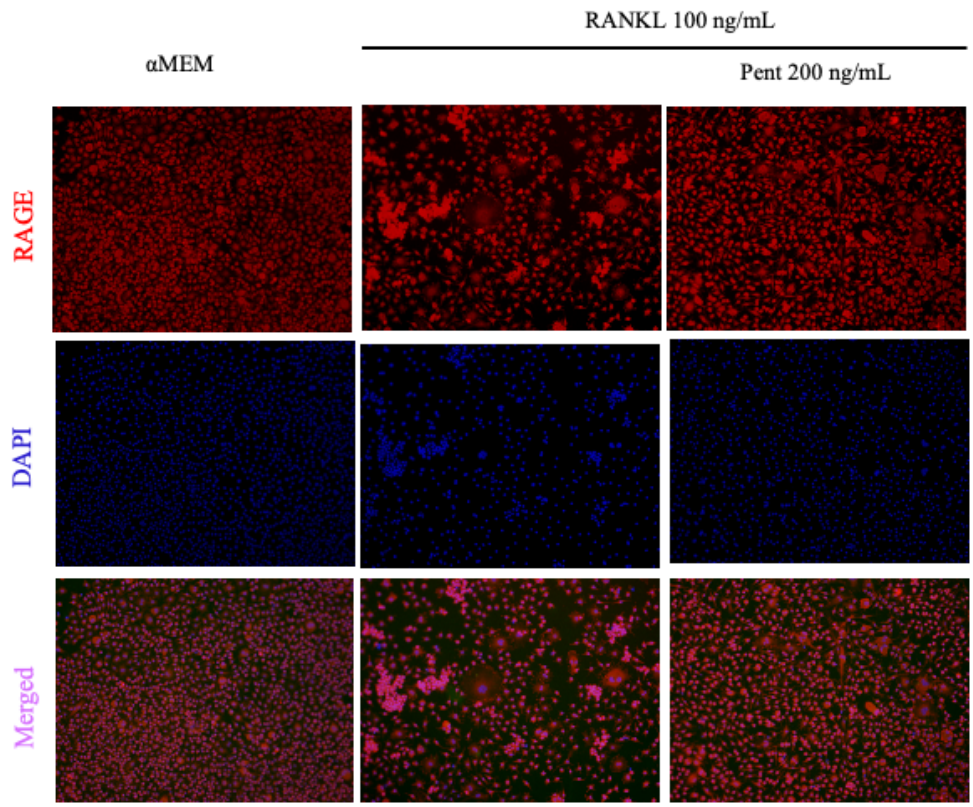

Figure 17: Role of free pentosidine on HMGB1 and RAGE expression. (A) HMGB1, (B) RAGE expression. Microscopic images are shown at 60X magnification for HMGB1 and 10X for RAGE.

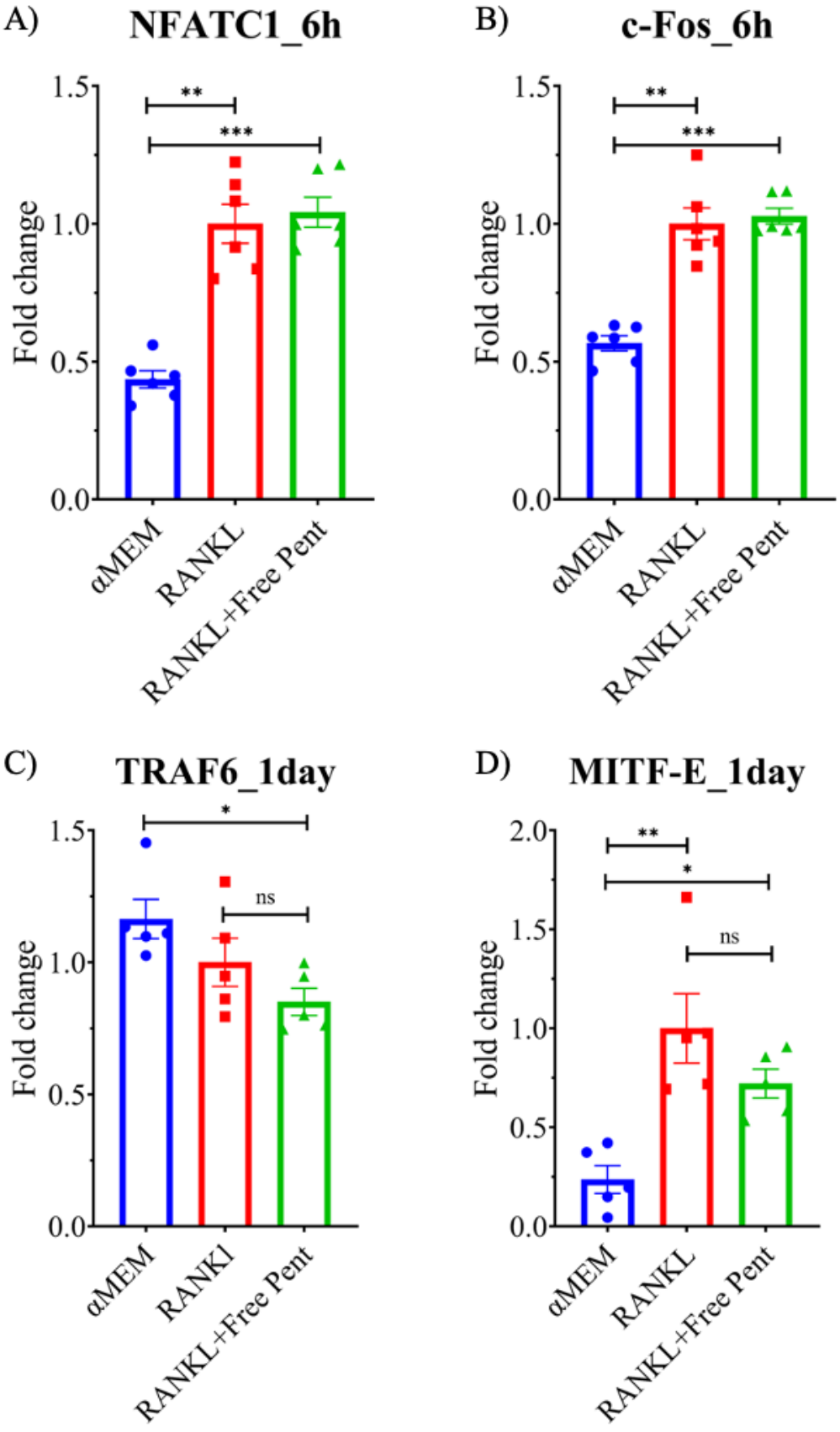
A)
NFATC1_6h
Fold change
1.5
1.0
0.5
0.0
**
***
αMEM
RANKL
RANKL+Free Pent
B)
c-Fos_6h
Fold change
1.5
1.0
0.5
0.0
**
***
αMEM
RANKL
RANKL+Free Pent
C)
TRAF6_1day
Fold change
1.5
1.0
0.5
0.0
*
ns
αMEM
RANKl
RANKL+Free Pent
D)
MITF-E_1day
Fold change
2.0
1.5
1.0
0.5
0.0
**
*
ns
αMEM
RANKL
RANKL+Free Pent

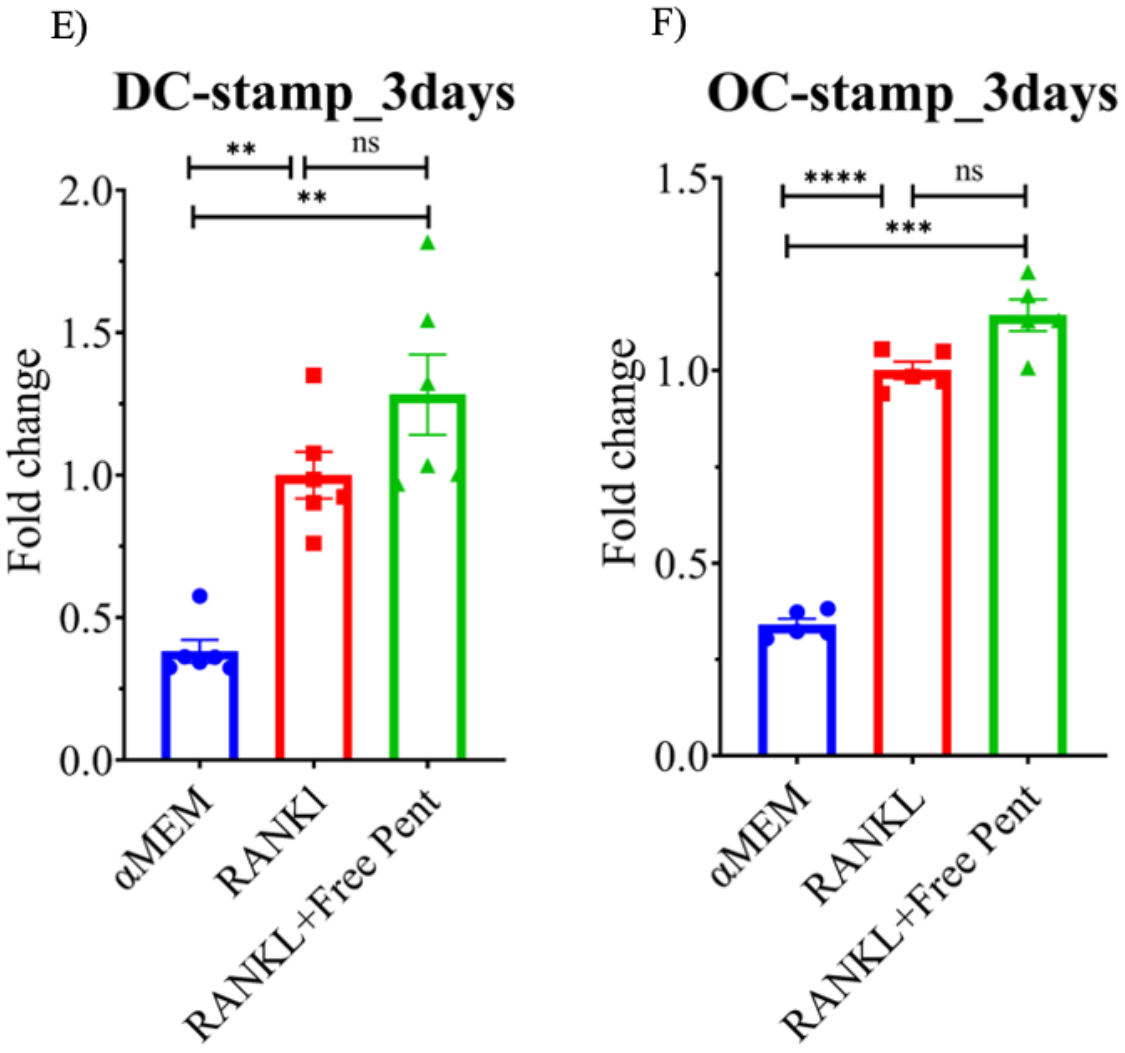
E)
DC-stamp_3days
**
ns
**
2.0
1.5
1.0
0.5
0.0
Fold change
αMEM
RANKl
RANKL+Free Pent
F)
OC-stamp_3days
****
ns
***
1.5
1.0
0.5
0.0
Fold change
αMEM
RANKL
RANKL+Free Pent

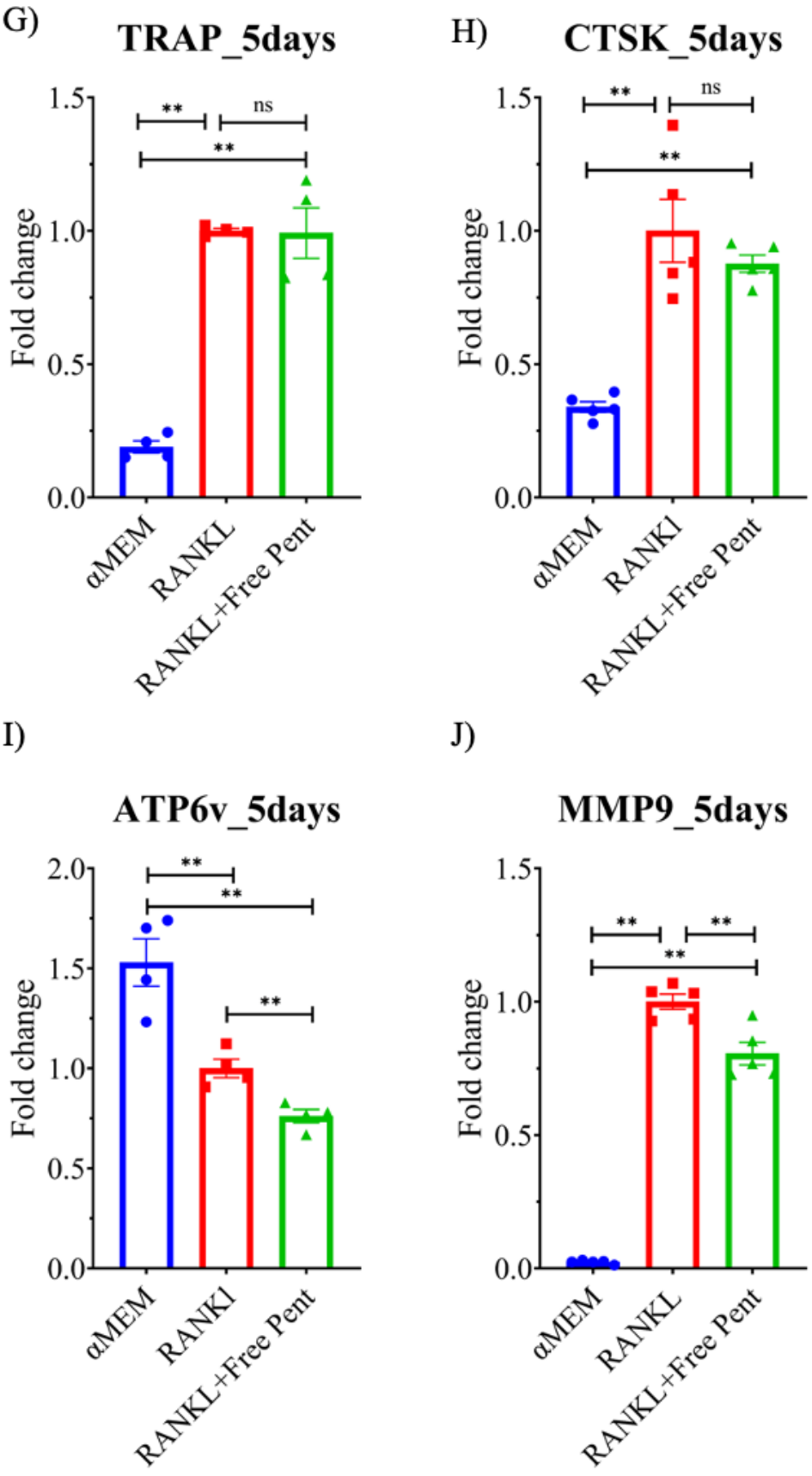
G)
TRAP_5days
Fold change
1.5
1.0
0.5
0.0
**
ns
**
αMEM
RANKL
RANKL+Free Pent
H)
CTSK_5days
Fold change
1.5
1.0
0.5
0.0
**
ns
**
αMEM
RANKl
RANKL+Free Pent
I)
ATP6v_5days
Fold change
2.0
1.5
1.0
0.5
0.0
**
**
**
αMEM
RANKl
RANKL+Free Pent
J)
MMP9_5days
Fold change
1.5
1.0
0.5
0.0
**
**
**
αMEM
RANKL
RANKL+Free Pent

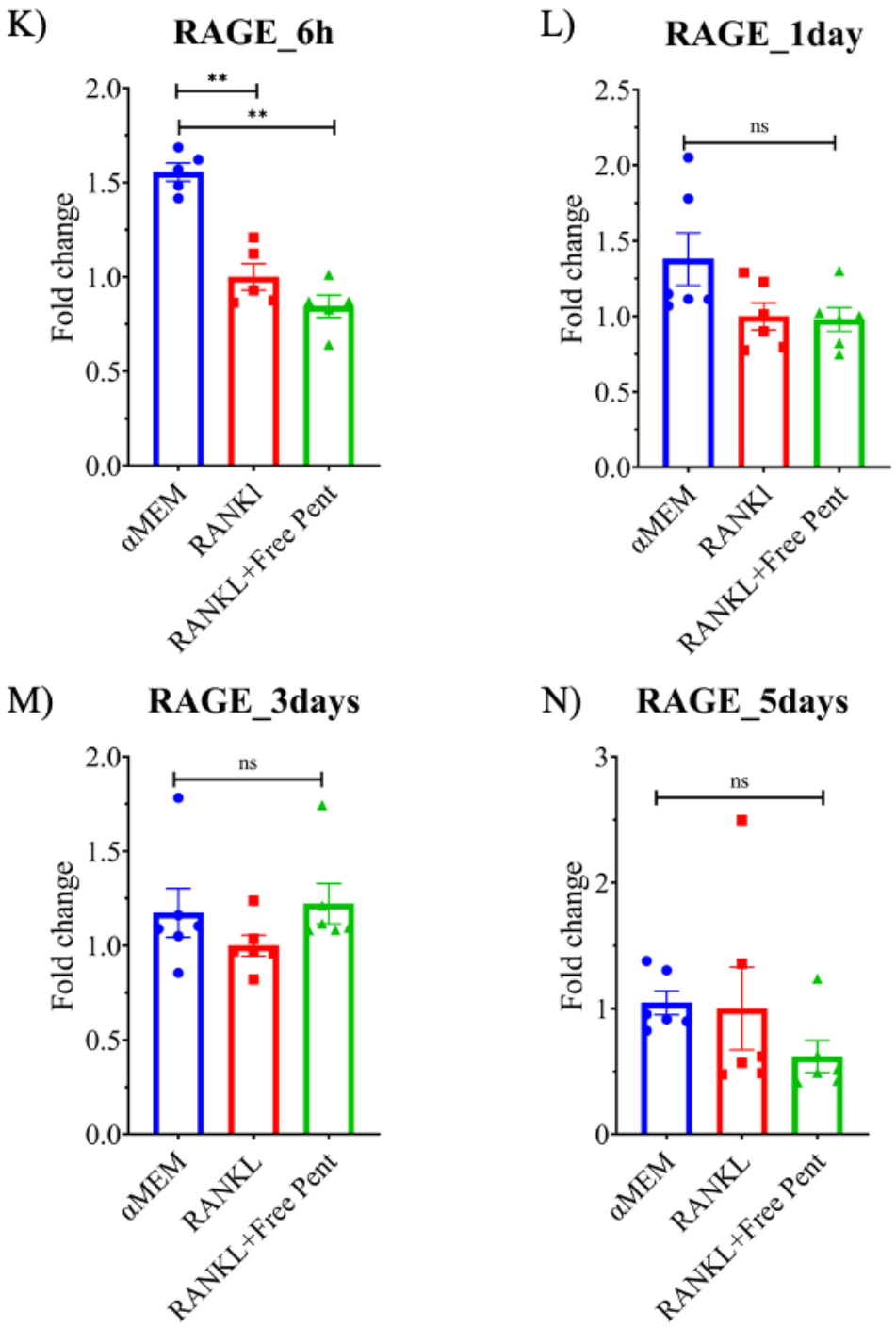

Figure 18: Role of free pentosidine on osteoclastogenic gene expression. Values are means±SEM, *p<0.05, ** p<0.01, ***p<0.001, ****p<0.0001, ns-non-significant.

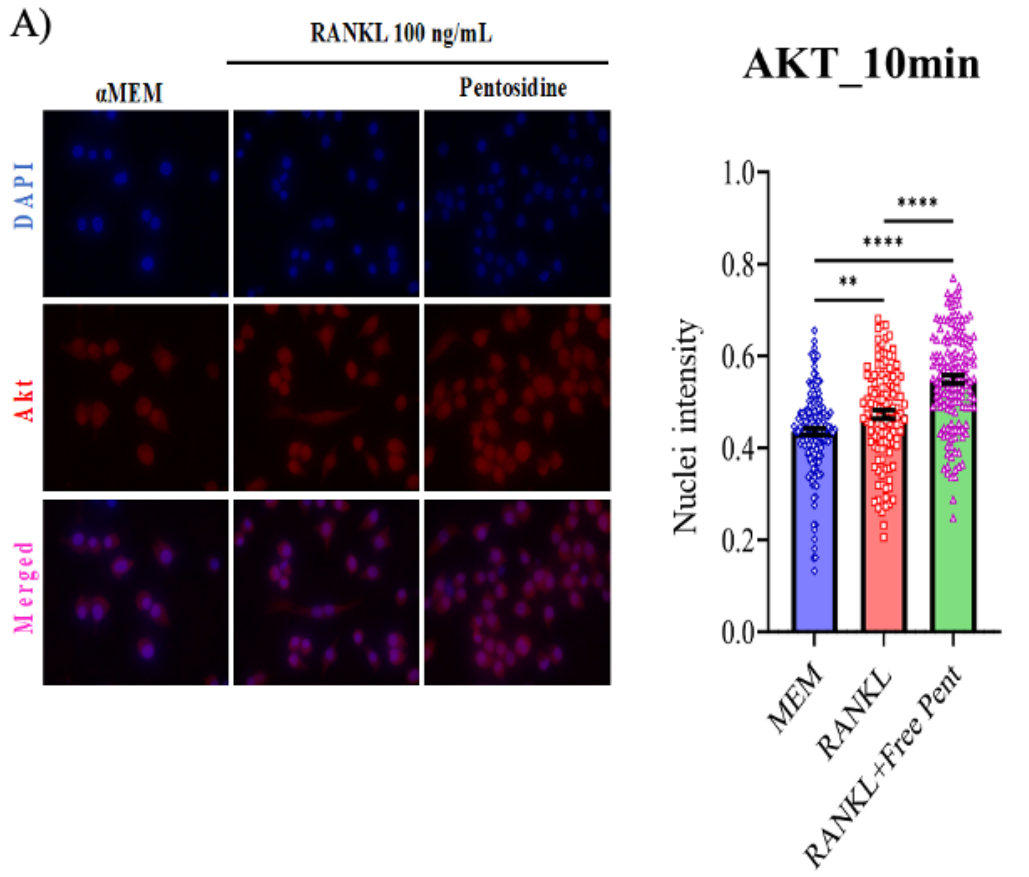
A)
RANKL 100 ng/mL
αMEM
Pentosidine
DAPI
Akt
Merged
AKT_10min
Nuclei intensity
1.0
0.8
0.6
0.4
0.2
0.0
**
****
****
MEM
RANKL
RANKL+Free Pent

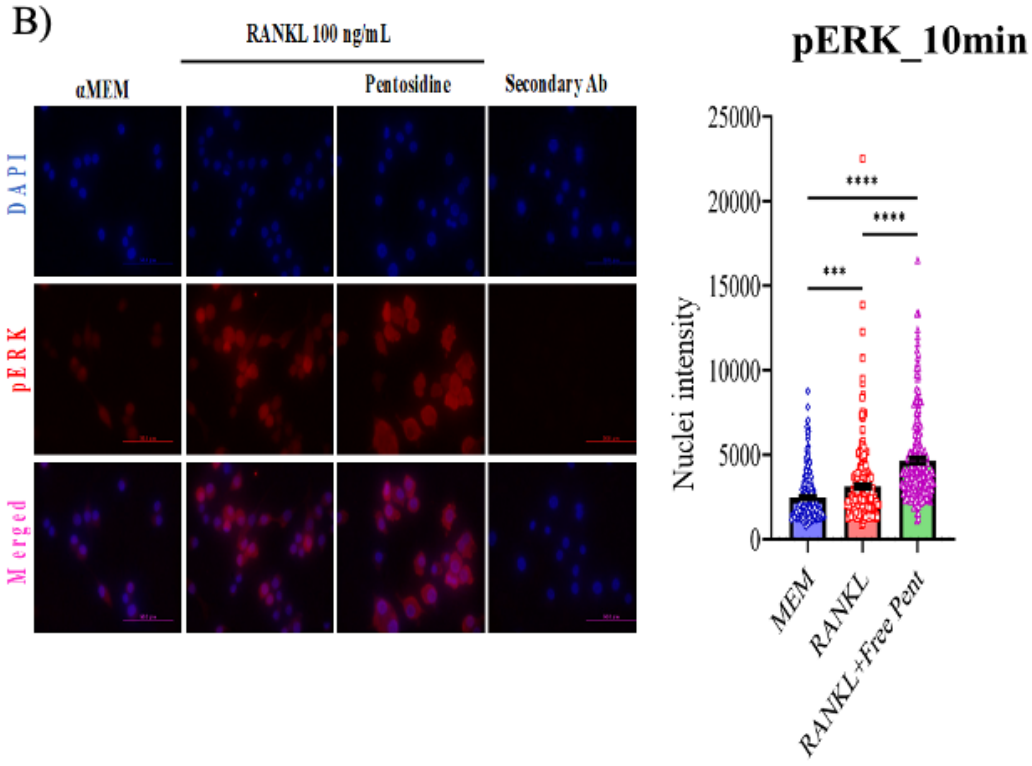
B)
RANKL 100 ng/mL
αMEM
Pentosidine
Secondary Ab
DAPI
pERK
Merged
pERK_10min
Nuclei intensity
25000
20000
15000
10000
5000
0
***
****
****
MEM
RANKL
RANKL+Free Pent

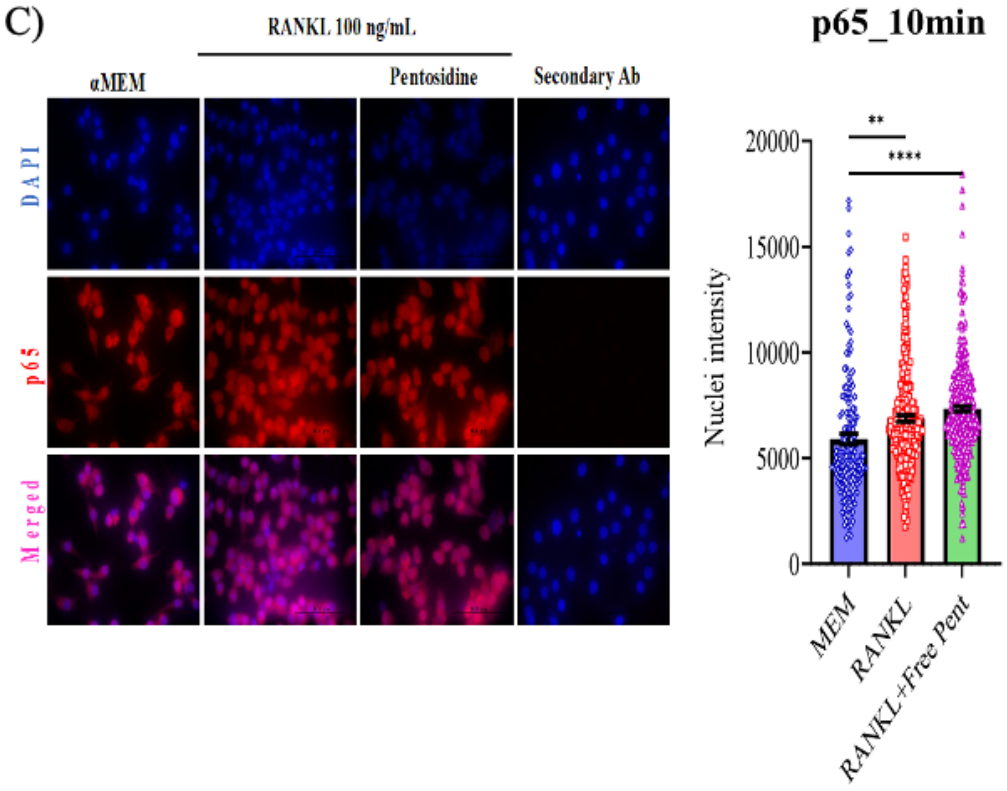
C)
RANKL 100 ng/mL
αMEM
Pentosidine
Secondary Ab
DAPI
p65
Merged
p65_10min
Nuclei intensity
20000
15000
10000
5000
0
**
****
MEM
RANKL
RANKL+Free Pent

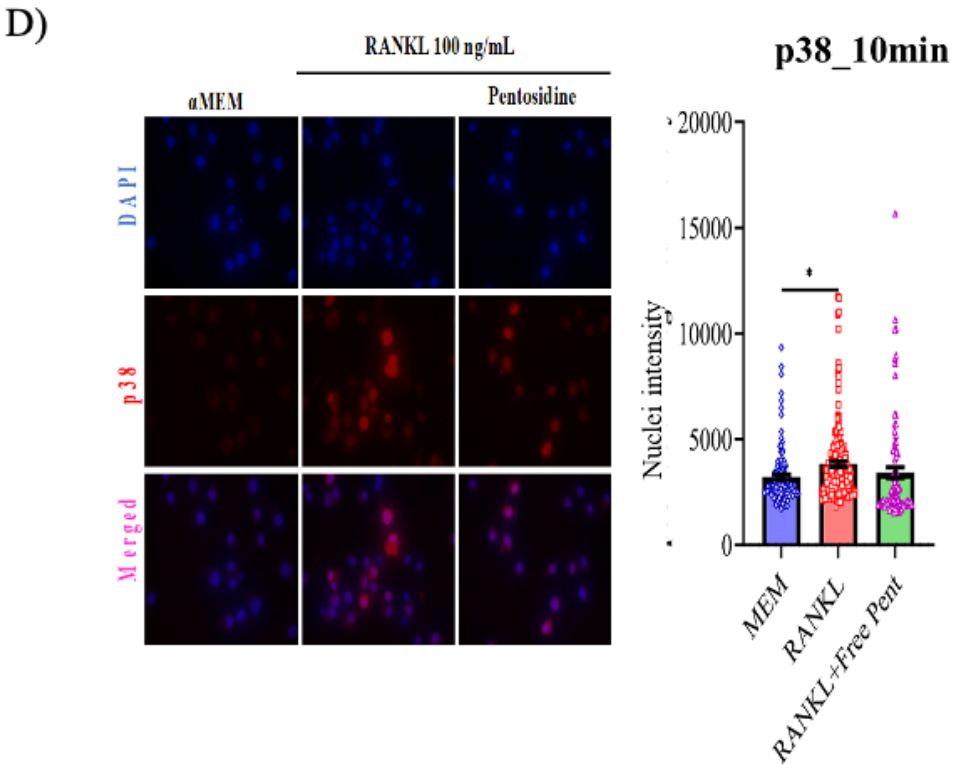
D)
RANKL 100 ng/mL
αMEM
Pentosidine
DAPI
p38
Merged
p38_10min
Nuclei intensity
20000
15000
10000
5000
0
*
MEM
RANKL
RANKL+Free Pent

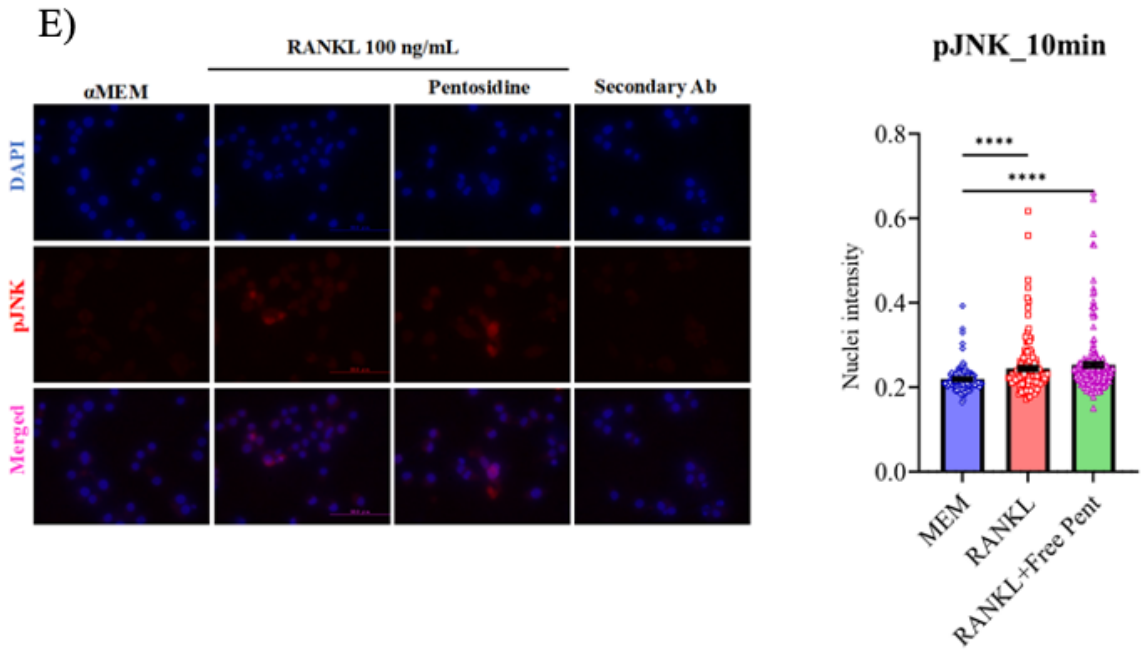

Figure 19: Different pathway activation by free pentosidine. Values are means±SEM, *p<0.05, ** p<0.01, ***p<0.001, ****p<0.0001.